Comparative Life-Cycle Analyses Reveal Interacting Climatic and Biotic Drivers of Population Responses to Climate Change

Authors

Esin Ickin[1], Eva Conquet[1], Briana Abrahms[3], Steve Albon[4], Daniel T. Blumstein[5,6], Monica L. Bond[1,7], P. Dee Boersma[3], Tyler J. Clark-Wolf[3,8], Tim Clutton-Brock[9,10,11], Aldo Compagnoni[12,13], Tomáš Dostálek[14,33], Sanne M. Evers[2,13,15], Claudia Fichtel[16], Marlène Gamelon[17], David García-Callejas[18,19], Michael Griesser[20,21], Brage B. Hansen[22,23], Stéphanie Jenouvrier[24], Kurt Jerstad[25], Peter M. Kappeler[26,16], Kate Layton-Matthews[27], Derek E. Lee[7], Francisco Lloret[28,29], Maarten JJE Loonen[30], Anne-Kathleen Malchow[31], Marta Manser[1,10,11], Julien Martin[32], Ana Morales-González[2], Zuzana Münzbergová[14,33], Chloé R. Nater[34], Neville Pillay[35], Maud Quéroué[36], Ole W. Røstad[37], María T Sánchez Mejía[28,29], Carsten Schradin[38,35], Bernt-Erik Sæther[39], Arpat Ozgul[1], Maria Paniw[2,1*]

* Corresponding author: Maria Paniw, maria.paniw@ebd.csic.es

Affiliations

1 Department of Evolutionary Biology and Environmental Sciences, University of Zurich, Zurich, Switzerland

2 Department of Conservation Biology and Global Change, Estación de Doñana (EBD-CSIC), Seville, Spain

3 Department of Biology, Center for Ecosystem Sentinels, University of Washington, Seattle, Washington, USA

4 The James Hutton Institute, Craigiebuckler, Aberdeen AB15 8QH, UK

5 Department of Ecology and Evolutionary Biology, University of California Los Angeles, Los Angeles, USA

6 The Rocky Mountain Biological Laboratory, Crested Butte, CO, USA

7 Wild Nature Institute, Concord, New Hampshire, USA

8 Department of Wildland Resources and Ecology Center, Utah State University, Logan, Utah, USA

9 Department of Zoology, University of Cambridge, Cambridge, UK

10 Kalahari Research Trust, Kuruman River Reserve, Kuruman, Northern Cape, South Africa.

11 Mammal Research Institute, University of Pretoria, Hatfield, South Africa

12 Martin Luther University Halle-Wittenberg, Am Kirchtor 1, 06108, Halle (Saale), Germany

13 German Centre for Integrative Biodiversity Research (iDiv), Leipzig, Germany

14 Department of Population Ecology, Institute of Botany, Czech Academy of Sciences, Průhonice, Czech Republic

15 Department of Community Ecology, Helmholtz Centre for Environmental Research – UFZ, Halle (Saale), Germany

16 Behavioral Ecology and Sociobiology Unit, German Primate Center, Leibniz Institute for Primate Research, Göttingen, Germany

17 Laboratoire de Biométrie et Biologie Evolutive, UMR 5558, CNRS, Université Claude Bernard Lyon 1, Villeurbanne, France

18 Centre for Integrative Ecology, School of Biological Sciences, University of Canterbury, Private Bag 4800, Christchurch 8140, Aotearoa New Zealand

19 Manaaki Whenua-Landcare Research, PO Box 69040, Lincoln 7640, Aotearoa New Zealand

20 Center for the Advanced Study of Collective Behavior, University of Konstanz, 78457 Konstanz, Germany

21 Department of Collective Behaviour, Max Planck Institute of Animal Behavior, 78457 Konstanz, Germany

22 Gjærevoll Centre for Biodiversity Foresight Analyses, Norwegian University of Science and Technology (NTNU), Trondheim, Norway

23 Department of Terrestrial Ecology, Norwegian Institute of Nature Research (NINA), Trondheim, Norway

24 Biology Department, Woods Hole Oceanographic Institution, Woods Hole, Massachusetts, USA

25 Jerstad Viltforvaltning, Mandal, Norway

26 Department of Sociobiology/Anthropology, Johann-Friedrich-Blumenbach Institute of Zoology and Anthropology, University of Göttingen, Göttingen, Germany

27 Department Oslo, Norwegian Institute for Nature Research, Trondheim, Norway

28 Center for Ecological Research and Forestry Applications (CREAF), Cerdanyola del Vallès 08193, Spain

29 Department Animal Biology, Plant Biology and Ecology, Universitat Autònoma Barcelona, Cerdanyola del Vallès 08193, Spain

30 Arctic Centre, Faculty of Arts, University of Groningen, PO Box 716, NL-9700 AS Groningen, Netherlands

31 Theoretical Ecology, Universität Regensburg, Regensburg, Germany

32 Department of Biology, University of Ottawa, Canada

33 Department of Botany, Faculty of Science, Charles University, Prague, Czech Republic

34 Department of Terrestrial Biodiversity, Norwegian Institute for Nature Research, Trondheim, Norway

35 School of Animal, Plant and Environmental Sciences, University of the Witwatersrand, South Africa

36 CEFE, Univ Montpellier, CNRS, EPHE, IRD, Montpellier, France

37 Department of Ecology and Natural Resource Management, Norwegian University of Life Sciences, Ås, Norway

38 Université de Strasbourg, CNRS, IPHC UMR 7178, F-67000 Strasbourg, France

39 Department of Biology, Centre for Biodiversity Dynamics, Norwegian University of Science and Technology (NTNU), Trondheim, Norway

Abstract

Responses of natural populations to climate change are driven by how multiple climatic and biotic factors affect survival and reproduction, and ultimately shape population dynamics. Yet, we lack a general understanding of the role of such mechanisms in moderating climate-change impacts across different species. Here, we synthesize how the joint effects of climate and biotic interactions on different vital rates impact population change, using 41 species from trees to primates. We show that the effects of multiple climatic drivers tend to exacerbate population responses to climate change in most species. Importantly however, density feedbacks consistently buffer the effects of climate drivers on populations. In all species considered in our analyses, such interactions among climate and density had starkly different effects depending on the age, size, or life-cycle stage of individuals, highlighting that climate-change impacts can hardly be inferred from single drivers or ages or life-cycle stages, regardless of the life-history of species. Our work thus advances our ability to make generalizations about key pathways of climate-change impacts on populations.

Short: From shrubs to primates, understanding climate-change impacts requires us to look at how individuals interact with each other.

MAIN TEXT

Introduction

Among the multiple challenges for biodiversity conservation, the increasing severity of climate change, interacting with other global-change drivers, is of particular concern *(1)*. Understanding how populations of plants and animals respond to such complex interactions is a priority for

theoretical and applied research and management *(2)*. Populations in natural communities are structured by variation in genetic and phenotypic traits, and often also developmental stages, which determine how different rates of survival and reproduction are spread throughout the life cycle *(3)*. In structured populations, climatic effects on population abundances are then filtered by how different biotic and abiotic drivers (including climate) affect trait-, age-, or stage-specific survival and reproduction *(4–13)*. For instance, population persistence may be particularly affected when several climatic factors simultaneously reduce survival and reproduction of several life-cycle stages, accelerating population decline *(5)*. In particular compound effects of hotter and drier climatic conditions on individuals can have strong negative impacts on natural populations and communities *(14, 15)*, especially in combination with land-use change *(16)*. However, populations may also be buffered from adverse climatic effect, when vital rates with higher impact on population growth, i.e., adult survival, exhibit the least temporal variability and thus stabilize population fitness *(18, 22–24)*. Furthermore, a decrease in one vital rate under climate stress (e.g., recruitment) can be compensated with increases in other vital rates, such as survival of the remaining recruits or adults, under negative density feedbacks *(6, 7, 20)*. This occurs because, when individuals compete for resources, negative climatic effects on abundance will also ease competition *(6, 26)*, which can allow the populations to recover faster from or show higher resilience to adverse climatic effects *(27)*. The role of density dependence may be particularly important in assessing climate-change effects on population dynamics *(26)*. Therefore, to broadly understand the impacts of climate change in complex natural systems, we need to understand how intrinsic mechanisms interact to mediate such impacts on natural populations *(28, 29)*.

Despite substantial progress to synthesize the sensitivity of populations to climatic variation, comparative studies have largely overlooked complex mechanisms of interacting drivers and vital rates that generate variation in population-level metrics. For instance, previous studies have linked global indices of temperature and rainfall to abundances or population growth rates to show that terrestrial populations of plants and animals with shorter generation times are relatively more sensitive to climatic variation *(21, 30)*. Despite producing important insights, such analyses have not investigated vital-rate responses to climatic factors and did not consider biotic drivers. A recent study compared the relative effect on plant population growth rates of perturbing abiotic vs. biotic drivers, but did not assess how simultaneous effects of different drivers on different vital rates affect populations *(31)*. This contrasts with the growing consensus that complex

interactions among vital rates and biotic and climatic drivers complicate projections of persistence under climate change *(28, 32–36)*.

We synthesize, for the first time, how interacting climatic and biotic drivers change population dynamics across taxa by affecting different vital rates such as reproduction and juvenile and adult survival. Given the evidence for the importance of interactions among abiotic and biotic factors on population dynamics *(5–12)*, we hypothesized (H1) that the simultaneous effects of climatic drivers and density dependence (whenever density feedbacks are present in population dynamics) can buffer population-level responses to climatic perturbations. Secondly, we hypothesized (H2) that changes of population growth rate under climatic perturbations cannot be predicted from perturbing single vital rates, even if those vital rates contribute strongly to population dynamics, given that climatic and biotic drivers typically affect vital rates differently and non-linearly, making their aggregated effect more complex to predict *(33–35)*.

We reviewed the ecological literature and identified studies that quantitatively linked at least two climatic drivers or one climatic and one biotic driver to at least two vital rates. Following *(33)*, we defined climatic drivers as direct measures of temperature or precipitation, i.e., not drivers that affected climate indirectly, such as the Southern Annular Mode (i.e., *Catharacta lönnbergi* from *(37)*; see *Supporting Materials* for a complete list of selection criteria). Among the biotic drivers, we distinguished intraspecific density dependence and interspecific interactions. We then built structured population models and used them to compute sensitivities of population growth rates *(38)* to a given climatic driver, either accounting for simultaneous effects of all other drivers on vital rates or keeping other drivers fixed, thus reducing the complexity of environmental effects. We also compared the effects of perturbing different single vital rates to understand whether population-level sensitivities are driven by changes in specific vital rates. When testing our hypotheses, we controlled for potential confounding factors, most importantly the life-history strategy of populations, which has been shown to strongly mediate population responses to environmental change *(19, 21)*. We created a database making all data and code freely available online, to allow researchers to link age- or stage-specific vital rates to population responses under environmental change for further analyses such as forecasts.

Results

We extracted data from 23 studies including 41 species (15 birds, 8 mammals, and 18 plant species). Among these species, 18 matrix population models, eight integral projection models, five integrated population models, and 10 individual-based models were used, and vital rates were typically modeled using generalized linear models. For an overview of life-history strategies, covariates, and demographic status of the species included in this comparative study, see Table S6. For each species, we calculated the scaled absolute sensitivities (|S|), i.e., changes in the population growth rate, λ, to observed climatic variation (standardized differences between maximum and minimum climatic values) *(31)*. In most studies, we calculated λ for either a single (meta)population or a representative average population across the habitat range, as in the case of eight bird species *(39)* and 11 Mediterranean tree species *(40)*. However, three studies (see Supporting Materials) modeled different populations. Here, we averaged sensitivities across populations to calculate species-specific average sensitivities to climate comparable across species *(31)*. Additional analyses showed that such averaging did not affect results (Table S4).

We modeled the variation in |S| using a modified meta-regression approach *(41)*, where we pooled the results from all studies into one generalized linear hierarchical model. Our model included average age at maturity, a proxy for the fast-slow continuum of life-history strategies *(42)*. As expected, slower-paced species had lower absolute sensitivities of λ (|S|) to climatic drivers compared to faster-paced species (Fig. 1; Table 1; $\beta_{Maturity} = -1.13 \pm 0.19$). These patterns agree with theoretical expectations (i.e., demographic buffering hypothesis; *(18, 25)*) and previous empirical studies *(19, 21, 30, 43)* and suggest that fast-paced life-histories across taxa are more labile to, or track, climatic fluctuations, whereas slow-paced life histories buffer population dynamics from multiple climatic effects *(18, 19, 21)*.

<u>Population responses to climate variation are more buffered when density feedbacks are explicitly considered (H1)</u>

Across life histories, sensitivities |S| to changes in a focal climatic driver were lower for populations where intraspecific density dependence explicitly affected vital rates, as opposed to populations where vital rates were largely modeled as a function of climatic and other abiotic variables, but not density dependence ($\beta_{DensityYes} = -1.00 \pm 0.56$; Table 1; Fig. 1; Fig. S1). These differences in sensitivities were strongest when we accounted for the full complexity of environmental effects in sensitivity analyses (Fig. S1). This is because, under such full-complexity analyses, we adjusted for observed changes in intraspecific density when the focal

perturbed climatic driver was at its minimum and maximum. Such covariation with density moderated the impact of the climatic driver and lowered the differences in λ under changes in the climatic driver (Fig. S2). In turn, |S| increased by holding density dependence constant when perturbing a climatic driver ($\beta_{NoCovariation:Density}$ = 0.40 ± 0.19). On the other hand, |S| decreased for models without density dependence when we held other climatic drivers constant and thus reduced the compound effects of climatic drivers (Table 1; $\beta_{NoCovariation}$ = -0.25 ± 0.11; Table 1; Fig. 1). Our results therefore suggest that interactions between climate and density may be critical in moderating climate-change impacts on populations across a wide range of taxa *(5–12, 44, 45)*. On the other hand, synergistic effects of different climatic drivers can have a stronger impact on population dynamics than considering the effects of such drivers in isolation.

Sensitivity of the population growth rate to climate cannot be predicted from climate responses of single vital rates (H2)

We perturbed climatic drivers in each vital-rate model separately for 26 species to understand how different vital rates mediate the sensitivity of λ (|S|) to these drivers. For the remaining species, we could not perturb single vital rates due to the complexity of the models. A generalized linear regression model revealed that |S| was not driven by specific vital rates (Table 2). Fast-paced life histories, i.e., ones with a lower age at maturity *(43)* were relatively more sensitive to climate perturbations in reproduction and survival of non-reproductive individuals than slow-paced life histories (Fig. S5). This is to be expected as reproduction contributes relatively more to population dynamics of fast-paced species *(19)*. Our results provide further evidence that fast-paced life histories buffer critical vital rates from climatic perturbations less than slow-paced ones *(18, 19, 22, 23)*; the latter typically showing lowest sensitivities when perturbing climate effects on adult survival, a critical vital rate *(46)*. However, a closer look at sensitivities of λ to vital-rate specific effects of climatic drivers revealed a complex picture (Fig. 2). Across life-histories, λ can be equally affected by perturbations in several vital rates, and some vital rates showed strong responses to one environmental variable, but weak responses to other variables (Fig. 2; Figs. S11 – S38).

Overall, our results showed that growth-rate sensitivities, |S|, varied substantially among species/studies (Table 1; Table 2). While the fixed and random effects in our GLMMs jointly explained > 80 % of the variance in |S|, the proportion of variance attributed to random effects was always relatively higher (see Tables S1-S5). The effect of species explained > 50 % of the

random variation in the model. We also note that while 20 studies included only one species, three modeled several species, and we could not completely separate species and study effect - attempting to do so resulted in overparameterized models. Although we accounted for potential variables that may have confounded our results, i.e., number of vital rates modeled and average number of parameters per vital rate, one reason for such high variance among species or studies may be the varying complexity among studies in model design or the specific climatic variable considered – complexity that we could not account for in our analysis. On the other hand, high variability in responses to environmental drivers among species have also been observed in recent studies *(30, 33, 47, 48)*. Thus, while we can discern generalizable patterns in population responses to climatic perturbations, only the inclusion of a wider range of future studies can disentangle the complex sources of context-dependent variation in population dynamics.

Discussion

Natural populations of plants and animals are increasingly affected by climate change worldwide *(49, 50)*. By identifying under what context populations are more susceptible to negative effects of climatic drivers, we can prioritize conservation efforts and develop targeted strategies to mitigate adverse effects. Our comparative analyses shed light on some common demographic pathways through which populations of plants, mammals, and birds respond to complex interactions of climatic and biotic drivers. We show that simultaneous effects of multiple climatic drivers increase population sensitivity to climate change, while interactions between density dependence and climate are key in moderating effects of multiple climate drivers. Further, it is necessary to understand the effects of climatic drivers across the full life cycle of species – not just single vital rates. Our results have important implications for our understanding on how resilient populations are to climate change.

Recent studies have emphasized that future climate risks to natural populations and humans will be exacerbated by compound effects of climate drivers *(1, 51)*. While previous research has focused on understanding such compound effects on single species or populations (reviewed in e.g., *30, 34, 52*), our results provide the first comparative evidence that synergistic effects of different climatic drivers can have a strong impact on population dynamics. Compound climatic effects, such as low rainfall and high temperature, often constitute climatic extremes (e.g., hot droughts, *(51)*), which are becoming increasingly common *(1)* and can have strong, non-additive effects on physiological processes of plants *(53)* and animals *(54)*, negatively affecting population fitness *(5, 32, 55)*. In meerkats (*Suricata suricatta*), for instance, extreme heat in a relatively dry

rainy season can lead to substantial loss of body mass and increased risks of deadly disease outbreaks *(56)*. We note, however, that our study assessed changes in the magnitude, but not in the direction of population responses to perturbations in climate. Therefore, compound effects such as unusually warm and rainy reproductive seasons, may also lead to strong increases in population growth *(56)*. This caveat is particularly relevant considering that fast life histories showed the strongest sensitivities to climate perturbations. Fast life histories are known to track environmental fluctuations *(25)*, which can allow them to increase population size rapidly when favorable climatic conditions follow unfavorable ones, or to adapt to changing environmental conditions more rapidly *(57)*.

Climatic factors do not affect populations in isolation; other abiotic and biotic factors also play a role, and their impacts vary among populations and individuals within those populations *(34, 58)*. Our results suggest that across taxa, adverse climate effects can be buffered by decreasing densities and thus easing the effects of intraspecific density, when present in populations *(5, 7)*. In turn, for populations that increase in abundance under climate change, negative density dependence may increase population fluctuations under adverse environmental conditions *(36)*. Other studies have also demonstrated the importance of density feedbacks in regulating population responses under land-use change *(59)* or disease outbreaks *(60, 61)*, while populations of some social species that show non-linear responses to population densities may be particularly susceptible to climate change if adverse climatic effects reduce optimal densities *(5)*. Similarly, climate change also affects populations through changes in interspecific interactions such as predation, competition, or facilitation *(12, 62)*. However, interspecific interactions are still very rarely explicitly modeled when projecting population dynamics *(33)*. Disentangling the relative contributions of climate and density dependence on population dynamics can require complex analyses, but studies that have done such breakdown of relative contributions have found that varying the effects of intra- or interspecific density dependence in vital rates produces the strongest responses at the population level (e.g., *12, 62, 63*).

Despite this growing evidence on the importance of assessing interactions of abiotic and biotic effects when quantifying population persistence under climate change *(4, 5, 13, 31, 33)*, such assessments can be challenging. Unlike climatic variables that are often included as continuous covariates in vital-rate models and are easily perturbed, interactions with individuals of the same population or even different species took on many complex forms in the population models we

used in this study. While 30 % of species in our database explicitly included density dependence in their models, some studies only included indirect or static measures of biotic effects. For example, the tree species in our analysis had a colonization factor in their models, which was indirectly related to density, but was decoupled from climate variables in vital rates *(40)*. Similarly, the models of *Certhia familiaris*, *Linaria cannabina*, *Lophophanes cristatus*, *Prunella collaris*, *Prunella modularis*, *Pyrrhula pyrrhula*, *Sitta europaea*, and *Turdus torquatus* did not contain density as a continuous driver in their vital-rate models (which was required for our sensitivity analyses), but density served as a fixed species-specific parameter affecting fecundity *(39)*. As our results highlight that density feedbacks may be a general mechanism that moderates population fluctuations under climate change for a range of taxa, broadening comparative analyses that can account for complex density effects is an important step forward in population ecology.

Density feedbacks are not equally important in all populations *(64)*. However, the potential effects of density feedbacks have not been tested in many recent population models *(33)*, likely due to a combination of lack of data and model complexity. In addition, most frameworks to predict biodiversity loss under global change do not explicitly model dynamic interactions between density and global-change drivers *(65)*. We thus emphasize that including density feedbacks in the climate-demography models, for instance using population density or population size as a covariate in models *(12, 36)*, may be key to understand how resilient natural populations are to climate change.

Ultimately, the effects of climate change on population dynamics are filtered by the strength and direction of driver effects on different vital rates, and how much the latter contribute to population dynamics (e.g., *(4–13, 19, 22, 26, 32, 35, 36, 37)*). An important finding of our study is that, for any life history, even slow-paced ones where adult survival is the key vital rate driving population dynamics *(19)*, we could not predict changes in population growth from perturbing single vital rates. This suggests that the manner in which interacting effects of different abiotic and biotic drivers filter through vital rates to affect population dynamics is highly context dependent *(13)*. Rainfall scarcity or extreme temperatures may differently affect individuals depending on the habitat, season, and life-cycle stage considered (e.g., *(5, 32)*), or depending on how other species in a given community are responding to climate change *(62)*. The complexity of the life cycle may also indicate how much a population is buffered from adverse environmental

effects *(52)*. Some species have dormant life-cycle stages that can protect populations from environmental fluctuations *(62)*. Dispersal, which was modeled in some studies considered here (see Supporting Materials), can stabilize decreasing populations and allow individuals to track new suitable habitats, and may itself be strongly mediated by climate *(66)*. Therefore, from trees to primates, identifying how different abiotic and biotic factors impact populations across their full life cycle is key to be able to target conservation efforts towards certain factors during certain times of the life cycle.

Our work has advanced comparative demographic analyses in two important ways. First, we standardized sensitivity analyses across a wide variety of population models, ranging from classic matrix population models to integrated population and integral projection models, and individual-based models. By including the experts for each study system, we ensured that our methods did not produce inadvertent errors. Second, we provide a freely accessible and dynamic (i.e., constantly updated) database of population models that was compiled for this study. This offers an ideal basis to expand the number of studies and analyses in the future – for instance, forecasting how changes of local climatic drivers may affect populations and whether such effects can be approximated by global climate indices *(67)*. We also recognize several limitations of our work. One limitation is that we could not account for taxonomic and geographical biases as we relied on available high-quality structured models that integrate multiple environmental factors (see *Supporting Materials* for study-specific details). Such tailored models are available for specific terrestrial plants, mammals, and birds, but are still lacking for many invertebrate species *(68, 69)*, where relatively little is known on the demographic pathways through which climate change impacts abundance *(70)*. We also have a geographic bias in our data as most study systems are from the Northern Hemisphere. Additionally, we only considered studies published in English. These types of biases can limit our ability to generalize patterns and employ conservation efforts based on comparative analyses *(71, 72)*.

When searching the literature for appropriate studies, we also discovered that reproducibility of ecological studies remains a problem. Of the 76 studies that met our search criteria, we could only replicate population models of 24 %. For the remaining studies, data and code to replicate analyses were not freely available and could often not be reproduced even when in contact with authors. Thus, we emphasize that making not just data but also code available is an important step towards reproducible comparative analyses in ecology *(73)*.

Our comparative analyses provide evidence that interactions among biotic and abiotic drivers, and the complex effects of such multiple drivers on different vital rates, hinder simplistic predictions of population persistence under climate change. We emphasize the need to recognize and incorporate interactions between climate and density dependence into full life-cycle models in order to understand and potentially mitigate the threat that climate change poses on natural populations.

Materials and Methods

Literature search

Our main objective was to collect code and data from studies which (i) modeled vital rates (e.g., survival, growth, reproduction) in natural populations as a function of at least two climatic variables or one climatic and one biotic variable; and (ii) constructed structured population models from which population growth rates could be obtained. We focused on studies where data were obtained in natural, unmanipulated populations (i.e., discarding experimental studies); and where the environmental variables were continuous so that we could calculate means and standard errors (see equation 1). We therefore excluded studies that constructed models for good/bad, dry/wet environments, etc. To obtain suitable studies, we performed a targeted review of the literature. We first considered a recent review, which revealed a lack of understanding regarding comprehensive demographic responses to climate change for terrestrial mammals including 87 species *(33)*. From the publications in this review, we selected those that met our criteria. To supplement data from this list of studies, we conducted a Web of Science search using the search terms from *(33)* and also checked the Padrino database *(74)* as well as *(75)* (Details in SI). To be included in our database, vital-rate models had to be reproducible, i.e., the regression models were fully reported, including their formula, coefficients, and standard errors. We were able to obtain data from 23 studies that met all these criteria.

As the first step of the analysis, we prepared a standardized protocol to build and perturb different structured population models, to maximize the ease of comparison across studies (https://github.com/EsinIckin/Comparative-demography-project). For help with conducting these analyses for the selected models, we contacted the authors of relevant studies. We extracted regression coefficients from tables to rebuild vital-rate models when possible; alternatively, the latter were provided by the authors of a given study. We then reconstructed population models

from these vital rates, and the authors from the original papers reviewed these models to ensure that they were correct. In some cases, authors already provided the R code to rebuild the population model (for more information see Supporting Materials). The environmental covariate data were also obtained from the authors of the papers. All studies built structured population models based on > 7 years of demographic data collection and/or using data across the distribution range of species, and the range of environmental covariate values was sufficient to robustly build and perturb structured population models (see SI on study-specific details).

Next, we compared among the species how perturbations in climatic variables affects long-term population fitness, λ, i.e., the sensitivity of λ to climatic drivers. For studies that provided matrix population models or integral projection models, we calculated λ as the annual asymptotic population growth rate using R package popbio version 2.7 *(76)*. For studies that developed individual-based or integrated models, we calculated λ as the mean of annual growth rates over at least 50 years from at least 100 simulations (see Supporting Materials for study-specific details; Figs. S38-S52). To obtain sensitivities of λ to climatic drivers, we calculated λ under minimum and maximum values of a climatic driver while (i) accounting for the actual observed values of other drivers when the focal driver was at its minimum or maximum (sensitivities with **covariation**) or (ii) holding the other drivers constant at their average values (sensitivities **without covariation**). When studies modeled random year effects consistently across vital rates, we set the years to ones where a climatic driver was at its minimum or maximum in analyses; and otherwise, we held them constant (see Table S7 for details). We then calculated the scaled sensitivities according to Morris et al. *(31)* for each population and driver (Equation 1):

$$|S| = \left|\frac{\lambda_{max}-\lambda_{min}}{(d_{max}-d_{min})/\mathrm{SD}_d}\right| \quad \text{Equation 1}$$

The driver values d_{max} and d_{min} produced the population growth rates when the driver was set to its maximum value (λ_{max}) and its minimum value (λ_{min}). The denominator of the scaled sensitivity |S| is the difference in the driver levels in standard deviation (SD) units. The *scaled* sensitivity makes it possible to compare |S| across different studies and driver types *(31)*. We tested the robustness of the sensitivity metric by comparing |S| to the most common type of metric for summarizing outcomes in ecological meta-analyses: log response ratios (see *Alternative sensitivity parameterizations* in Supporting Materials).

We accounted for uncertainties around all |S| estimates by resampling parameters from vital-rate models and recalculating λ and |S| each time. More specifically, if a study reported the standard errors of the regression coefficients, we simulated the parameter distributions and sampled parameters from it, whereas in the case of Bayesian regressions, we sampled parameters from the MCMC posteriors. We produced 100 |S| estimates for most species but had to use fewer samples in some cases due to computational limits (see species-specific details in SI). In three cases, we averaged |S| over different populations to get species-specific results. However, this averaging did not affect our overall conclusions (see Table S4).

Further, we perturbed the climatic drivers in each vital rate separately whenever possible (Figs. S12 – S38 for the specific vital rates in each species' model), in the same manner as above, to get vital-rate specific |S|. In this case, all environmental driver values covaried with the focal driver in the perturbed vital-rate but were held at their average values in other vital rates. Lastly, for populations where intraspecific density dependence was explicitly considered as a driver in vital-rate models, we performed additional perturbations: We accounted for the actual observed values of other climatic or biotic drivers when perturbing a focal climatic driver (sensitivities with covariation), but held densities constant. We did this to test how much |S| depended on density dependence moderating the effects climatic changes.

Statistical analyses

We used a generalized linear mixed model (GLMM), assuming a Gamma distributed response under a log link function, to understand the underlying mechanisms influencing population-level sensitivities |S| to climate change. We chose the Gamma distribution because the scaled sensitivities were positive values larger than zero. The resulting model fit well to observed data (Fig. 1), and model fit was substantially better than using a log-normal distribution, based on AIC and residual plots *(77)*. We included log(age at sexual maturity) as a covariate for the effect of life-history speed on |S|. To test (H1) whether accounting for the simultaneous effect of biotic interactions decreased |S|, we incorporated as predictor variables: covariation with other drivers when λ was calculated under minimum/maximum values of a focal driver (accounted for or not), intraspecific density effects (incorporated or not in vital-rate models), and the interaction between the two. We focused on intraspecific density effects to analyze the role of biotic interactions in population dynamics because this was the most common type of biotic variables included in vital

rate models across species (see Table S6). We also controlled for a potential effect of model complexity on |S|, by including the log(number of vital rates) and log(mean parameters per vital rate) in each population model. To address potential phylogenetic differences or among species, taxonomic groups and species were integrated as nested random effects on the model intercept, respectively. To account for differences among taxonomic groups and species in how much driver covariation affects |S|, the same nested random effects were also applied on the slope of the covariation variable.

To test (H2) whether specific vital rates were driving |S|, we repeated the GLMMs using |S| calculated by perturbing climatic drivers in single vital rates. To facilitate comparisons among species, we grouped the vital rates of each species into three main types: survival of non-reproductive individuals (including juveniles), survival of reproductive individuals, and reproduction (including reproductive success and recruitment). We excluded trait change (including growth and maturation) as a vital rate, as it was only modeled in four species: *Marmota flaviventer*, *Rhabdomys pumilio*, *Suricata suricatta*, and *Protea repens*. The resulting GLMM had a similar structure as the one for the global |S|, with two differences. First, as we calculated vital-rate specific |S| without simplifying driver covariation in specific vital rates, covariation was not included in the model. Second, as we held variables constant in non-perturbed vital rates, we simplified the model structure further by excluding whether species included or excluded density feedbacks in vital-rate and population models. We included main vital-rate type as a covariate and tested whether the climatic effects of different vital rates on |S| differed among life histories, via the effects of log(age at maturity), and used an interaction term of vital rate and age at sexual maturity.

We calculated marginal and conditional R^2 for all GLMMs to quantify the variance in the data explained by the fixed effects and random and fixed effects, respectively *(78)*. We made all the data and code available online, along with the templates, ensuring that future analyses follow the same structure (https://github.com/EsinIckin/Comparative-demography-project).

References

1. J. Zscheischler, S. Westra, B. J. J. M. van den Hurk, S. I. Seneviratne, P. J. Ward, A. Pitman, A. AghaKouchak, D. N. Bresch, M. Leonard, T. Wahl, X. Zhang, Future climate risk from compound events. *Nature Clim Change* **8**, 469–477 (2018).

2. D. Leclère, M. Obersteiner, M. Barrett, S. H. Butchart, A. Chaudhary, A. De Palma, F. A. DeClerck, M. Di Marco, J. C. Doelman, M. Dürauer, Bending the curve of terrestrial biodiversity needs an integrated strategy. *Nature* **585**, 551–556 (2020).

3. B. Ebenman, L. Persson, *Size-structured populations: Ecology and evolution* (Springer Science & Business Media, 2012).

4. T. Coulson, E. A. Catchpole, S. D. Albon, B. J. T. Morgan, J. M. Pemberton, T. H. Clutton-Brock, M. J. Crawley, B. T. Grenfell, Age, Sex, Density, Winter Weather, and Population Crashes in Soay Sheep. *Science* **292**, 1528–1531 (2001).

5. M. Paniw, N. Maag, G. Cozzi, T. Clutton-Brock, A. Ozgul, Life history responses of meerkats to seasonal changes in extreme environments. *Science* **363**, 631–635 (2019).

6. T. E. Reed, V. Grøtan, S. Jenouvrier, B.-E. Sæther, M. E. Visser, Population growth in a wild bird is buffered against phenological mismatch. *Science* **340**, 488–491 (2013).

7. B. B. Hansen, M. Gamelon, S. D. Albon, A. M. Lee, A. Stien, R. J. Irvine, B.-E. Sæther, L. E. Loe, E. Ropstad, V. Veiberg, More frequent extreme climate events stabilize reindeer population dynamics. *Nature Communications* **10**, 1616 (2019).

8. M. Lima, N. C. Stenseth, F. M. Jaksic, Population dynamics of a South American rodent: seasonal structure interacting with climate, density dependence and predator effects. *Proc Biol Sci* **269**, 2579–2586 (2002).

9. C. Barbraud, H. Weimerskirch, Climate and density shape population dynamics of a marine top predator. *Proc. R. Soc. Lond. B* **270**, 2111–2116 (2003).

10. P. Sanczuk, K. De Pauw, E. De Lombaerde, M. Luoto, C. Meeussen, S. Govaert, T. Vanneste, L. Depauw, J. Brunet, S. A. Cousins, Microclimate and forest density drive plant population dynamics under climate change. *Nature Climate Change* **13**, 840–847 (2023).

11. N. Chr. Stenseth, H. Viljugrein, T. Saitoh, T. F. Hansen, M. O. Kittilsen, E. Bølviken, F. Glöckner, Seasonality, density dependence, and population cycles in Hokkaido voles. *Proc. Natl. Acad. Sci. U.S.A.* **100**, 11478–11483 (2003).

12. C. R. Nater, K. J. Van Benthem, C. I. Canale, C. Schradin, A. Ozgul, Density feedbacks mediate effects of environmental change on population dynamics of a semidesert rodent. *Journal of Animal Ecology* **87**, 1534–1546 (2018).

13. S. Jenouvrier, Impacts of climate change on avian populations. *Glob Change Biol* **19**, 2036–2057 (2013).

14. A. R. Bourne, S. J. Cunningham, C. N. Spottiswoode, A. R. Ridley, Hot droughts compromise interannual survival across all group sizes in a cooperatively breeding bird. *Ecology Letters* **23**, 1776–1788 (2020).

15. T. H. Larsen, Upslope Range Shifts of Andean Dung Beetles in Response to Deforestation: Compounding and Confounding Effects of Microclimatic Change. *Biotropica* **44**, 82–89 (2012).

16. M. L. Forister, A. C. McCall, N. J. Sanders, J. A. Fordyce, J. H. Thorne, J. O'Brien, D. P. Waetjen, A. M. Shapiro, Compounded effects of climate change and habitat alteration shift patterns of butterfly diversity. *Proc. Natl. Acad. Sci. U.S.A.* **107**, 2088–2092 (2010).

17. S. C. Stearns, *The evolution of life histories* (Oxford University Press, 1992).

18. C. H. Hilde, M. Gamelon, B.-E. Sæther, J.-M. Gaillard, N. G. Yoccoz, C. Pélabon, The demographic buffering hypothesis: evidence and challenges. *Trends in Ecology & Evolution* **35**, 523–538 (2020).

19. W. F. Morris, C. A. Pfister, S. Tuljapurkar, C. V. Haridas, C. L. Boggs, M. S. Boyce, E. M. Bruna, D. R. Church, T. Coulson, D. F. Doak, S. Forsyth, J.-M. Gaillard, C. C. Horvitz, S. Kalisz, B. E. Kendall, T. M. Knight, C. T. Lee, E. S. Menges, Longevity can buffer plant and animal populations against changing climatic variability. *Ecology* **89**, 19–25 (2008).

20. J. L. McDonald, M. Franco, S. Townley, T. H. Ezard, K. Jelbert, D. J. Hodgson, Divergent demographic strategies of plants in variable environments. *Nature ecology & evolution* **1**, 0029 (2017).

21. A. Compagnoni, S. Levin, D. Z. Childs, S. Harpole, M. Paniw, G. Römer, J. H. Burns, J. Che-Castaldo, N. Rüger, G. Kunstler, Herbaceous perennial plants with short generation time have stronger responses to climate anomalies than those with longer generation time. *Nature Communications* **12**, 1824 (2021).

22. B.-E. Sæther, Ø. Bakke, Avian life history variation and contribution of demographic traits to the population growth rate. *Ecology* **81**, 642–653 (2000).

23. J.-M. Gaillard, N. G. Yoccoz, Temporal variation in survival of mammals: a case of environmental canalization? *Ecology* **84**, 3294–3306 (2003).

24. C. Le Coeur, N. G. Yoccoz, R. Salguero-Gómez, Y. Vindenes, Life history adaptations to fluctuating environments: combined effects of demographic buffering and lability. *Ecology Letters* **25**, 2107–2119 (2022).

25. W. F. Morris, D. F. Doak, Buffering of life histories against environmental stochasticity: accounting for a spurious correlation between the variabilities of vital rates and their contributions to fitness. *The American Naturalist* **163**, 579–590 (2004).

26. B. Peeters, V. Grøtan, M. Gamelon, V. Veiberg, A. M. Lee, J. M. Fryxell, S. D. Albon, B. Sæther, S. Engen, L. E. Loe, B. B. Hansen, Harvesting can stabilise population fluctuations and buffer the impacts of extreme climatic events. *Ecology Letters* **25**, 863–875 (2022).

27. E. Conquet *et al.*, https://doi.org/10.32942/X24G93 (2024).

28. M. C. Urban, G. Bocedi, A. P. Hendry, J.-B. Mihoub, G. Pe'er, A. Singer, J. R. Bridle, L. G. Crozier, L. De Meester, W. Godsoe, A. Gonzalez, J. J. Hellmann, R. D. Holt, A. Huth, K. Johst, C. B. Krug, P. W. Leadley, S. C. F. Palmer, J. H. Pantel, A. Schmitz, P. A. Zollner, J. M. J. Travis, Improving the forecast for biodiversity under climate change. *Science* **353**, aad8466 (2016).

29. A. M. de Roos, Dynamic population stage structure due to juvenile–adult asymmetry stabilizes complex ecological communities. *Proceedings of the National Academy of Sciences* **118**, e2023709118 (2021).

30. J. Jackson, C. Le Coeur, O. Jones, Life history predicts global population responses to the weather in terrestrial mammals. *eLife* **11**, e74161 (2022).

31. W. F. Morris, J. Ehrlén, J. P. Dahlgren, A. K. Loomis, A. M. Louthan, Biotic and anthropogenic forces rival climatic/abiotic factors in determining global plant population growth and fitness. *Proc. Natl. Acad. Sci. U.S.A.* **117**, 1107–1112 (2020).

32. T. J. Clark-Wolf, P. Dee Boersma, G. A. Rebstock, B. Abrahms, Climate presses and pulses mediate the decline of a migratory predator. *Proc. Natl. Acad. Sci. U.S.A.* **120**, e2209821120 (2023).

33. M. Paniw, T. D. James, C. Ruth Archer, G. Römer, S. Levin, A. Compagnoni, J. Che-Castaldo, J. M. Bennett, A. Mooney, D. Z. Childs, A. Ozgul, O. R. Jones, J. H. Burns, A. P. Beckerman, A. Patwary, N. Sanchez-Gassen, T. M. Knight, R. Salguero-Gómez, The myriad of complex demographic responses of terrestrial mammals to climate change and gaps of knowledge: A global analysis. *Journal of Animal Ecology* **90**, 1398–1407 (2021).

34. T. G. Benton, S. J. Plaistow, T. N. Coulson, Complex population dynamics and complex causation: devils, details and demography. *Proc. R. Soc. B.* **273**, 1173–1181 (2006).

35. V. Radchuk, C. Turlure, N. Schtickzelle, Each life stage matters: the importance of assessing the response to climate change over the complete life cycle in butterflies. *Journal of Animal Ecology* **82**, 275–285 (2013).

36. M. Gamelon, V. Grøtan, A. L. K. Nilsson, S. Engen, J. W. Hurrell, K. Jerstad, A. S. Phillips, O. W. Røstad, T. Slagsvold, B. Walseng, N. C. Stenseth, B.-E. Sæther, Interactions between demography and environmental effects are important determinants of population dynamics. *Sci. Adv.* **3**, e1602298 (2017).

37. M. Quéroué, C. Barbraud, F. Barraquand, D. Turek, K. Delord, N. Pacoureau, O. Gimenez, Multispecies integrated population model reveals bottom-up dynamics in a seabird predator–prey system. *Ecological Monographs* **91**, e01459 (2021).

38. H. Caswell, *Matrix population models: Construction, analysis, and interpretation*, 2nd ed (Sinauer Associates, 2001).

39. A.-K. Malchow, F. Hartig, J. Reeg, M. Kéry, D. Zurell, Demography–environment relationships improve mechanistic understanding of range dynamics under climate change. *Phil. Trans. R. Soc. B* **378**, 20220194 (2023).

40. D. García-Callejas, R. Molowny-Horas, J. Retana, Projecting the distribution and abundance of Mediterranean tree species under climate change: a demographic approach. *Journal of Plant Ecology* **10**, 731–743 (2017).

41. J. Koricheva, J. Gurevitch, K. Mengersen, Eds., *Handbook of meta-analysis in ecology and evolution* (Princeton University Press, 2013).

42. K. Healy, T. H. G. Ezard, O. R. Jones, R. Salguero-Gómez, Y. M. Buckley, Animal life history is shaped by the pace of life and the distribution of age-specific mortality and reproduction. *Nat Ecol Evol* **3**, 1217–1224 (2019).

43. J. Forcada, P. N. Trathan, E. J. Murphy, Life history buffering in Antarctic mammals and birds against changing patterns of climate and environmental variation. *Global Change Biology* **14**, 2473–2488 (2008).

44. P. Turchin, "Population regulation: Old arguments and a new synthesis" in *Population Dynamics*, (Elsevier, 1995), pp. 19–40.

45. N. J. C. Tyler, M. C. Forchhammer, N. A. Øritsland, Nonlinear effects of climate and density in the dynamics of a fluctuating population of reindeer. *Ecology* **89**, 1675–1686 (2008).

46. F. A. Campos, W. F. Morris, S. C. Alberts, J. Altmann, D. K. Brockman, M. Cords, A. Pusey, T. S. Stoinski, K. B. Strier, L. M. Fedigan, Does climate variability influence the demography of wild primates? Evidence from long-term life-history data in seven species. *Global Change Biology* **23**, 4907–4921 (2017).

47. J. Van De Walle, R. Fay, J.-M. Gaillard, F. Pelletier, S. Hamel, M. Gamelon, C. Barbraud, F. G. Blanchet, D. T. Blumstein, A. Charmantier, K. Delord, B. Larue, J. Martin, J. A. Mills, E. Milot, F. M. Mayer, J. Rotella, B.-E. Saether, C. Teplitsky, M. Van De Pol, D. H. Van Vuren, M. E. Visser, C. P. Wells, J. Yarrall, S. Jenouvrier, Individual life histories: Neither slow nor fast, just diverse. *Proc. R. Soc. B.* **290**, 20230511 (2023).

48. F. E. Buderman, J. H. Devries, D. N. Koons, A life-history spectrum of population responses to simultaneous change in climate and land use. *Journal of Animal Ecology* **92**, 1267–1284 (2023).

49. K. Calvin, *et al.*, "IPCC, 2023: Climate Change 2023: Synthesis Report. Contribution of working groups I, II and III to the sixth assessment report of the intergovernmental panel on climate change [Core Writing Team, H. Lee and J. Romero (eds.)]. IPCC, Geneva, Switzerland," First (Intergovernmental Panel on Climate Change (IPCC), 2023).

50. C. D. Thomas, J. K. Hill, B. J. Anderson, S. Bailey, C. M. Beale, R. B. Bradbury, C. R. Bulman, H. Q. P. Crick, F. Eigenbrod, H. M. Griffiths, W. E. Kunin, T. H. Oliver, C. A. Walmsley, K. Watts, N. T. Worsfold, T. Yardley, A framework for assessing threats and benefits to species responding to climate change. *Methods Ecol Evol* **2**, 125–142 (2011).

51. K. E. King, E. R. Cook, K. J. Anchukaitis, B. I. Cook, J. E. Smerdon, R. Seager, G. L. Harley, B. Spei, Increasing prevalence of hot drought across western North America since the 16th century. *Sci. Adv.* **10**, eadj4289 (2024).

52. M. González-Suárez, E. Revilla, Variability in life-history and ecological traits is a buffer against extinction in mammals. *Ecology Letters* **16**, 242–251 (2013).

53. U. Feller, I. I. Vaseva, Extreme climatic events: impacts of drought and high temperature on physiological processes in agronomically important plants. *Front. Environ. Sci.* **2** (2014).

54. A. R. Bourne, S. J. Cunningham, C. N. Spottiswoode, A. R. Ridley, Hot droughts compromise interannual survival across all group sizes in a cooperatively breeding bird. *Ecology Letters* **23**, 1776–1788 (2020).

55. R. M. Harris, L. J. Beaumont, T. R. Vance, C. R. Tozer, T. A. Remenyi, S. E. Perkins-Kirkpatrick, P. J. Mitchell, A. B. Nicotra, S. McGregor, N. R. Andrew, Biological responses to the press and pulse of climate trends and extreme events. *Nature climate change* **8**, 579–587 (2018).

56. M. Paniw, C. Duncan, F. Groenewoud, J. A. Drewe, M. Manser, A. Ozgul, T. Clutton-Brock, Higher temperature extremes exacerbate negative disease effects in a social mammal. *Nature Climate Change* **12**, 284–290 (2022).

57. M. Schmid, M. Paniw, M. Postuma, A. Ozgul, F. Guillaume, A trade-off between robustness to environmental fluctuations and speed of evolution. *The American Naturalist* **200**, E16–E35 (2022).

58. P. L. Zarnetske, D. K. Skelly, M. C. Urban, Biotic multipliers of climate change. *Science* **336**, 1516–1518 (2012).

59. A. E. Stears, B. Heidel, M. Paniw, R. Salguero-Gómez, D. C. Laughlin, Negative density dependence promotes persistence of a globally rare yet locally abundant plant species *Oenothera coloradensis*. *Oikos*, e10673 (2024).

60. R. Woodroffe, C. A. Donnelly, G. Wei, D. R. Cox, F. J. Bourne, T. Burke, R. K. Butlin, C. L. Cheeseman, G. Gettinby, P. Gilks, S. Hedges, H. E. Jenkins, W. T. Johnston, J. P. McInerney, W. I. Morrison, L. C. Pope, Social group size affects *Mycobacterium bovis* infection in European badgers (*Meles meles*). *Journal of Animal Ecology* **78**, 818–827 (2009).

61. E. E. Brandell, A. P. Dobson, P. J. Hudson, P. C. Cross, D. W. Smith, A metapopulation model of social group dynamics and disease applied to Yellowstone wolves. *Proc. Natl. Acad. Sci. U.S.A.* **118**, e2020023118 (2021).

62. M. Paniw, *et al.*, Pathways to global-change effects on biodiversity: New opportunities for dynamically forecasting demography and species interactions. *Proc. R. Soc. B.* **290**, 20221494 (2023).

63. K. Layton-Matthews, B. B. Hansen, V. Grøtan, E. Fuglei, M. J. J. E. Loonen, Contrasting consequences of climate change for migratory geese: Predation, density dependence and carryover effects offset benefits of high-arctic warming. *Global Change Biology* **26**, 642–657 (2020).

64. S. Herrando-Pérez, S. Delean, B. W. Brook, C. J. A. Bradshaw, Strength of density feedback in census data increases from slow to fast life histories. *Ecology and Evolution* **2**, 1922–1934 (2012).

65. M. C. Urban, J. M. Travis, D. Zurell, P. L. Thompson, N. W. Synes, A. Scarpa, P. R. Peres-Neto, A.-K. Malchow, P. M. James, D. Gravel, Coding for life: designing a platform for projecting and protecting global biodiversity. *BioScience* **72**, 91–104 (2022).

66. J. M. J. Travis, M. Delgado, G. Bocedi, M. Baguette, K. Bartoń, D. Bonte, I. Boulangeat, J. A. Hodgson, A. Kubisch, V. Penteriani, M. Saastamoinen, V. M. Stevens, J. M. Bullock, Dispersal and species' responses to climate change. *Oikos* **122**, 1532–1540 (2013).

67. A. K. Snover, N. J. Mantua, J. S. Littell, M. A. Alexander, M. M. Mcclure, J. Nye, Choosing and Using Climate-Change Scenarios for Ecological-Impact Assessments and Conservation Decisions. *Conservation Biology* **27**, 1147–1157 (2013).

68. J. P. van der Sluijs, Insect decline, an emerging global environmental risk. *Current Opinion in Environmental Sustainability* **46**, 39–42 (2020).

69. D. L. Wagner, E. M. Grames, M. L. Forister, M. R. Berenbaum, D. Stopak, Insect decline in the Anthropocene: death by a thousand cuts. *Proceedings of the National Academy of Sciences* **118**, e2023989118 (2021).

70. C. L. Boggs, The fingerprints of global climate change on insect populations. *Current Opinion in Insect Science* **17**, 69–73 (2016).

71. L. J. Martin, B. Blossey, E. Ellis, Mapping where ecologists work: Biases in the global distribution of terrestrial ecological observations. *Frontiers in Ecology and the Environment* **10**, 195–201 (2012).

72. K. Konno, M. Akasaka, C. Koshida, N. Katayama, N. Osada, R. Spake, T. Amano, Ignoring non-English-language studies may bias ecological meta-analyses. *Ecology and Evolution* **10**, 6373–6384 (2020).

73. S. M. Powers, S. E. Hampton, Open science, reproducibility, and transparency in ecology. *Ecol Appl* **29** (2019).

74. S. C. Levin, S. Evers, T. Potter, M. P. Guerrero, D. Z. Childs, A. Compagnoni, T. M. Knight, R. Salguero-Gómez, Rpadrino: An R package to access and use PADRINO , an open access database of Integral Projection Models. *Methods Ecol Evol* **13**, 1923–1929 (2022).

75. J. Ehrlén, W. F. Morris, T. von Euler, J. P. Dahlgren, Advancing environmentally explicit structured population models of plants. *Journal of Ecology* **104**, 292–305 (2016).

76. C. Stubben, B. Milligan, Estimating and analyzing demographic models using the popbio package in R. *Journal of Statistical Software* **22**, 1–23 (2007).

77. F. Hartig, DHARMa: Residual Diagnostics for Hierarchical (Multi-Level / Mixed) Regression Models, (2016); https://doi.org/10.32614/CRAN.package.DHARMa.

78. S. Nakagawa, H. Schielzeth, A general and simple method for obtaining R^2 from generalized linear mixed-effects models. *Methods Ecol Evol* **4**, 133–142 (2013).

SI References

79. C. R. Nater, K. J. Van Benthem, C. I. Canale, C. Schradin, A. Ozgul, Density feedbacks mediate effects of environmental change on population dynamics of a semidesert rodent. *Journal of Animal Ecology* **87**, 1534–1546 (2018).

80. A. Ozgul, C. Fichtel, M. Paniw, P. M. Kappeler, Destabilizing effect of climate change on the persistence of a short-lived primate. *Proc. Natl. Acad. Sci. U.S.A.* **120**, e2214244120 (2023).

81. W. F. Morris, J. Ehrlén, J. P. Dahlgren, A. K. Loomis, A. M. Louthan, Biotic and anthropogenic forces rival climatic/abiotic factors in determining global plant population growth and fitness. *Proc. Natl. Acad. Sci. U.S.A.* **117**, 1107–1112 (2020).

82. M. Quéroué, C. Barbraud, F. Barraquand, D. Turek, K. Delord, N. Pacoureau, O. Gimenez, Multispecies integrated population model reveals bottom-up dynamics in a seabird predator–prey system. *Ecological Monographs* **91**, e01459 (2021).

83. M. Gamelon, V. Grøtan, A. L. K. Nilsson, S. Engen, J. W. Hurrell, K. Jerstad, A. S. Phillips, O. W. Røstad, T. Slagsvold, B. Walseng, N. C. Stenseth, B.-E. Sæther, Interactions between demography and environmental effects are important determinants of population dynamics. *Sci. Adv.* **3**, e1602298 (2017).

84. D. García-Callejas, R. Molowny-Horas, J. Retana, Projecting the distribution and abundance of Mediterranean tree species under climate change: A demographic approach. *JPECOL* rtw081 (2016). https://doi.org/10.1093/jpe/rtw081.

85. M. L. Bond, D. E. Lee, M. Paniw, Extinction risks and mitigation for a megaherbivore, the giraffe, in a human-influenced landscape under climate change. *Global Change Biology* **29**, 6693–6712 (2023).

86. R. Salguero-Gómez, O. R. Jones, C. R. Archer, C. Bein, H. De Buhr, C. Farack, F. Gottschalk, A. Hartmann, A. Henning, G. Hoppe, G. Römer, T. Ruoff, V. Sommer, J. Wille, J. Voigt, S. Zeh, D. Vieregg, Y. M. Buckley, J. Che-Castaldo, D. Hodgson, A. Scheuerlein, H. Caswell, J. W. Vaupel, COMADRE : a global data base of animal demography. *Journal of Animal Ecology* **85**, 371–384 (2016).

87. R. Salguero-Gómez, O. R. Jones, C. R. Archer, Y. M. Buckley, J. Che-Castaldo, H. Caswell, D. Hodgson, A. Scheuerlein, D. A. Conde, E. Brinks, H. De Buhr, C. Farack, F. Gottschalk, A. Hartmann, A. Henning, G. Hoppe, G. Römer, J. Runge, T. Ruoff, J. Wille, S. Zeh, R. Davison, D. Vieregg, A. Baudisch, R. Altwegg, F. Colchero, M. Dong, H. De Kroon, J. Lebreton, C. J. E. Metcalf, M. M. Neel, I. M. Parker, T. Takada, T. Valverde, L. A. Vélez-Espino, G. M. Wardle, M. Franco, J. W. Vaupel, The COMPADRE P lant M atrix D atabase: an open online repository for plant demography. *Journal of Ecology* **103**, 202–218 (2015).

88. S. C. Levin, S. Evers, T. Potter, M. P. Guerrero, D. Z. Childs, A. Compagnoni, T. M. Knight, R. Salguero-Gómez, Rpadrino: An R package to access and use PADRINO , an open access database of Integral Projection Models. *Methods Ecol Evol* **13**, 1923–1929 (2022).

89. J. Ehrlén, W. F. Morris, T. von Euler, J. P. Dahlgren, Advancing environmentally explicit structured population models of plants. *Journal of Ecology* **104**, 292–305 (2016).

90. M. Paniw, T. D. James, C. Ruth Archer, G. Römer, S. Levin, A. Compagnoni, J. Che-Castaldo, J. M. Bennett, A. Mooney, D. Z. Childs, A. Ozgul, O. R. Jones, J. H. Burns, A. P. Beckerman, A. Patwary, N. Sanchez-Gassen, T. M. Knight, R. Salguero-Gómez, The myriad

of complex demographic responses of terrestrial mammals to climate change and gaps of knowledge: A global analysis. *Journal of Animal Ecology* **90**, 1398–1407 (2021).

91. C. Stubben, B. Milligan, Estimating and analyzing demographic models using the popbio package in R. *Journal of Statistical Software* **22**, 1–23 (2007).

92. H. Caswell, Matrix population models: Construction, analysis, and interpretation, 2nd ed (Sinauer Associates, 2001).

93. A.-K. Malchow, F. Hartig, J. Reeg, M. Kéry, D. Zurell, Demography–environment relationships improve mechanistic understanding of range dynamics under climate change. *Phil. Trans. R. Soc. B* **378**, 20220194 (2023).

94. E. Conquet *et al.*, https://doi.org/10.32942/X24G93 (2024).

95. A. Ozgul, C. Fichtel, M. Paniw, P. M. Kappeler, Destabilizing effect of climate change on the persistence of a short-lived primate. *Proc. Natl. Acad. Sci. U.S.A.* **120**, e2214244120 (2023).

96. S. Nakagawa, E. S. A. Santos, Methodological issues and advances in biological meta-analysis. *Evol Ecol* **26**, 1253–1274 (2012).

97. M. J. Lajeunesse, Bias and correction for the log response ratio in ecological meta-analysis. *Ecology* **96**, 2056–2063 (2015).

98. J. D. Wilson, The breeding biology and population history of the dipper *Cinclus cinclus* on a Scottish river system. *Bird Study* **43**, 108–118 (1996).

99. N. P. Myhrvold, E. Baldridge, B. Chan, D. Sivam, D. L. Freeman, S. K. M. Ernest, An amniote life-history database to perform comparative analyses with birds, mammals, and reptiles: Ecological Archives E096-269. *Ecology* **96**, 3109–3109 (2015).

100. T. J. Clark-Wolf, P. Dee Boersma, G. A. Rebstock, B. Abrahms, Climate presses and pulses mediate the decline of a migratory predator. *Proc. Natl. Acad. Sci. U.S.A.* **120**, e2209821120 (2023).

101. S. Jenouvrier, M. Desprez, R. Fay, C. Barbraud, H. Weimerskirch, K. Delord, H. Caswell, Climate change and functional traits affect population dynamics of a long-lived seabird. *Journal of Animal Ecology* **87**, 906–920 (2018).

102. H. Weimerskirch, J. Clobert, P. Jouventin, Survival in five southern albatrosses and its relationship with their life history. *The Journal of Animal Ecology* 1043–1055 (1987).

103. M. Desprez, S. Jenouvrier, C. Barbraud, K. Delord, H. Weimerskirch, Linking oceanographic conditions, migratory schedules and foraging behaviour during the non-breeding season to reproductive performance in a long-lived seabird. *Functional Ecology* **32**, 2040–2053 (2018).

104. K. Layton-Matthews, B. B. Hansen, V. Grøtan, E. Fuglei, M. J. J. E. Loonen, Contrasting consequences of climate change for migratory geese: Predation, density dependence and

carryover effects offset benefits of high-arctic warming. *Global Change Biology* **26**, 642–657 (2020).

105. J. M. Black, M. Owen, Reproductive Performance and Assortative Pairing in Relation to Age in Barnacle Geese. *Journal of Animal Ecology* **64**, 234–244 (1995).

106. K. Layton-Matthews, A. Ozgul, M. Griesser, The interacting effects of forestry and climate change on the demography of a group-living bird population. *Oecologia* **186**, 907–918 (2018).

107. S. Jenouvrier, M. Holland, J. Stroeve, C. Barbraud, H. Weimerskirch, M. Serreze, H. Caswell, Effects of climate change on an emperor penguin population: analysis of coupled demographic and climate models. *Global Change Biology* **18**, 2756–2770 (2012).

108. S. Jenouvrier, H. Caswell, C. Barbraud, H. Weimerskirch, Mating Behavior, Population Growth, and the Operational Sex Ratio: A Periodic Two-Sex Model Approach. *The American Naturalist* **175**, 739–752 (2010).

109. D. E. Lee, M. L. Bond, "Giraffe metapopulation demography" in *Tarangire: Human-Wildlife Coexistence in a Fragmented Ecosystem*, Ecological Studies., C. Kiffner, M. L. Bond, D. E. Lee, Eds. (Springer International Publishing, 2022), pp. 189–207.

110. D. E. Lee, G. G. Lohay, D. R. Cavener, M. L. Bond, Using spot pattern recognition to examine population biology, evolutionary ecology, sociality, and movements of giraffes: A 70-year retrospective. *Mamm Biol* **102**, 1055–1071 (2022).

111. M. L. Bond, A. Ozgul, Derek. E. Lee, Effect of local climate anomalies on giraffe survival. *Biodivers Conserv* **32**, 3179–3197 (2023).

112. M. Paniw, D. Z. Childs, K. B. Armitage, D. T. Blumstein, J. G. A. Martin, M. K. Oli, A. Ozgul, Assessing seasonal demographic covariation to understand environmental-change impacts on a hibernating mammal. *Ecology Letters* **23**, 588–597 (2020).

113. P. M. Kappeler, F. P. Cuozzo, C. Fichtel, J. U. Ganzhorn, S. Gursky-Doyen, M. T. Irwin, S. Ichino, R. Lawler, K. A.-I. Nekaris, J.-B. Ramanamanjato, Long-term field studies of lemurs, lorises, and tarsiers. *Journal of Mammalogy* **98**, 661–669 (2017).

114. M. Eberle, P. M. Kappeler, Sex in the dark: Determinants and consequences of mixed male mating tactics in Microcebus murinus, a small solitary nocturnal primate. *Behavioral Ecology and Sociobiology* **57**, 77–90 (2004).

115. S. Schliehe-Diecks, M. Eberle, P. M. Kappeler, Walk the line—dispersal movements of gray mouse lemurs (Microcebus murinus). *Behav Ecol Sociobiol* **66**, 1175–1185 (2012).

116. B. B. Hansen, M. Gamelon, S. D. Albon, A. M. Lee, A. Stien, R. J. Irvine, B.-E. Sæther, L. E. Loe, E. Ropstad, V. Veiberg, More frequent extreme climate events stabilize reindeer population dynamics. *Nature Communications* **10**, 1616 (2019).

117. C. Schradin, A. K. Lindholm, J. Johannesen, I. Schoepf, C. Yuen, B. König, N. Pillay, Social flexibility and social evolution in mammals: a case study of the African striped mouse (*Rhabdomys pumilio*). *Molecular Ecology* **21**, 541–553 (2012).

118. M. Paniw, N. Maag, G. Cozzi, T. Clutton-Brock, A. Ozgul, Life history responses of meerkats to seasonal changes in extreme environments. *Science* **363**, 631–635 (2019).

119. C. R. Nater, N. E. Eide, Å. Ø. Pedersen, N. G. Yoccoz, E. Fuglei, Contributions from terrestrial and marine resources stabilize predator populations in a rapidly changing climate. *Ecosphere* **12**, e03546 (2021).

120. Z. Tablado, E. Revilla, Contrasting Effects of Climate Change on Rabbit Populations through Reproduction. *PLoS ONE* **7**, e48988 (2012).

121. M. Paniw, D. García-Callejas, F. Lloret, R. D. Bassar, J. Travis, O. Godoy, Pathways to global-change effects on biodiversity: new opportunities for dynamically forecasting demography and species interactions. *Proc. R. Soc. B.* **290**, 20221494 (2023).

122. T. Dostálek, Z. Münzbergová, Comparative population biology of critically endangered dracocephalum austriacum (lamiaceae) in two distant regions. *Folia Geobot* **48**, 75–93 (2013).

123. M. Paniw, P. F. Quintana-Ascencio, F. Ojeda, R. Salguero-Gómez, Interacting livestock and fire may both threaten and increase viability of a fire-adapted Mediterranean carnivorous plant. *Journal of Applied Ecology* **54**, 1884–1894 (2017).

124. 46. T. E. X. Miller, S. M. Louda, K. A. Rose, J. O. Eckberg, Impacts of insect herbivory on cactus population dynamics: Experimental demography across an environmental gradient. *Ecological Monographs* **79**, 155–172 (2009).

125. J. R. Ohm, T. E. X. Miller, Balancing anti-herbivore benefits and anti-pollinator costs of defensive mutualists. *Ecology* **95**, 2924–2935 (2014).

126. S. M. Evers, T. M. Knight, D. W. Inouye, T. E. X. Miller, R. Salguero-Gómez, A. M. Iler, A. Compagnoni, Lagged and dormant season climate better predict plant vital rates than climate during the growing season. *Global Change Biology* **27**, 1927–1941 (2021).

127. A. Compagnoni, A. J. Bibian, B. M. Ochocki, H. S. Rogers, E. L. Schultz, M. E. Sneck, B. D. Elderd, A. M. Iler, D. W. Inouye, H. Jacquemyn, T. E. X. Miller, The effect of demographic correlations on the stochastic population dynamics of perennial plants. *Ecological Monographs* **86**, 480–494 (2016).

128. C. Merow, A. M. Latimer, A. M. Wilson, S. M. McMahon, A. G. Rebelo, J. A. Silander, On using integral projection models to generate demographically driven predictions of species' distributions: development and validation using sparse data. *Ecography* **37**, 1167–1183 (2014).

129. D. Le Maitre, "Life history and reproductive ecology of selected proteaceae in the mountain Fynbos Vegetation of the South-Western Cape," University of Cape Town. (1999).

130. M. Plummer, JAGS: A program for analysis of Bayesian graphical models using Gibbs sampling in *Proceedings of the 3rd International Workshop on Distributed Statistical Computing*, (Vienna, Austria, 2003), pp. 1–10.

131. A.-K. Malchow, F. Hartig, J. Reeg, M. Kéry, D. Zurell, Demography–environment relationships improve mechanistic understanding of range dynamics under climate change. *Phil. Trans. R. Soc. B* **378**, 20220194 (2023).

132. IUCN, Certhia familiaris: BirdLife International: The IUCN Red List of Threatened Species 2017: e.T22735060A111155023. https://doi.org/10.2305/IUCN.UK.2017-1.RLTS.T22735060A111155023.en. Deposited 1 October 2016.

133. IUCN, Linaria cannabina: BirdLife International: The IUCN Red List of Threatened Species 2018: e.T22720441A132139778. https://doi.org/10.2305/IUCN.UK.2018-2.RLTS.T22720441A132139778.en. Deposited 9 August 2018.

134. IUCN, Lophophanes cristatus: BirdLife International: The IUCN Red List of Threatened Species 2016: e.T22711810A87427182. https://doi.org/10.2305/IUCN.UK.2016-3.RLTS.T22711810A87427182.en. Deposited 1 October 2016.

135. IUCN, Prunella collaris: BirdLife International: The IUCN Red List of Threatened Species 2016: e.T22718617A88039291. https://doi.org/10.2305/IUCN.UK.2016-3.RLTS.T22718617A88039291.en. Deposited 1 October 2016.

136. IUCN, Prunella modularis: BirdLife International: The IUCN Red List of Threatened Species 2018: e.T22718651A132118966. https://doi.org/10.2305/IUCN.UK.2018-2.RLTS.T22718651A132118966.en. Deposited 9 August 2018.

137. IUCN, Pyrrhula pyrrhula: BirdLife International: The IUCN Red List of Threatened Species 2018: e.T22720671A132141969. https://doi.org/10.2305/IUCN.UK.2018-2.RLTS.T22720671A132141969.en. Deposited 9 August 2018.

138. IUCN, Sitta europaea: BirdLife International: The IUCN Red List of Threatened Species 2018: e.T103879804A132199203. https://doi.org/10.2305/IUCN.UK.2018-2.RLTS.T103879804A132199203.en. Deposited 9 August 2018.

139. IUCN, Turdus torquatus: BirdLife International: The IUCN Red List of Threatened Species 2019: e.T22708768A155629409. https://doi.org/10.2305/IUCN.UK.2018-2.RLTS.T22708768A155629409.en. Deposited 9 August 2018.

140. M. Gamelon, V. Grøtan, A. L. K. Nilsson, S. Engen, J. W. Hurrell, K. Jerstad, A. S. Phillips, O. W. Røstad, T. Slagsvold, B. Walseng, N. C. Stenseth, B.-E. Sæther, Interactions between demography and environmental effects are important determinants of population dynamics. *Sci. Adv.* **3**, e1602298 (2017).

141. IUCN, Cinclus cinclus: BirdLife International: The IUCN Red List of Threatened Species 2018: e.T22708156A131946814. https://doi.org/10.2305/IUCN.UK.2018-2.RLTS.T22708156A131946814.en. Deposited 9 August 2018.

142. N. P. Myhrvold, E. Baldridge, B. Chan, D. Sivam, D. L. Freeman, S. K. M. Ernest, An amniote life-history database to perform comparative analyses with birds, mammals, and reptiles: Ecological Archives E096-269. *Ecology* **96**, 3109–3109 (2015).

143. M. Quéroué, C. Barbraud, F. Barraquand, D. Turek, K. Delord, N. Pacoureau, O. Gimenez, Multispecies integrated population model reveals bottom-up dynamics in a seabird predator–prey system. *Ecological Monographs* **91**, e01459 (2021).

144. IUCN, Halobaena caerulea: BirdLife International: The IUCN Red List of Threatened Species 2020: e.T22698102A181599271. https://doi.org/10.2305/IUCN.UK.2020-3.RLTS.T22698102A181599271.en. Deposited 12 August 2020.

145. S. Jenouvrier, M. Desprez, R. Fay, C. Barbraud, H. Weimerskirch, K. Delord, H. Caswell, Climate change and functional traits affect population dynamics of a long-lived seabird. *Journal of Animal Ecology* **87**, 906–920 (2018).

146. IUCN, Thalassarche melanophris: BirdLife International: The IUCN Red List of Threatened Species 2018: e.T22698375A132643647. https://doi.org/10.2305/IUCN.UK.2018-2.RLTS.T22698375A132643647.en. Deposited 7 August 2018.

147. T. J. Clark-Wolf, P. Dee Boersma, G. A. Rebstock, B. Abrahms, Climate presses and pulses mediate the decline of a migratory predator. *Proc. Natl. Acad. Sci. U.S.A.* **120**, e2209821120 (2023).

148. IUCN, Spheniscus magellanicus: BirdLife International: The IUCN Red List of Threatened Species 2020: e.T22697822A157428850. https://doi.org/10.2305/IUCN.UK.2020-3.RLTS.T22697822A157428850.en. Deposited 20 August 2020

149. A. Ozgul, C. Fichtel, M. Paniw, P. M. Kappeler, Destabilizing effect of climate change on the persistence of a short-lived primate. *Proc. Natl. Acad. Sci. U.S.A.* **120**, e2214244120 (2023).

150. IUCN, Microcebus murinus: Reuter, K.E., Blanco, M., Ganzhorn, J. & Schwitzer, C.: The IUCN Red List of Threatened Species 2020: e.T163314248A182239898. https://doi.org/10.2305/IUCN.UK.2020-3.RLTS.T163314248A182239898.en. Deposited 5 April 2020.

151. IUCN, Rangifer tarandus: Gunn, A.: The IUCN Red List of Threatened Species 2016: e.T29742A22167140. https://doi.org/10.2305/IUCN.UK.2016-1.RLTS.T29742A22167140.en. Deposited 24 December 2015.

152. C. R. Nater, N. E. Eide, Å. Ø. Pedersen, N. G. Yoccoz, E. Fuglei, Contributions from terrestrial and marine resources stabilize predator populations in a rapidly changing climate. *Ecosphere* **12**, e03546 (2021).

153. IUCN, Vulpes lagopus: Angerbjörn, A. & Tannerfeldt, M.: The IUCN Red List of Threatened Species 2014: e.T899A57549321. https://doi.org/10.2305/IUCN.UK.2014-2.RLTS.T899A57549321.en. Deposited 20 June 2014.

154. C. R. Nater, K. J. Van Benthem, C. I. Canale, C. Schradin, A. Ozgul, Density feedbacks mediate effects of environmental change on population dynamics of a semidesert rodent. *Journal of Animal Ecology* **87**, 1534–1546 (2018).

155. IUCN, Rhabdomys pumilio: Du Toit, N., Pillay, N., Ganem, G. & Relton, C.: The IUCN Red List of Threatened Species 2019: e.T112168517A22402072. https://doi.org/10.2305/IUCN.UK.2019-1.RLTS.T112168517A22402072.en. Deposited 23 May 2016.

156. C. Schradin, A. K. Lindholm, J. Johannesen, I. Schoepf, C. Yuen, B. König, N. Pillay, Social flexibility and social evolution in mammals: a case study of the African striped mouse (*Rhabdomys pumilio*). *Molecular Ecology* **21**, 541–553 (2012).

157. M. Paniw, D. Z. Childs, K. B. Armitage, D. T. Blumstein, J. G. A. Martin, M. K. Oli, A. Ozgul, Assessing seasonal demographic covariation to understand environmental-change impacts on a hibernating mammal. *Ecology Letters* **23**, 588–597 (2020).

158. IUCN, Marmota flaviventris: Cassola, F.: The IUCN Red List of Threatened Species 2016: e.T42457A115189809. https://doi.org/10.2305/IUCN.UK.2016-3.RLTS.T42457A22257543.en. Deposited 8 August 2016.

159. M. Paniw, N. Maag, G. Cozzi, T. Clutton-Brock, A. Ozgul, Life history responses of meerkats to seasonal changes in extreme environments. *Science* **363**, 631–635 (2019).

160. IUCN, Suricata suricatta: Jordan, N.R. & Do Linh San, E.: The IUCN Red List of Threatened Species 2015: e.T41624A45209377. https://doi.org/10.2305/IUCN.UK.2015-4.RLTS.T41624A45209377.en. Deposited 28 February 2015.

161. M. L. Bond, D. E. Lee, M. Paniw, Extinction risks and mitigation for a megaherbivore, the giraffe, in a human-influenced landscape under climate change. *Global Change Biology* **29**, 6693–6712 (2023).

162. IUCN, Giraffa camelopardalis: Muller, Z., Bercovitch, F., Brand, R., Brown, D., Brown, M., Bolger, D., Carter, K., Deacon, F., Doherty, J.B., Fennessy, J., Fennessy, S., Hussein, A.A., Lee, D., Marais, A., Strauss, M., Tutchings, A. & Wube, T.: The IUCN Red List of Threatened Species 2018: e.T9194A136266699. https://doi.org/10.2305/IUCN.UK.2016-3.RLTS.T9194A136266699.en. Deposited 9 July 2016.

163. C. Merow, A. M. Latimer, A. M. Wilson, S. M. McMahon, A. G. Rebelo, J. A. Silander, On using integral projection models to generate demographically driven predictions of species' distributions: development and validation using sparse data. *Ecography* **37**, 1167–1183 (2014).

164. D. Le Maitre, "Life history and reproductive ecology of selected proteaceae in the mountain Fynbos Vegetation of the South-Western Cape," University of Cape Town. (1999).

165. IUCN, Protea repens: Rebelo, A.G., Mtshali, H. & von Staden, L.: The IUCN Red List of Threatened Species 2020: e.T113214987A185583475. https://doi.org/10.2305/IUCN.UK.2020-3.RLTS.T113214987A185583475.en. Deposited 12 June 2019.

166. D. García-Callejas, R. Molowny-Horas, J. Retana, Projecting the distribution and abundance of Mediterranean tree species under climate change: A demographic approach. *JPECOL* rtw081 (2016). https://doi.org/10.1093/jpe/rtw081.

167. J. R. Packham, P. A. Thomas, M. D. Atkinson, T. Degen, Biological flora of the British Isles: Fagus sylvatica. *Journal of Ecology* **100**, 1557–1608 (2012).

168. IUCN, Fagus sylvatica: Barstow, M. & Beech, E.: The IUCN Red List of Threatened Species 2018: e.T62004722A62004725. https://doi.org/10.2305/IUCN.UK.2018-1.RLTS.T62004722A62004725.en. Deposited 12 January 2017.

169. E. W. Jones, Biological flora of the British Isles. (1959).

170. IUCN, Quercus faginea: Jerome, D. & Vazquez, F.: The IUCN Red List of Threatened Species 2018: e.T78916251A78916554. https://doi.org/10.2305/IUCN.UK.2018-2.RLTS.T78916251A78916554.en. Deposited 1 November 2017.

171. IUCN, Quercus ilex: Rankou, H., M'SOU , S., Barstow, M., Harvey-Brown, Y. & Martin, G.: The IUCN Red List of Threatened Species 2017: e.T62537A3116134. https://doi.org/10.2305/IUCN.UK.2017-3.RLTS.T62537A3116134.en. Deposited 27 January 2017.

172. IUCN, Quercus pyrenaica: Gorener, V., Harvey-Brown, Y. & Barstow, M.: The IUCN Red List of Threatened Species 2017: e.T78972170A78972188. https://doi.org/10.2305/IUCN.UK.2017-3.RLTS.T78972170A78972188.en. Deposited 2 February 2017.

173. IUCN, Quercus robur: Barstow, M. & Khela, S.: The IUCN Red List of Threatened Species 2017: e.T63532A3126467. https://doi.org/10.2305/IUCN.UK.2017-3.RLTS.T63532A3126467.en. Deposited 13 February 2017.

174. IUCN, Pinus nigra: Farjon, A.: The IUCN Red List of Threatened Species 2013: e.T42386A2976817. https://doi.org/10.2305/IUCN.UK.2013-1.RLTS.T42386A2976817.en. Deposited 12 August 2011.

175. R. Calama Sainz, R. Manso González, M. E. Lucas Borja, J. M. Espelta Morral, M. Piqué Nicolau, F. Bravo Oviedo, C. E. del Peso Taranco, M. Pardos Mínguez, Natural regeneration in Iberian pines: A review of dynamic processes and proposals for management. (2017).

176. IUCN, Pinus pinea: Farjon, A.: The IUCN Red List of Threatened Species 2013: e.T42391A129160976. https://doi.org/10.2305/IUCN.UK.2013-1.RLTS.T42391A2977175.en. Deposited 16 August 2011.

177. IUCN, Quercus suber: Barstow, M. & Harvey-Brown, Y.: The IUCN Red List of Threatened Species 2017: e.T194237A2305530. https://doi.org/10.2305/IUCN.UK.2017-3.RLTS.T194237A2305530.en. Deposited 30 January 2017.

178. J. Julio Camarero, E. Gutiérrez, Response of Pinus uncinata recruitment to climate warming and changes in grazing pressure in an isolated population of the Iberian system (ne Spain). *Arctic, Antarctic, and Alpine Research* **39**, 210–217 (2007).

179. IUCN, Pinus uncinata: Farjon, A.: The IUCN Red List of Threatened Species 2017: e.T43945544A161578748. https://doi.org/10.2305/IUCN.UK.2017-2.RLTS.T43945544A161578748.en. Deposited 9 May 2016.

180. IUCN, Pinus halepensis: Farjon, A.: The IUCN Red List of Threatened Species 2013: e.T42366A2975569. https://doi.org/10.2305/IUCN.UK.2013-1.RLTS.T42366A2975569.en. Deposited 5 August 2011.

181. IUCN, Pinus pinaster: Farjon, A.: The IUCN Red List of Threatened Species 2013: e.T42390A2977079. https://doi.org/10.2305/IUCN.UK.2013-1.RLTS.T42390A2977079.en. Deposited 15 August 2011.

182. IUCN, Pinus sylvestris: Gardner, M.: The IUCN Red List of Threatened Species 2013: e.T42418A2978732. https://doi.org/10.2305/IUCN.UK.2013-1.RLTS.T42418A2978732.en. Deposited 31 January 2011.

183. M. Paniw, P. F. Quintana-Ascencio, F. Ojeda, R. Salguero-Gómez, Interacting livestock and fire may both threaten and increase viability of a fire-adapted Mediterranean carnivorous plant. *Journal of Applied Ecology* **54**, 1884–1894 (2017).

184. M. Paniw, D. García-Callejas, F. Lloret, R. D. Bassar, J. Travis, O. Godoy, Pathways to global-change effects on biodiversity: new opportunities for dynamically forecasting demography and species interactions. *Proc. R. Soc. B.* **290**, 20221494 (2023).

185. IUCN, Cistus libanotis: Rivers, M.C., Monteiro-Henriques, T., García Murillo, P.G., Buira, A., Fraga i Arquimbau, P. & Carapeto, A.: The IUCN Red List of Threatened Species 2017: e.T96425363A96425962. https://doi.org/10.2305/IUCN.UK.2017-3.RLTS.T96425363A96425962.en. Deposited 26 September 2016.

186. S. M. Evers, T. M. Knight, D. W. Inouye, T. E. X. Miller, R. Salguero-Gómez, A. M. Iler, A. Compagnoni, Lagged and dormant season climate better predict plant vital rates than climate during the growing season. *Global Change Biology* **27**, 1927–1941 (2021).

187. A. Compagnoni, A. J. Bibian, B. M. Ochocki, H. S. Rogers, E. L. Schultz, M. E. Sneck, B. D. Elderd, A. M. Iler, D. W. Inouye, H. Jacquemyn, T. E. X. Miller, The effect of demographic correlations on the stochastic population dynamics of perennial plants. *Ecological Monographs* **86**, 480–494 (2016).

188. J. R. Ohm, T. E. X. Miller, Balancing anti-herbivore benefits and anti-pollinator costs of defensive mutualists. *Ecology* **95**, 2924–2935 (2014).

189. IUCN, Cylindropuntia imbricata: Hernández, H.M., Cházaro, M. & Gómez-Hinostrosa, C.: The IUCN Red List of Threatened Species 2020: e.T152144A183111167. https://doi.org/10.2305/IUCN.UK.2020-3.RLTS.T152144A183111167.en. Deposited 29 April 2009.

190. T. Dostálek, Z. Münzbergová, Comparative population biology of critically endangered dracocephalum austriacum (lamiaceae) in two distant regions. *Folia Geobot* **48**, 75–93 (2013).

191. M. B. (Red L. Unit), IUCN Red List of Threatened Species: Dracocephalum austriacum. *IUCN Red List of Threatened Species* (2011).

192. BirdLife International (2024) Species factsheet: Barnacle Goose *Branta leucopsis*. Downloaded from https://datazone.birdlife.org/species/factsheet/barnacle-goose-branta-leucopsis on 14/11/2024.

193. BirdLife International (2024) Species factsheet: Siberian Jay *Perisoreus infaustus*. Downloaded from https://datazone.birdlife.org/species/factsheet/siberian-jay-perisoreus-infaustus on 17/11/2024.

194. Z. Tablado, E. Revilla, Contrasting Effects of Climate Change on Rabbit Populations through Reproduction. *PLoS ONE* **7**, e48988 (2012).

195. M. C. Díaz Barradas, M. A. Mateos, R. Orellana, M. Zunzunegui, F. García Novo, Changes in the canopy structure of the Mediterranean shrub *Lavandula stoechas* after disturbance. *J Vegetation Science* **10**, 449–456 (1999).

196. BirdLife International (2024) Species factsheet: Emperor Penguin *Aptenodytes forsteri*. Downloaded from https://datazone.birdlife.org/species/factsheet/emperor-penguin-aptenodytes-forsteri on 26/11/2024.

Acknowledgments

Funding

Spanish Ministry of Economy and Competitiveness (MINECO) and by the European Social Fund through the Ramón y Cajal Program (RYC2021-033192-I) (MP)

PID2022-141004OA-I00 funded by MCIN/AEI/ 10.13039/501100011033 and by "ERDF A way of making Europe" (MP).

Swiss National Science Foundation Grant (31003A_182286) (MP, EC, AO).

Research Council Norway (grants 216051, 223257, 276080, and 343398) (BHH).

National Geographic Society, the University of California Los Angeles (Faculty Senate and Division of Life Sciences) (DTB)

RMBL research fellowship and the U.S. National Science Foundation (NSF IDBR-0754247 and DEB-1119660 and 1557130 (DTB),

DBI 0242960, 07211346 and 1226713 (DTB)

The Deutsche Forschungsgemeinschaft (Ka 1082/5-1, 8-1, 10-1, 33-1, Fi 929/9-1) (PMK, CF).

Swiss National Science Foundation Postdoc.Mobility grants (P500PB_206670/1 and P5R5PB_217704) (MLB).

Long-term research development project No. RVO 67985939 of the Czech Academy of Sciences (TD, ZM)

Author contributions: For a detailed contribution table, please see https://github.com/EsinIckin/Comparative-demography-project.

Conceptualization: MP, AO, EI

Methodology: EI, MP, AO

Modelling: EI, MP, EC

Data and code: All authors

Visualization: EI, MP

Supervision: MP, OA, EC

Writing—original draft: MP, IE

Writing—review & editing: All authors

Competing interests: The authors declare no competing interest

Data and material availability: All data are code are available on https://github.com/EsinIckin/Comparative-demography-project. All analyses are fully reproducible.

Supplementary Materials: Separate pdf file

Figures and Tables

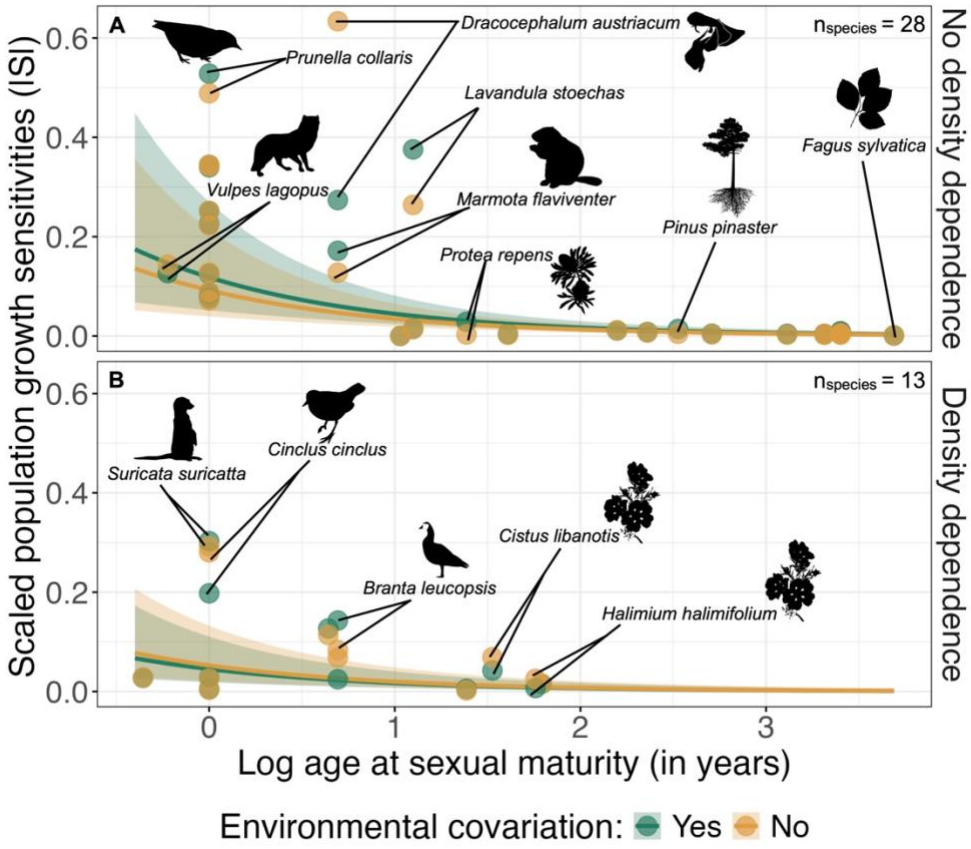

Figure 1. Scaled sensitivities of population growth rates to climate, |S|, are lower when accounting for density dependence in vital rates. Sensitivities are shown for species where density effects were not modeled explicitly (A) or were added (B) as covariates in vita-rate models. Different colors indicate sensitivity analyses under full environmental complexity (covariation with other drivers considered when perturbing a focal climate driver in vital-rate models) or reduced complexity (keeping other drivers as their average values when perturbing a focal driver). The shaded areas indicate 95% model prediction intervals (see Table 1 for model coefficients). The points show the observed mean sensitivity values of each species and perturbation scenario. We labeled some example species across different life histories and taxa.

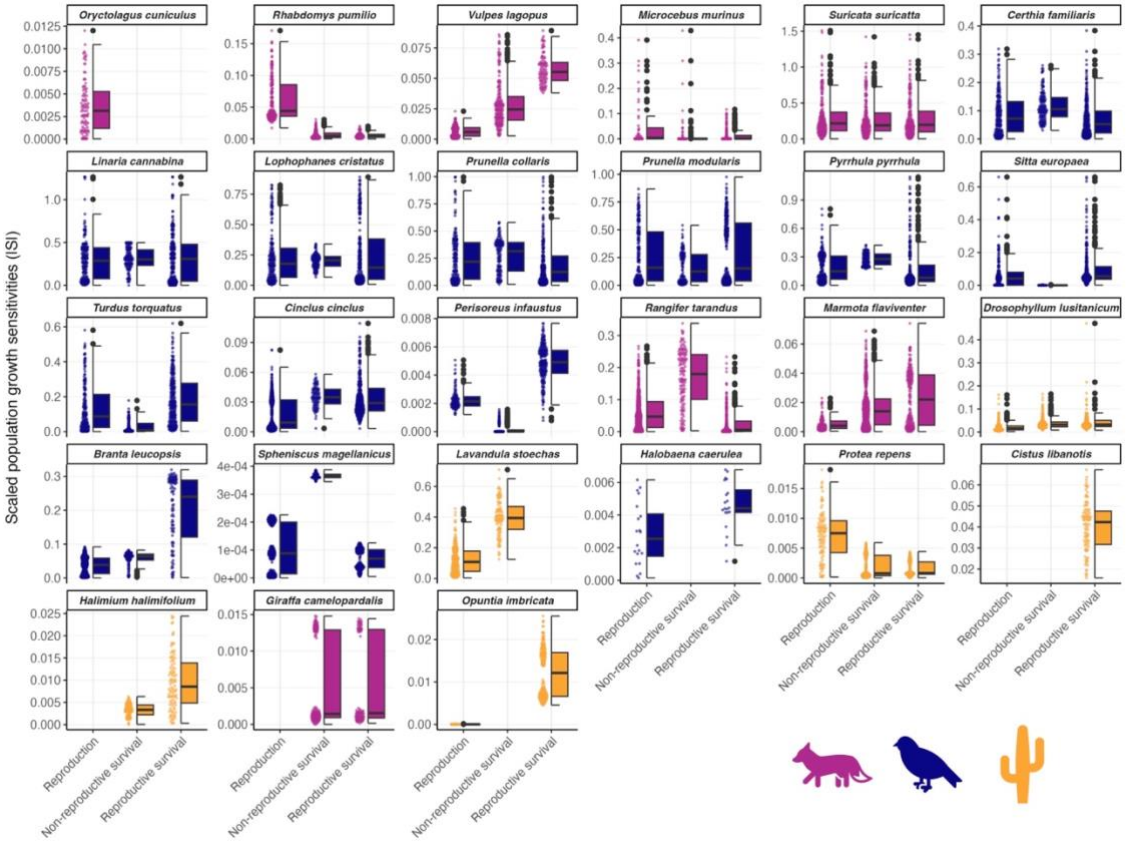

Figure 2. For any species, scaled sensitivities of population growth rates (|S|) vary substantially when perturbing single vital rates. Perturbations are shown for the species where we could perturb single vital rates. The plots are ordered by ascending age at sexual maturity and the colors indicate the taxa mammals, birds, and plants. The points represent |S| for each species, driver, vital rate, and parameter sample in vital-rate models. The boxplots display the distribution of |S|, including the median (central line), the interquartile range (box), and the range of the data (whiskers), with outliers shown as black points ($n_{\text{samples per species and vital rate}} = 100$, $n_{\text{sample for } \textit{Halobaena caerulea} \textit{ per vital rate}} = 50$; see Supporting Materials). If some sensitivities of some vital rates are missing, it's because these species did not have a climatic variable (but could have a biotic variable) in this specific vital rate.

Table 1. Output of model assessing how age at sexual maturity, covariation with other drivers, presence of density feedbacks in vital-rate models and other covariates affected scaled sensitivities of population growth rates to changes in climate, |S|.

A Fixed Effects	Coefficient	SE	P
Intercept	-3.085	0.945	**0.001**
$Covariation_{no}$	-0.250	0.112	**0.026**
$Density_{yes}$	-1.004	0.556	0.070
Age at sexual maturity	-0.991	0.200	**<0.001**
Number of vital rates	-0.221	0.501	0.660
Parameters per vital rate	0.760	0.497	0.127
$Covariation_{no}$:$Density_{yes}$	0.470	0.192	**0.014**
B Random Effects	Variance	SD	Prop. variance
Species/Group (Intercept)	1.738	1.318	0.633
Species/Group $Covariation_{no}$	0.241	0.473	0.088
Group (Intercept)	<0.001	<0.001	<0.01
Group $Covariation_{no}$	<0.001	<0.001	<0.01
Residual	0.767	0.757	0.279
Marginal R^2 (variance explained by fixed effects): 0.300			
Conditional R^2 (variance explained by fixed and random effects): 0.829			

The fixed effects (A) and random effects (B) of the generalized linear mixed model with gamma log link are shown here. The coefficient, standard error (SE), and p-value are reported for each fixed effect, whereas variance and standard deviation (SD) are reported for each random effect, as well as prop. variance, which indicates the proportion of the total random-effect variance explained by different grouping variables. Nested random effects were incorporated due to multiple observations within species and groups ($n_{samples}$ = 17’240, $n_{species}$ = 41, n_{groups} = 3). Bold p-values indicate statistical significance ($\alpha = 0.05$).

Table 2. Output of model assessing how age at sexual maturity, vital-rate type, presence of density feedbacks in vital-rate models, and other covariates affected scaled sensitivities of population growth rates to changes in climate, |S|, calculated by perturbing individual vital rates.

A Fixed Effects	Coefficient	SE	P
Intercept	-3.324	1.143	**0.003**
Vital rate$_{\text{non-reproductive survival}}$	-0.620	0.385	0.107
Vital rate$_{\text{reproductive survival}}$	0.030	0.363	0.936
Age at sexual maturity	-2.157	0.529	**<0.001**
Number of vital rates	-0.738	0.564	0.191
Parameters per vital rate	0.850	0.541	0.117
Age at sex. mat.:vital rate$_{\text{non-reproductive survival}}$	1.412	0.596	**0.012**
Age at sex. mat.:vital rate$_{\text{reproductive survival}}$	1.097	0.491	**0.025**
B Random Effects	Variance	SD	Prop. variance
Species/Group (Intercept)	2.057	1.434	0.272
Species/Group Vital rate$_{\text{non-reproductive survival}}$	2.336	1.528	0.283
Species/Group Vital rate$_{\text{reproductive survival}}$	2.078	1.442	0.264
Group (Intercept)	<0.001	<0.001	<0.01
Group Vital rate$_{\text{non-reproductive survival}}$	<0.001	<0.001	<0.01
Group Vital rate$_{\text{reproductive survival}}$	<0.001	<0.001	<0.01
Residual	0.957	0.998	0.180
Marginal R^2 (variance explained by fixed effects): 0.271			
Conditional R^2 (variance explained by fixed and random effects): 0.878			

The fixed effects (A) and random effects (B) of the generalized linear mixed model with gamma log link are shown here. The coefficient, standard error (SE), and p-value are reported for each fixed effect, whereas variance and standard deviation (SD) are reported for each random effect, as well as prop. variance, which indicates the proportion of the total random-effect variance explained by different grouping variables. Nested random effects were incorporated due to multiple observations within species and groups ($n_{samples}$ = 13'040, $n_{species}$ = 26, n_{groups} = 3). Bold p-values indicate statistical significance ($\alpha = 0.05$). Note that while perturbing one vital rate at a time, we accounted for covariation with other factors in the focal rate but set the covariates in the other vital-rate models to their mean values.

Supplementary Materials for

Comparative Life-Cycle Analyses Reveal Interacting Climatic and Biotic Drivers of Population Responses to Climate Change

Ickin *et al*.

* Corresponding authors: Esin Ickin and Maria Paniw. Email: ickin.esin@gmail.com; maria.paniw@ebd.csic.es

All data and code are freely available on this repository, and we intend to continue adding more to this database in the future: https://github.com/EsinIckin/Comparative-demography-project

This PDF file includes:

Supplementary text

Figures S1 to S53

Tables S1 to S6

SI References

Supplementary text, figures, and tables

Selection of studies

We used the following selection criteria for a study to be included in our database:

- A study had to be conducted on a wild natural population (i.e. *(79)*).
- Quantitative models had to link at least two climatic, or one climatic and one biotic driver, to at least one vital rates (i.e., *(80)*).
- The above drivers needed to be continuous for us to calculate the maximum, minimum, mean, and standard deviation, making results comparable across studies. This also allowed for perturbations with covariation, accounting for observed values of other drivers when the focal driver was at its extremes (i.e., *(81)*).
- To facilitate comparisons, climatic drivers had to be direct measures of temperature or precipitation, meaning it couldn't be a driver that influences climate, such as the Southern Annular Mode (i.e., *Catharacta lönnbergi* from *(82)*).
- The study should have constructed a structured population model such as a matrix population model, integrated population model, integral projection model, or individual-based model *(80, 83–85)*.

To find suitable studies, we first searched open databases on structured population models. We searched through the original papers in COMADRE and COMPARDE databases on matrix population models *(86, 87)*. We also searched the open database Padrino, which has been collecting studies that parameterized vital rates as functions of traits and other covariates to build integral projection models *(88)*. We also examined the database collected in *(89)*, who compiled information on studies examining the relationship between environmental drivers and population growth rates in plants using structured population models. Lastly, we considered the studies published in *(90)*.

To consider additional papers that were not part of the previous databases, we also searched Web of Science (WoS). For this, we used the search term:

TS = (("vital rate" OR demograph* OR population OR life-history OR "life history" OR model) AND (climat* OR precipitation OR rain* OR temperature OR weather OR density)).

We acknowledge that we could have missed other relevant studies if our search terms were not mentioned in the title, abstract, or key words. Initial selection of studies from the above-listed databases showed that it was difficult to obtain all necessary data for our analyses from studies published prior to 2016. This was because information in the papers was not sufficient to replicate the models, we could not reach the authors of the studies, or they were not able to provide all the necessary information. We therefore restricted our WoS search to the most recent years (2016-2023). This yielded over three million results. We ordered the results by relevance and scanned through the first 300 papers, as further results were not relevant to our selection criteria.

Sensitivity analyses

We used different perturbations of climatic variables in underlying vital-rate models to calculate long-term population growth rates – which approximate population fitness under environmental change. In cases where we constructed matrix population or integral projection models (see *Details on Study Species*)**,** we calculated the asymptotic population growth rate (λ), using the R package popbio version 2.7 *(91)*. For individual-based models, we calculated λ as the long-term average of N_{t+1}/N_t after projecting the population dynamics for at least 50 time steps and discarding the first 5-50 time steps to exclude an effect of transient dynamics in simulations (see *Details on Study Species*). We verified visually that λ calculated from simulations converged, corresponding to a distribution of growth rates that fluctuated with the same magnitude and direction across simulations (Figs. S30 – S43).

All perturbations included calculating λ under minimum (d_{min}) and maximum (d_{max}) values of a climatic driver (d) observed during a study period. In doing so, we used the actual observed values of other covariates when the focal driver was at its minimum or maximum (covariation) to account for the full complexity of environmental fluctuations and their effects on demography. We compared these perturbations to simplified ones, where we kept the remaining environmental covariates in vital-rate models fixed at their average values (no covariation) when perturbing a focal driver, which is typically done in classic sensitivity analyses *(92)*. We then calculated the absolute scaled sensitivities, |S|, for each population and climatic driver *(81)* (**Equation 1**):

$$|S| = \left| \frac{\lambda_{max} - \lambda_{min}}{(d_{max} - d_{min})/\mathrm{SD}_d} \right|$$

The denominator of |S| is the difference in the driver levels in SD (standard deviation) units. This allows to compare the sensitivities of λ to drivers that vary over different scales, i.e., across different studies *(81)*. We used the absolute values of S because we were interested in the magnitude of the driver's effects on λ rather than the direction. We also calculated uncertainties around |S| from standard errors of regression coefficients or from MCMC posterior distributions in those cases where vital rates were modeled using Bayesian regression. In the first situation, we used parametric bootstrapping; that is, we simulated the distributions of the regression coefficients based on their mean and SE and then ran the sensitivity analyses again by taking 100 parameter samples from the distribution. In the case of Bayesian regressions, we took 100 samples directly from the MCMC posterior distributions. We also tested other parameterizations of sensitivities to assess how much our choice of how to assess sensitivities affected results (see *Alternative sensitivity parameterizations* below). All analyses were conducted in R version 4.2.2.

In most studies, we calculated λ for either a single (meta)population or a representative average population across the habitat range. For the eight bird species, Malchow et al. developed a model using data from two sources. The species included *Certhia familiaris*, *Linaria cannabina*, *Lophophanes cristatus*, *Prunella collaris*, *Prunella modularis*, *Pyrrhula pyrrhula*, *Sitta europaea*, and *Turdus torquatus*, and the data covered 2585 sites across Switzerland *(93)*. Although the individual-based models were spatially explicit, we adopted the matrix model and simulated mean population growth rates and mean sensitivities for each species across sites. Similarly, the 11 Mediterranean tree species *Fagus sylvatica*, *Quercus faginea*, *Quercus ilex*, *Quercus robur/petraea*, *Pinus nigra*, *Pinus pinea*, *Quercus suber*, *Pinus uncinata*, *Pinus halepensis*, *Pinus pinaster*, and *Pinus sylvestris* were located across the continental territory of Spain in a 1 km x 1 km grid system *(84)* and we first calculated the scaled sensitivities and then averaged across the grid. In the case of *Drosophyllum lusitanicum*, Conquet et al. *(94)* included eight distinct populations, for which we first conducted the sensitivity analyses separately, and then averaged the results across sites. The study species *Dracocephalum austriacum* and *Perisoreus infaustus* also included four and two populations, respectively, for which we again first calculated the sensitivities separately, and then averaged the results across sites. We did this averaging in the main analyses to compare results at the species level. However, we performed additional analyses where we separated the different populations for *Drosophyllum lusitanicum*, *Dracocephalum austriacum*, and *Perisoreus infaustus* (see Table S4).

To understand the underlying mechanisms influencing population-level sensitivities to climate change ($|S_c|$), we fit a global generalized linear mixed model (GLMM), assuming a Gamma distribution with a log link function (**Equation 2**):

$$\log(|S_c|) = \mu_1 + \beta_1 * \mathrm{COV} + \beta_2 * \mathrm{DENS} + \beta_3 * \log(\mathrm{MAT}) + \beta_4 * \log(\mathrm{VR}) + \beta_5 * \log(\mathrm{PAR}) + \beta_6 * (\mathrm{COV} \times \mathrm{DENS}),$$

where μ_1 is the intercept, β_1 is the slope for the variable covariation (COV) which is categorical (no/yes), β_2 is the slope for the variable density (DENS; i.e., density dependence explicitly included in vital-rate models) which is also categorical with two levels (no/yes), β_3 is the slope for the log-transformed age at sexual maturity (MAT), β_4 is the slope for the log-transformed total number of vital rates that had climatic or biotic covariates (VR), β_5 is the slope for the log-transformed mean number of parameters per vital rate (PAR), and β_6 is the slope for the interaction of covariation and density. To address potential phylogenetic differences or variances within species, taxonomic groups and species were integrated as nested random intercepts, and covariation was added as a random slope.

We also fitted a simpler model, where we averaged sensitivities |S|, based on perturbations that considered the full complexity (i.e., covariation) of environmental drivers, across all perturbed drivers for each species. As Fig. S1 demonstrates, average |S| were significantly lower for species where vital-rate models included density dependence.

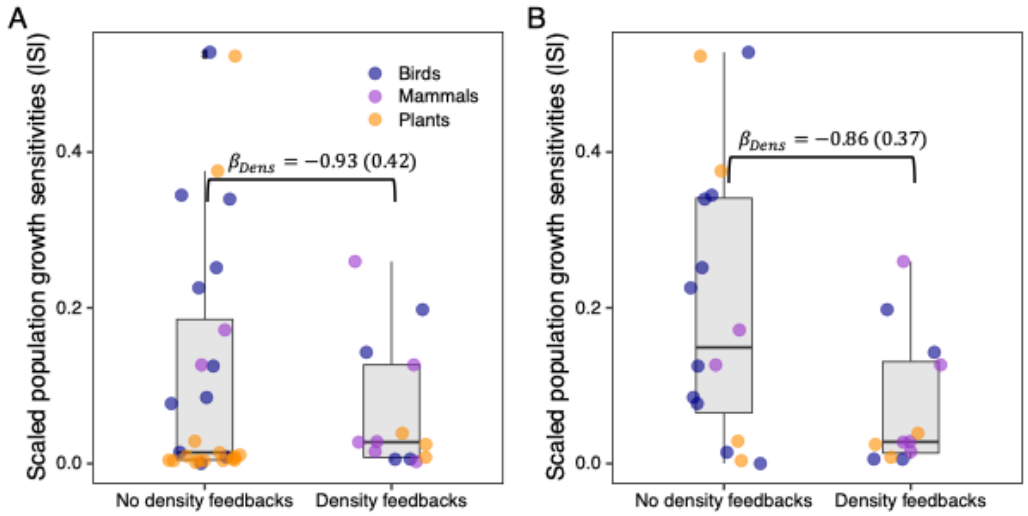

Figure S1. Scaled sensitivities of population growth rate to climate (|S|) averaged across all drivers for the 41 species used in the comparative analysis. The points represent the calculated averages, and the boxplots display the distribution of these averages among species where vital-rate models included or excluded density dependence. The boxplots show the median (central line), the interquartile range (box), and the range of the data (whiskers), with outliers shown as black points. A GLMM (with a Gamma link family) was used to model the average sensitivities as a function of presence or absence of density dependence, with species group as a random effect on the mean, and mean (SE) β estimates are shown. All calculations and plotting were done on the full dataset (A) or omitting species with very large or small ages at sexual maturity (B).

To investigate further whether the patterns (|S| lower for species where vital-rate models included density dependence) were driven by the effect of density dependence in vital-rate models, we performed additional perturbations for those species that modeled density dependence: We repeated the perturbations of climatic drivers considering covariation with other biotic and abiotic covariates, but not with density (keeping density fixed). |S| increased for most populations with modeled density dependence when changes in the effects of density dependence were fixed in perturbations (Fig. S2).

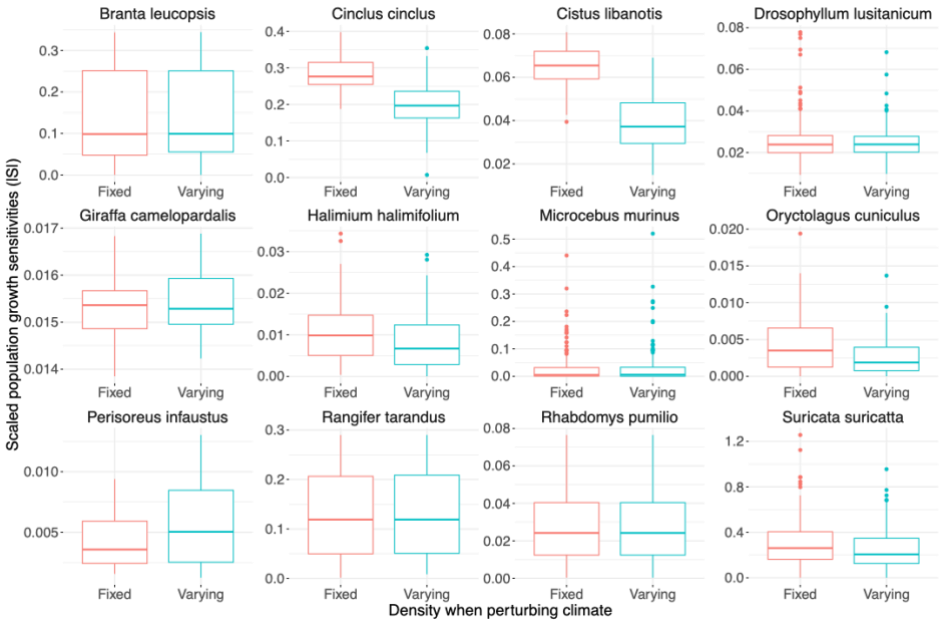

Figure S2. Scaled sensitivities of population growth rates to climate, |S|, for species where density dependence was considered explicitly in vital-rate models. |S| were calculated either keeping density fixed at their average values (but considering covariation with other environmental drivers) or considering covariation with density (along with other drivers, as in the global analysis in the main text) when perturbing a focal climate driver in vital-rate models. Boxplots summarize |S| across all resampled values for all focal climate drivers.

We then fitted an additional GLMM to see whether fixing interactions with density in full complexity perturbations still resulted in populations with density dependence having a lower |S| (**Equations 3**):

$$\log\left(\left|S_{cfixDensity}\right|\right) = \mu_1 + \beta_2 * \mathrm{DENS} + \beta_3 * \log(\mathrm{MAT}) + \beta_4 * \log(\mathrm{VR}) + \beta_5 * \log(\mathrm{PAR})$$

Parameter estimates from this model showed that, compared to results from the full global model (Equation 2), the effect of density decreases, and is not significant, β_2 = -0.711($\pm$0.589) (see sensitivity_fixed_density.R).

We performed the global analyses (Equation 2) separately for plants, where we had a good representation of age at maturity and studies that included and excluded density dependence in vital-rate models. The results represented well the general results where all taxa were included (Fig. S3). We note that we simplified the random error structure to allow the model to converge (Table S1).

Table S1. Output of model assessing how age at maturity, covariation with other drivers, presence of density dependence in vital-rate models, and other covariates affected scaled sensitivities of population growth rates of **plant species** to observed variation in climatic drivers.

A Fixed Effects	Coefficient	SE	P
Intercept	-0.788	1.743	0.651
$Covariation_{no}$	-0.483	0.042	**<0.001**
$Density_{yes}$	-1.102	1.081	0.308
Age at maturity	-1.386	0.296	**<0.001**
Number of Vital Rates	0.093	0.923	0.919
Parameters per Vital Rate	-0.149	0.577	0.796
$Covariation_{no}$:$Density_{yes}$	1.455	0.068	**<0.001**
B Random Effects	Variance	SD	Prop. variance
Species (Intercept)	0.396	0.629	0.483
Residual	0.454	0.674	0.517
Marginal R^2 (variance explained by fixed effects): 0.559			
Conditional R^2 (variance explained by fixed and random effects): 0.785			

The fixed effects (A) and random effects (B) of the generalized linear mixed model with gamma log link are shown here. The coefficient, standard error (SE), and p-value are reported for each fixed effect. Whereas variance and standard deviation (SD) are reported for each random effect. Random effects were incorporated due to multiple observations within species ($n_{samples}$ = 3420, $n_{species}$ = 18). Bold p-values indicate significance (α = 0.05). Prop. variance indicates the proportion of the total random-effect variance explained by different grouping variables.

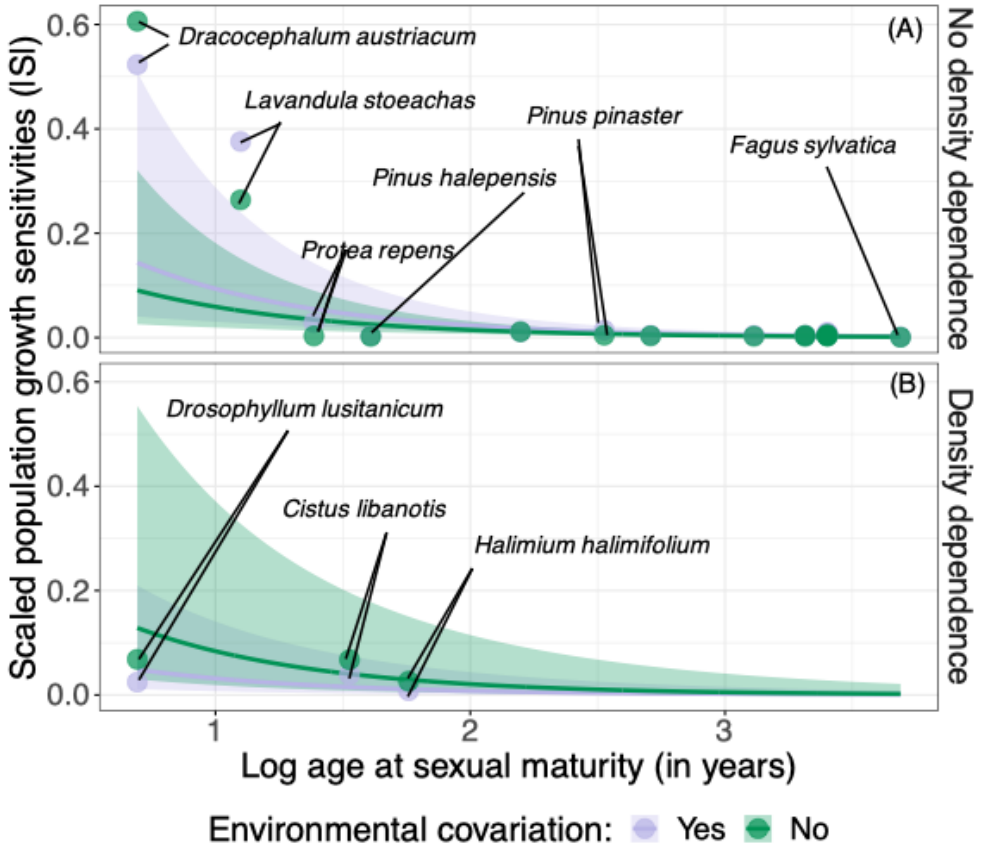

Figure S3. Scaled sensitivities of population growth rates to climate, |S|, across **plant species**. The age at sexual maturity in years (x-axis) is log-transformed using the natural logarithm. Sensitivities are shown for species where density dependence was not modeled (n =15) (A) or were added (n = 3) (B) as covariates in models. Different colors indicate sensitivity analyses where covariation with other environmental drivers was considered when perturbing a focal climate driver in vital-rate models or omitted by keeping other drivers as their average values. The shaded areas indicate 95% model prediction intervals. The points show the observed mean sensitivity values of each species. We labeled some example species across different life histories and taxa.

We also assessed the differences between the sensitivities to temperature and rain ($|S_{TR}|$) by fitting another GLMM like above but this time untangling the climatic drivers (**Equation 4**):

$$\log(|S_{TR}|) = \mu_2 + \beta_1 * \mathrm{COV} + \beta_2 * \mathrm{DENS} + \beta_3 * \log(\mathrm{MAT}) + \beta_4 * \mathrm{DRIVER} + \beta_7 * (\mathrm{COV} \times \mathrm{DENS}) + \beta_8 * (\mathrm{COV} \times \mathrm{DRIVER}) + \beta_9 * (\mathrm{DENS} \times \mathrm{DRIVER}) + \beta_{11} * \log(\mathrm{VR}) + \beta_{12} * \log(\mathrm{PAR}),$$

where μ_2 is the intercept, α_1 is the slope for the variable covariation (COV) which is categorical (no/yes), β_2 is the slope for the variable density (DENS; i.e., density dependence present in vital-rate models) which is also categorical with two levels (no/yes), β_3 is the slope for the log-

transformed age at sexual maturity (MAT), β_4 is the slope for the driver (DRIVER), β_7 is the slope for the interaction of covariation and density, β_8 is the slope for the interaction of covariation and driver, β_9 is the slope for the interaction of density and driver, β_{10} is the slope for the log-transformed age at maturity (MAT), β_{11} is the slope for the log-transformed total number of vital rates that had climatic or biotic covariates (VR), and β_{12} is the slope for the log-transformed mean number of parameters per vital rate (PAR). To address potential phylogenetic differences or variances within species, taxonomic groups and species were integrated as nested random intercepts, and covariation was added as a random slope (Table S2; Fig. S4).

Table S2. Output of model assessing how age at maturity, covariation with other drivers, presence of density dependence in vital-rate models, driver type, and other covariates affected scaled sensitivities of population growth rates to changes in rain or temperature.

A Fixed Effects	Estimate	SE	P
Intercept	-3.474	1.010	**<0.001**
$Covariation_{no}$	-0.450	0.122	**<0.001**
$Density_{yes}$	-0.651	0.568	0.255
$Driver_{temp}$	0.297	0.028	**<0.001**
Age at Maturity	-0.983	0.204	**<0.001**
Number of Vital Rates	-0.141	0.526	0.788
Parameters per Vital Rate	0.748	0.501	0.136
$Covariation_{no}$:$Density_{yes}$	0.487	0.201	**0.015**
$Covariation_{no}$:$Driver_{temp}$	0.234	0.036	**<0.001**
$Density_{no}$:$Driver_{temp}$	-0.446	0.045	**<0.001**
B Random Effects	Variance	SD	Prop. variance
Species:Group			
Intercept	1.636	1.279	0.490
$Covariation_{yes}$	0.237	0.487	0.186
Group			
Intercept	<0.001	<0.001	<0.01
$Covariation_{yes}$	<0.001	<0.001	<0.01
Residual	0.715	0.846	0.324

Marginal R^2 (variance explained by fixed effects): 0.261

Conditional R^2 (variance explained by fixed and random effects): 0.824

The fixed effects (A) and random effects (B) of the generalized linear mixed model with gamma log link are shown here. The coefficient, standard error (SE), and p-value are reported for each fixed effect. Whereas variance and standard deviation (SD) are reported for each random effect. Random effects were incorporated due to multiple observations within species ($n_{samples}$ = 17'105, $n_{species}$ = 41, n_{groups} = 3). Bold p-values indicate significance (α = 0.05). Prop. variance indicates the proportion of the total random-effect variance explained by different grouping variables.

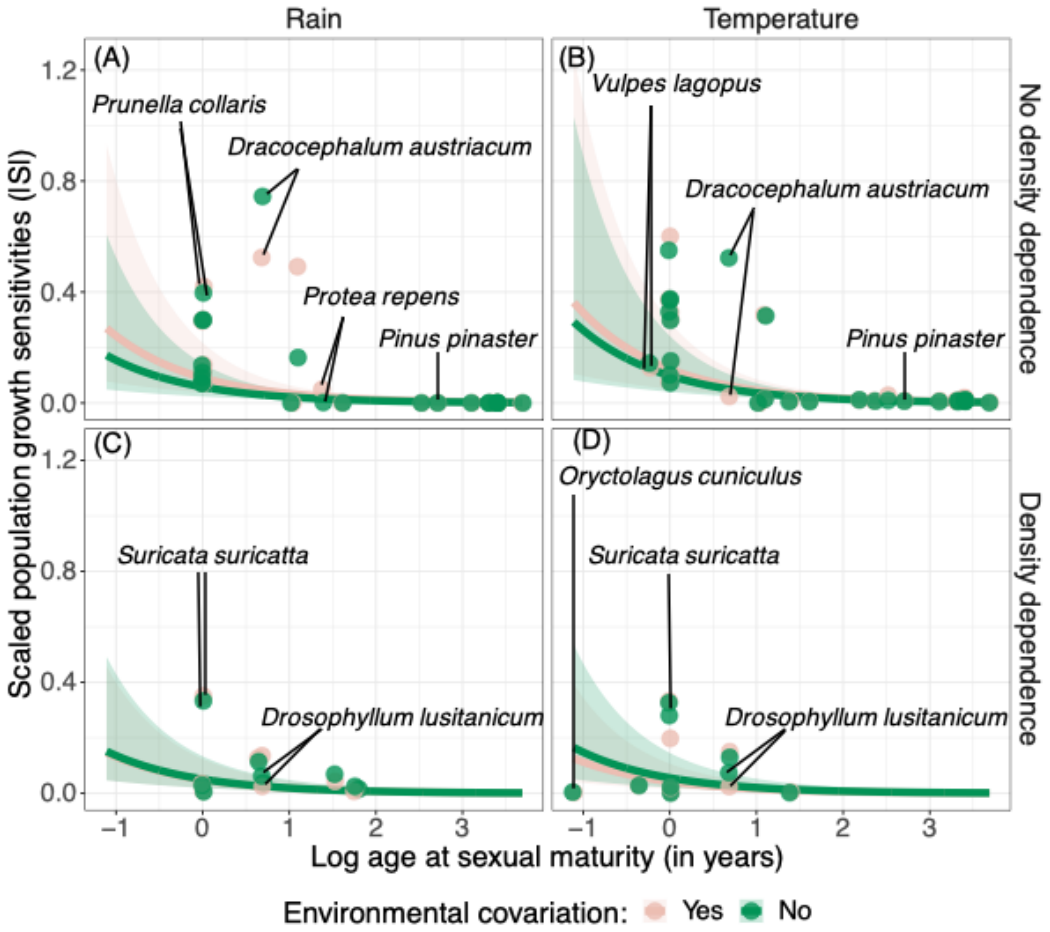

Figure S4. Scaled sensitivities of population growth rates to rain and temperature, |S|, across species. The age at sexual maturity in years (x-axis) is log-transformed using the natural logarithm. The sensitivities are shown for species where density dependence was not modeled in vital-rate models or were considered. Different colors indicate sensitivity analyses where covariation with other environmental drivers was considered when perturbing a focal climate driver in vital-rate models or omitted by keeping other drivers as their average values. The shaded areas indicate 95% model prediction intervals. The points are average |S| per species and driver modeled.

We also tested how specific vital rates were driving $|S_{VR}|$ and fitted a GLMM using |S| that we computed by perturbing climatic drivers in single vital rates (see methods in main text; Fig. S5).

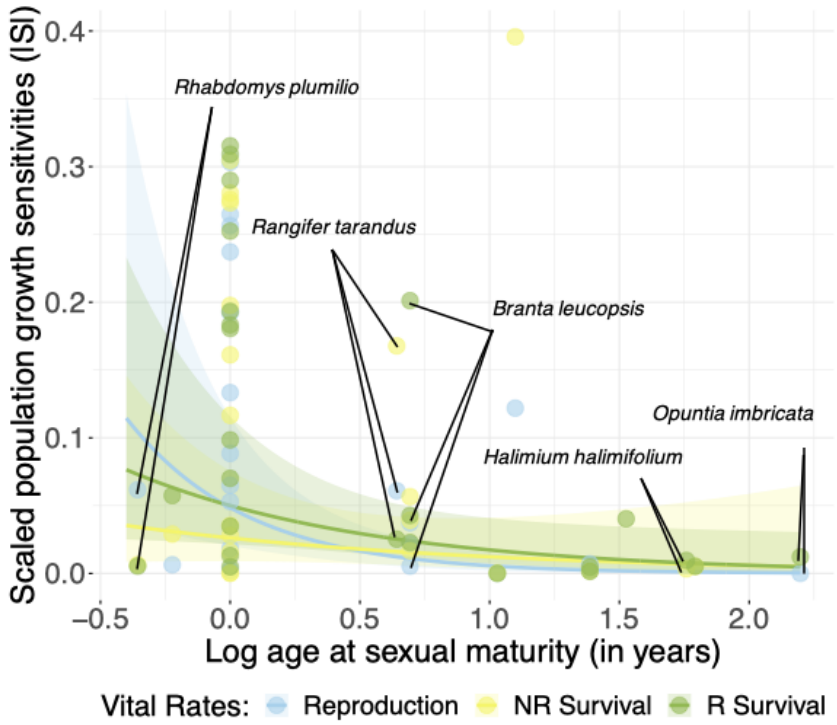

Figure S5. Scaled sensitivities of population growth rates to vital rates, |S|, across species. For each species, vital rates were categorized into three general categories (different colors. The age at sexual maturity in years (x-axis) is log-transformed using the natural logarithm. The shaded areas indicate 95% model prediction intervals. The points are average |S| per species and vital rate modeled.

To assess whether the length of the study affected any of our results, we included the variable study length as a covariate in the global GLMM (Equation 2). Study durations ranged from 3 to 40 years, with a mean of 21 years. Due to the wide range of study length, we used the natural logarithm of study length in the model. The results indicated that including study length as a covariate did not affect |S| ($\beta_{\text{study length}} = -0.38 \pm 0.47$).

In addition, although we obtained the majority of λ values analytically and we checked that λ calculated from simulations, i.e., as the long-term average of (N_{t+1}/N_t), converged, we additionally evaluated statistically whether including λ calculated from simulations affected our results. To do so, we re-parameterized the global model above removing the subset of species where λ was calculated from simulations. The results remained unchanged, with the exception

that the coefficient describing changes in sensitivities when perturbations were simplified (Covariation$_{no}$) showed relatively higher variability (see Table S3; Fig. S6).

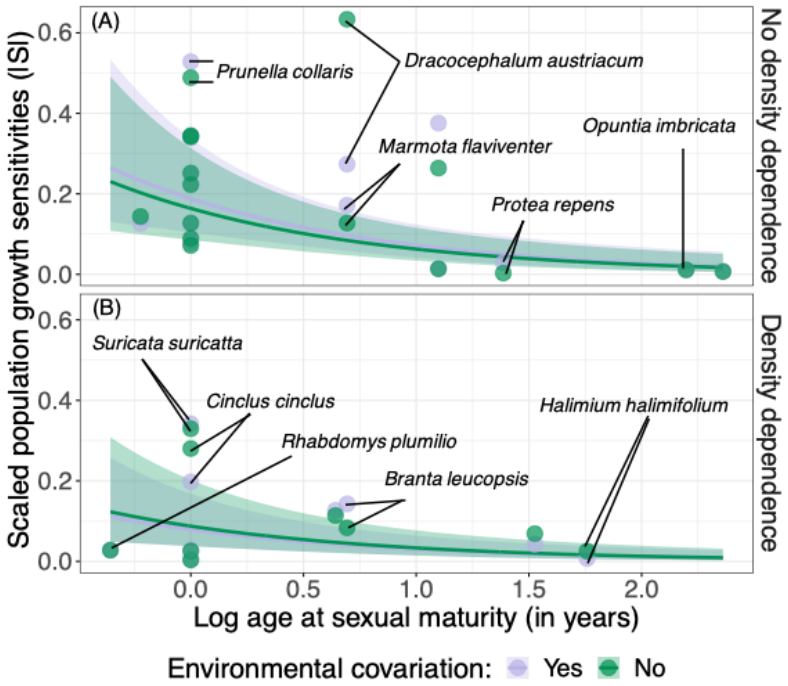

Figure S6. Scaled sensitivities of population growth rates to climate, |S|, **removing the subset of species where λ was calculated from simulations**. The age at sexual maturity in years (x-axis) is log-transformed using the natural logarithm. Sensitivities are shown for species where density dependence was not modeled (A) or were added (B) as covariates in models. Different colors indicate sensitivity analyses where covariation with other environmental drivers was considered when perturbing a focal climate driver in vital-rate models or omitted by keeping other drivers as their average values. The shaded areas indicate 95% model prediction intervals. The points show the observed mean sensitivity values of each species. We labeled some example species across different life histories and taxa.

Table S3. Output of model assessing how age at sexual maturity, covariation with other drivers, presence of density dependence in vital-rate models and other covariates affected scaled sensitivities of population growth rates to changes in climate, |S|, **removing the subset of species where λ was calculated from simulations**.

A Fixed Effects	Coefficient	SE	P
Intercept	-2.377	0.724	**0.001**
$Covariation_{no}$	-0.137	0.141	0.337
$Density_{yes}$	-0.865	0.431	**0.045**
Age at sexual maturity	-0.958	0.266	**<0.001**
Number of vital rates	-0.316	0.357	0.377
Parameters per vital rate	0.701	0.391	0.081
$Covariation_{no}$:$Density_{yes}$	0.238	0.236	0.313
B Random Effects	Variance	SD	Prop. variance
Species/Group (Intercept)	0.813	0.902	0.388
Species/Group $Covariation_{no}$	0.263	0.517	0.222
Group (Intercept)	<0.001	<0.001	<0.01
Group $Covariation_{no}$	<0.001	<0.001	<0.01
Residual	0.823	0.908	0390
Marginal R^2 (variance explained by fixed effects): 0.338			
Conditional R^2 (variance explained by fixed and random effects): 0.748			

The fixed effects (A) and random effects (B) of the generalized linear mixed model with gamma log link are shown here. The coefficient, standard error (SE), and p-value are reported for each fixed effect, whereas variance and standard deviation (SD) are reported for each random effect. Nested random effects were incorporated due to multiple observations within species and groups ($n_{samples}$ = 14'566, $n_{species}$ = 25, n_{groups} = 3). Bold p-values indicate statistical significance (α =0.05). Prop. variance indicates the proportion of the total random-effect variance explained by different grouping variables.

Finally, we repeated the global model, but maintaining |S| separate for different populations of *Drosophyllum lusitanicum*, *Dracocephalum austriacum*, and *Perisoreus infaustus.* We thus included another nested level of the random effect: population nested in species, which in turn was nested in group (mammals, birds, plants). As Table S4 shows, the results remained unchanged, and variance among populations did not contribute substantially to the random effect variance.

Table S4. Output of model assessing how age at sexual maturity, covariation with other drivers, presence of density dependence in vital-rate models and other covariates affected scaled sensitivities of population growth rates to changes in climate, |S|, **including a population random effect**.

A Fixed Effects	Coefficient	SE	P
Intercept	-3.007	0.958	**0.002**
$Covariation_{no}$	-0.252	0.112	**0.024**
$Density_{yes}$	-1.000	0.559	0.071
Age at sexual maturity	-1.032	0.199	**<0.001**
Number of vital rates	-0.321	0.504	0.523
Parameters per vital rate	0.844	0.491	0.091
$Covariation_{no}$:$Density_{yes}$	0.389	0.190	**0.040**
B Random Effects	Variance	SD	Prop. variance
Population/Species/Group (Intercept)	0.015	0.123	0.015
Population/Species/Group $Covariation_{no}$	0.050	0.222	0.042
Species/Group (Intercept)	1.724	1.313	0.447
Species/Group $Covariation_{no}$	0.174	0.417	0.142
Group (Intercept)	<0.001	<0.001	<0.01
Group $Covariation_{no}$	<0.001	<0.001	<0.01
Residual	0.738	0.859	0.293
Marginal R^2 (variance explained by fixed effects): 0.302			
Conditional R^2 (variance explained by fixed and random effects): 0.829			

The fixed effects (A) and random effects (B) of the generalized linear mixed model with gamma log link are shown here. The coefficient, standard error (SE), and p-value are reported for each fixed effect, whereas variance and standard deviation (SD) are reported for each random effect. Nested random effects were incorporated due to multiple observations within species and groups ($n_{samples}$ = 17'666, $n_{species}$ = 41, n_{groups} = 3). Bold p-values indicate statistical significance (α =0.05). Prop. variance indicates the proportion of the total random-effect variance explained by different grouping variables.

Alternative sensitivity parameterizations

When using the same data to calculate the range (maximum-minimum) and SD of a variable, there is necessarily a positive correlation between those two metrics (Fig. S7). This means that our scaling approach (Equation 1) results in a denominator that is similar across different species. One way to break this correlation is to calculate long-term SD of climatic drivers, while taking the range of values over a given shorter-term study period. In our comparative analysis, it was not possible to calculate long-term SD of climatic drivers in many studies we examined. However, in all studies but one (on the gray mouse lemur, *Microcebus murinus (95)*) the covariates in vital rate models did not show a large range (Fig. S7), and covariates were already scaled to represent *z* scores (mean = 0; SD = 1 regardless of range) for 23 species of the 41 species (Fig. S7). In other words, the covariates were already on a similar scale across most studies. The grey mouse lemur

was the only study that used raw climatic values with large ranges of temperatures (30°C – 32°C) and rainfall (621 mm – 1404 mm).

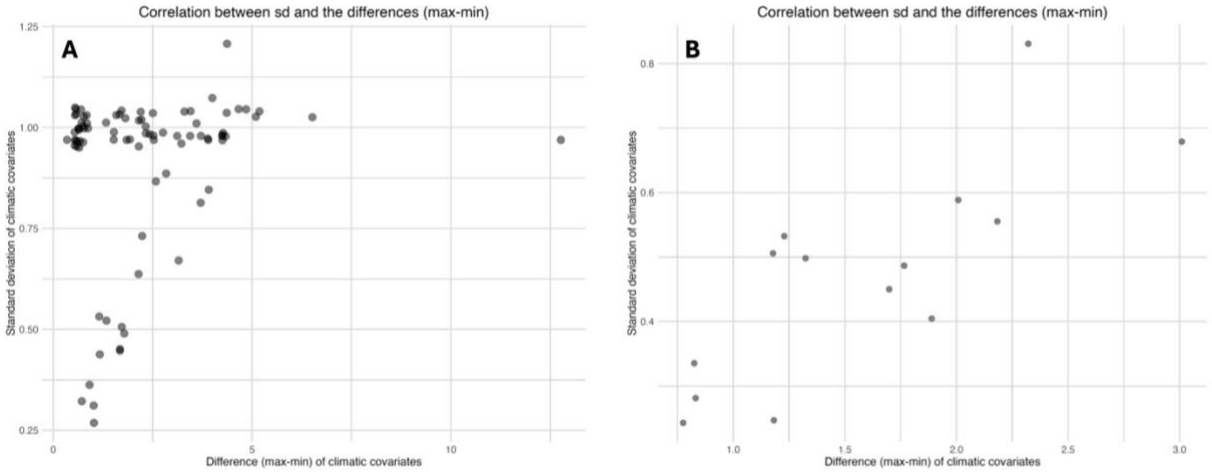

Figure S7. Relationship between observed ranges (maximum – minimum values) and standard deviations of climatic variables perturbed in this comparative study. These values were used to scale sensitivities of population growth rates, λ, across different studies (see Equation 1). The plots show (A) all ranges, including for studies where climatic drivers were already scaled in the original study (SD = 1); or (B) removing the latter drivers.

In addition, we calculated another sensitivity metric to test whether our scaling impacted our conclusions. We calculated the log response ratios (|L|) of perturbed population growth rates, λ, (**Equation 5**):

$$|L| = |\log(\lambda_{max}/\lambda_{min})|,$$

where *min* and *max* refer to λ calculated at the minimum and maximum values of a climatic driver. As with |S|, we considered absolute values as we were interested in the magnitude of the effects only. Log response ratios are the most common type of metric for summarizing outcomes in ecological meta-analyses *(96, 97)*, but do not account for different scales in perturbations *(81)*. As Fig. S8 and Table S5 show, our conclusions remain largely unchanged when considering |L| as sensitivity metric (except for a higher uncertainty associated with the main effect of "*Density in vital rate modes*"). This highlights that our results are not sensitive to different sensitivity parameterizations.

Table S5. Output of model assessing how age at sexual maturity, covariation with other drivers, presence of density dependence in vital-rate models and other covariates affected log response ratios, |L|.

A Fixed Effects	Coefficient	SE	P
Intercept	-2.587	0.894	**0.004**
$Covariation_{no}$	-0.281	0.127	0.027
$Density_{yes}$	-0.561	0.510	0.254
Age at sexual maturity	-0.378	0.181	**0.036**
Number of vital rates	0.209	0.464	0.652
Parameters per vital rate	0.451	0.451	0.316
$Covariation_{no}$:$Density_{yes}$	0.455	0.219	**0.037**
B Random Effects	Variance	SD	Prop. variance
Species/Group (Intercept)	1.954	1.398	0.470
Species/Group $Covariation_{no}$	0.374	0.612	0.206
Group (Intercept)	<0.001	<0.001	<0.01
Group $Covariation_{no}$	<0.001	<0.001	<0.01
Residual	0.933	0.966	0325
Marginal R^2 (variance explained by fixed effects): 0.101 Conditional R^2 (variance explained by fixed and random effects): 0.761			

The fixed effects (A) and random effects (B) of the generalized linear mixed model with gamma log link are shown here. The coefficient, standard error (SE), and p-value are reported for each fixed effect, whereas variance and standard deviation (SD) are reported for each random effect. Nested random effects were incorporated due to multiple observations within species and groups ($n_{samples}$ = 16'805, $n_{species}$ = 41, n_{groups} = 3). Bold p-values indicate statistical significance (α =0.05). Prop. variance indicates the proportion of the total random-effect variance explained by different grouping variables.

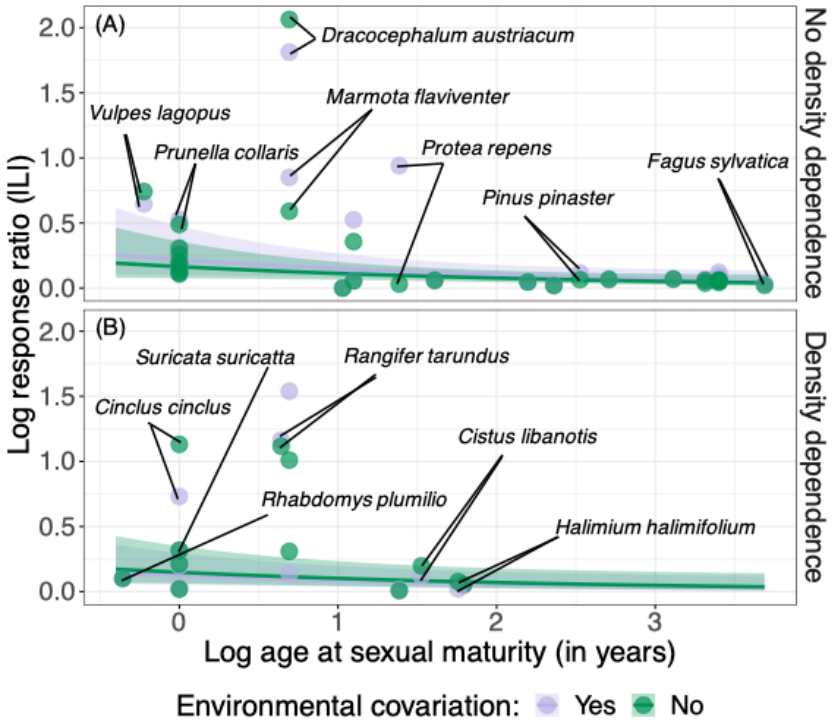

Figure S8. Log response ratios (|L|) of population growth rates, λ, under perturbations of climatic variables in vital-rate models. The age at sexual maturity in years (x-axis) is log-transformed using the natural logarithm. Response ratios are shown for species where density dependence was not modeled (A) or were added (B) as covariates in vital-rate models. Different colors indicate perturbations where covariation with other environmental drivers was considered when perturbing a focal climate driver in vital-rate models or omitted by keeping other drivers as their average values. The shaded areas indicate 95% model prediction intervals. The points show the observed mean sensitivity values of each species. We labeled some example species across different life histories and taxa.

Details on study species

Table S6. Overview of all the species included in this comparative study. The covariates used in the models were temperature (T), precipitation (P), intraspecific density (D1), interspecific density (D2), southern annular mode (SAM), sea surface temperature (SST), rain-on-snow (ROS), sea-ice concentration (SIC), food (B), potential evapotranspiration (PET), and latent climatic variable (Q). The IUCN status comprises of least concern (LC), vulnerable (VU), data deficient (DD), and unknown (?). The population trend categories, also obtained from the IUCN red list, are stable (=), increasing (+), decreasing (-), or unknown (?). The sources of the original studies the data were obtained from are listed in sources, alongside the sources of IUCN status, population trend, and age at sexual maturity if it was not obtained from the original study.

Species	Common name	Covariates	IUCN status	Population trend	Age at sex. maturity (years)	Source
Certhia familiaris	Eurasian treecreeper	T, P	LC	=	1	*(131, 132)*
Linaria cannabina	Common linnet	T, P	LC	-	1	*(131, 133)*
Lophophanes cristatus	Crested tit	T, P	LC	-	1	*(131, 134)*
Prunella collaris	Alpine accentor	T, P	LC	=	1	*(131, 135)*
Prunella modularis	Dunnock	T, P	LC	-	1	*(131, 136)*
Pyrrhula pyrrhula	Eurasian bullfinch	T, P	LC	-	1	*(131, 137)*
Sitta europaea	Eurasian nuthatch	T, P	LC	=	1	*(131, 138)*
Turdus torquatus	Ring ouzel	T, P	LC	=	1	*(131, 139)*
Cinclus cinclus	White-throated dipper	T, D1	LC	-	1	*(140, 141, 142)*
Halobaena caerulea	Blue petrel	SST, SAM, D1, D2, B, SAM	LC	-	4	*(142, 143, 144)*
Thalassarche melanophris	Black-browed albatross	SST winter, SST breeding season	LC	+	10.6	(142,*145*,*146*)
Spheniscus magellanicus	Magellanic penguin	T, P, SST	LC	-	2.8	(*142, 147, 148*)
Microcebus murinus	Gray mouse lemur	T, P, D1	LC	-	1	(*149, 150)*

Rangifer tarandus	Reindeer	ROS, D1	VU	-	1.9	(*142*, *151*)
Vulpes lagopus	Arctic fox	T, B	LC	=	0.8	(*142*, *152*, *153*)
Rhabdomys pumilio	Striped mouse	T, D1, B	LC	=	0.7	(*154*, *155*, *156*)
Marmota flaviventer	Yellow-bellied marmot	Q, D1	LC	=	2	*(157, 158)*
Suricata suricatta	Meerkat	T, P, D1	LC	=	1	*(159, 160)*
Giraffa camelopardalis	Masai giraffe	P, D1	VU	-	6	*(161, 162)*
Protea repens	Sugarbush	T, P	LC	=	4	*(163, 164, 165)*
Fagus sylvatica	Beech	T, P	LC	?	40	(166, 167, 168)
Quercus faginea	Honeydew oak	T, P	LC	?	30	(166, 169, 170)
Quercus ilex	Holly oak	T, P	LC	=	30	(166, 169, 171)
Quercus pyrenaica	Pyrenean oak	T, P	LC	=	30	(166, 169, 172)
Quercus robur	Common oak	T, P	LC	-	30	(166, 169, 173)
Pinus nigra	Black pine	T, P	LC	=	27.5	(166, 174, 175)
Pinus pinea	Stone pine	T, P	LC	=	22.5	(166, 175, 176)
Quercus suber	Cork oak	T, P	LC	-	30	(166, 169, 177)
Pinus uncinata	Mountain pine	T, P	LC	=	15	(166, 178, 179)
Pinus halepensis	Aleppo pine	T, P	LC	=	5	(166, 175, 180)

Pinus pinaster	Maritime pine	T, P	LC	+	12.5	(166, 175, 181)
Pinus sylvestris	Scots pine	T, P	LC	=	27.5	(166, 175, 182)
Drosophyllum lusitanicum	Dewy pine	T, D1	?	-	2	(183)
Halimium halimifolium	Yellow sun rose	P, D1, D2	?	-	5.8	(184)
Cistus libanotis	Rockrose	P, D1, D2	LC	-	4.6	(184, 185)
Opuntia imbricata	Devil's rope pear	T (multiple)	LC	+	9	(186–189)
Dracocephalum austriacum	Austrian dragonhead	T, P, PET	DD	-	2	(190, 191)
Branta leucopsis	Barnacle goose	T, P, D1, B	LC	=	2	*(192)*
Perisoreus infaustus	Siberian jay	P,T,D1	LC	=	1	(*193)*
Oryctolagus cuniculus	European rabbit	T,D1,B	EN	-	0.33	*(194)*
Lavandula stoechas	Lavender	T, P	?	?	3	*(195)*
Aptenodytes forsteri	Emperor penguin	SIC (multiple)	NT	-	3	*(196)*

414
415

Birds

Blue Petrel (*Halobaena caerulea*). The population of blue petrels was studied on Mayes Island in the Southern Ocean where they breed during the austral summer *(82)*. This species is long-lived and reaches sexual maturity at the age of four years *(82)*. The climate and population size information were obtained from the a GitHub repository (https://github.com/maudqueroue/MultispeciesIPM_SkuaPetrel) and the code for the vital rate models and the population model, as well as the regression coefficients were provided by the corresponding author of *(82)*. The authors built a multispecies integrated population model where the covariates in the vital-rate models for the petrel were: the Southern annular mode, sea surface temperature anomalies (SSTA), chlorophyll *a* concentration, and intra- and interspecific density. We classified SSTA as the only climatic driver "temperature". We calculated λ by projecting the population for 20 years, discarding the first ten years to account for transient dynamics. λ was then determined by calculating the changes in abundance per year using the formula and averaging it. We calculated uncertainties around λ for each perturbation scenario by resampling regression coefficients from the MCMC posteriors 10 times (instead of 50 or 100 due to the limits of computational power); and then recalculating λ.

The White-throated Dipper (*Cinclus cinclus)*. The study population of the white-throated dipper is located in the river system of Lyngdalselva in southern Norway *(83)*. The dipper is a small short-lived passerine bird with the average age at sexual maturity of one year *(98, 99)*. The climate data and population size information were obtained from the corresponding author of (83). The structure of the vital-rate models (survival and recruitment rates of the age classes 1-4) and the regression coefficients were obtained from the paper's supplementary materials Table S1 and Table S2, respectively *(83)*. The study integrated the recorded number of occupied nests, capture-recapture data of females, and data on reproductive success into a Bayesian integrated population model *(83)*. We built the matrix population model based on the life cycle illustrated in Figure 1 of the study *(83)*. Noticeably, the immigration rate was added as apparent recruitment per capita to age class 1 in our population model, after discussing it with the corresponding author. The covariates used in the vital-rate models were standardized mean winter temperature and density. We classified the former as "temperature" for our GLMMs. We calculated λ as the dominant eigenvalue of the matrix model for each perturbation scenario. We calculated

uncertainties around λ for each perturbation scenario by resampling regression coefficients 100 times using a gaussian distribution with SE given by the study; and then recalculating λ.

The Magellanic Penguin (*Spheniscus magellanicus*). The study population of the Magellanic penguins is located at the Punta Tombo colony in Argentina *(100)*. They typically reach sexual maturity at the age of 2.8 years *(99)*. The data and R code were obtained from the corresponding author's GitHub repository (https://github.com/teejclark/Press_Pulse) *(100)*. Clark-Wolf and colleagues built a pre-breeding, three-stage, female-only integrated population model *(100)*. The covariates used in the vital-rate models were the total precipitation between October 15 and December 15, temperature as the % of days per breeding season when maximum air temperature was higher than 25 °C, and sea surface temperature anomalies during breeding and migration season and their lagged versions. We classified precipitation as "rain" and the rest as "temperature" for our GLMMs. We calculated λ by running the model for 38 years, calculating λ = (N_{t+1}/N_t), and averaging it across all years. We only used the last 20 λ, discarding the first 18 years to account for transient dynamics. We calculated uncertainties around λ for each perturbation scenario by resampling regression coefficients from the MCMC posteriors that we obtained from the IPM 100 times; and then recalculating λ.

Swiss Birds. The study included eight Swiss breeding bird populations: Eurasian bullfinch (*Pyrrhula pyrrhula*), European crested tit (*Lophophanes cristatus*), Eurasian treecreeper (*Certhia familiaris*), Eurasian nuthatch (*Sitta europaea*), dunnock (*Prunella modularis*), common linnet (*Linaria cannabina*), ring ouzel (*Turdus torquatus*), and alpine accentor (*Prunella collaris*). The authors of the study chose bird species with age at maturity of one year that share common traits *(93)*. The climate data and the code were obtained from the author's GitHub repository: https://github.com/UP-macroecology/Malchow_DemogEnv_2022, and the regression coefficients for the models were provided directly by the authors *(93)*. A female-only, two-stage matrix population model with three vital rates was built for each species *(93)*. In the vital-rate models, five climatic covariates were used: mean temperature and total precipitation during the breeding season, mean temperature in fall, and total precipitation and minimum temperature during winter. Temperature-related covariates were categorized as "temperature", and precipitation-related ones as "rain". We calculated λ as the dominant eigenvalue of the matrix model for each perturbation scenario and for each species separately. We calculated uncertainties around λ for each perturbation scenario by resampling regression coefficients from the MCMC posteriors 100 times, and then recalculating λ. We conducted the analyses for each species separately, but they

all followed the same workflow. Although the individual-based models were spatially explicit (covering 2585 sites across Switzerland) *(93)*, we adopted the matrix model and simulated mean λ and mean |S| for each species across sites.

The Black-browed Albatross (*Thalassarche melanophris*). The study population is located at Kerguelen Island, in the colony of Cañon des Sourcils Noirs *(101)*. The black-browed albatross is a long-lived seabird, reaching sexual maturity at the age of 10.6 years *(99, 102)*. The climate data and code, including the model parameters, were provided by the corresponding author *(101)*. The authors built a matrix population model comprised of 25 states. The covariates used in the vital-rate models were standardized sea surface temperature (SST) in the juvenile sector during the wintering season (May to August), SST in the wintering sector of adults (July to September), and SST in the breeding sector (October of year t to March of year t+1) *(102)*. We classified all the climatic covariates as "temperature". We calculated λ as the dominant eigenvalue of the matrix model for each perturbation scenario. We calculated uncertainties around λ for each perturbation scenario by resampling regression coefficients 100 times using a gaussian distribution with SE extracted from Table S2.4b of a previous study *(103)*; and then recalculating λ.

The Barnacle Goose (*Branta leucopsis*). The study population was monitored in northwestern Svalbard where it breeds *(104)*. The Svalbard barnacle goose population overwinters at Solway Firth, Scotland, before flying to Svalbard for breeding in summer. The barnacle goose reaches sexual maturity at the age of 2 years *(105)*. The climate data and code, including the model parameters, were provided by the corresponding author *(104)*. The authors built a matrix population model comprised of 2 states, fledglings and adults. The covariates used in the vital-rate models were mean daily minimum temperatures October-March in Scotland and in April-May in Helgeland, mean precipitation in April-May in Helgeland, the flyway population size at the wintering grounds in Scotland, spring onset, adult numbers in Svalbard, and fox predation. We classified all the climatic covariates as "temperature" or "rainfall". We calculated λ as the dominant eigenvalue of the matrix model for each perturbation scenario. We calculated uncertainties around λ for each perturbation scenario by resampling regression coefficients 100 times using a multivariate Normal distribution based on the parameter covariance matrix.

The Siberian Jay (*Perisoreus infaustus*). Siberian jay individuals have been observed long-term near Arvidsjaur, northern Sweden. For this study, we had 15 years of data on 4341 sightings from

1166 individuals (*106)*. We used population models representing two populations: managed (in the southern area where scots pine and Norway spruce are thinned, harvested, and re-planted in 80–120 year cycles) and natural (northern area of the study site that has not been managed for at least 200 years). The jays reach sexual maturity at the age of 1 year. The climate data and code, including the model parameters, were provided by the corresponding author *(106)*. The authors built a periodic matrix population model that described transitions among juvenile, non-breeding, and breeding stages across winter and summer seasons. The covariates used in the vital-rate models were mean winter snow depth (December–March), average temperature during the breeding season (April–May), and population density. We classified all the climatic covariates as "temperature" or "precipitation". We calculated λ as the dominant eigenvalue of the annual product of the periodic matrix model for each perturbation scenario. We calculated uncertainties around λ for each perturbation scenario by resampling regression coefficients 100 times using a multivariate Normal distribution based on the parameter covariance matrix. We calculated sensitivities for the natural and managed population separately, and the averaged them across the two populations for the global analysis.

The emperor penguin (*Aptenodytes forsteri*). For this work, we used a long-term dataset on breeding emperor penguins at Dumont D'Urville, Terre Adélie, in Antarctica. The colony has been monitored every year, during the breeding season (March–December), from 1962 onwards. We used the demographic model in *(107)* constructed from capture histories from 1962-2005. The authors constructed a sex- (males and females) and stage-structured (pre-breeders, breeding pairs, non-breeder) periodic (seasonal) matrix population model following *(108)*. The climatic covariates in vital-rate models were proportional anomalies in sea-ice concentration (SIC), relative to the mean from 1979 to 2007 in the pre-breeding, laying, incubating, and rearing seasons. We categorized the SIC as "temperature" in our GLMMs. All data and code to construct and perturb the population model were made available by Jenouvrier and coauthors and can be found at: https://gitfront.io/r/fledge-whoi/zUbHbQtJq2XV/emperor-penguin-IUCN/ (CMR code). We calculated λ as the dominant eigenvalue of the annual product of the seasonal matrix population models for each perturbation scenario, after projecting population dynamics for 1000 years and letting the population vector converge to a stable distribution (projections were necessary because female/male ratios were used to model breeding and were generated within the model). We obtained the uncertainties around λ for each perturbation scenario using parametric bootstrapping to obtain variation in vital rate parameters (following the original study; *(107)*).

Mammals

The Masai Giraffe (*Giraffa camelopardalis tippelskirchi or G. tippelskirchi*). The metapopulation of female Masai giraffes studied here is located in northern Tanzania *(109–111)*. They reach sexual maturity at the age of 6 years *(85)*. The data and code were provided by the authors of *(85)* and can be found at https://github.com/MariaPaniw/Masai_giraffe_ibm. The study used long-term demographic data to develop a stochastic, socially structured individual-based model (IBM) *(85)*. The two covariates used in the model were population density and rainfall; the latter was classified as "rain" for our GLMMs. We ran the model for 150 seasons (4-month time steps), discarding the first 12 seasons to account for transient dynamics. λ was then determined by calculating the changes in abundance per year using the formula $\lambda = (N_{t+1}/N_t)$ and averaging it across all years. We ran the simulation 100 times to obtain the uncertainties around λ for each perturbation scenario.

The Yellow-bellied Marmot (*Marmota flaviventer*). The study population of these large rodents is located in the Upper East River Valley, Gothic, Colorado. They reach sexual maturity at the age of 2 years *(112)*. The data and code of the study were provided by the author of the study *(112)* and can also be found at https://datadryad.org/stash/dataset/doi:10.5061/dryad.4j0zpc87c. The authors of *(112)* built seasonal stage-, mass- and environmental-specific integral projection models (IPM) that account for seasonal demographic covariation using a latent climatic variable (Q) that depicts a measure of environmental quality *(112)*. We considered random year variation as a separate covariate, due to the way the demographic model was built. We considered Q as a climatic driver and composite of both rainfall and temperature (see *(112)*). We calculated λ as the dominant eigenvalue of the matrix of the IPM for each perturbation scenario. We calculated uncertainties around λ for each perturbation scenario by resampling regression coefficients 100 times from the MCMC posteriors, and then recalculating λ.

The Gray Mouse Lemur (*Microcebus murinus*). The study population of this small lemur is located in the Kirindy forest in Madagascar *(113)*. They are a short-lived species, reaching sexual maturity at the age of one year *(80, 114, 115)*. The climate and population-size data were provided by the corresponding author of *(80)*. We obtained the structure of the vital-rate models, regression coefficients, and their standard errors from Table 1 of their paper. We then rebuilt the MPM based on the annual life cycle illustrated in Figure 6 of their paper *(80)*. The model is a two-stage and

two-sex matrix population model *(80)*. The covariates used in the vital-rate models were monthly mean maximum temperature, monthly total rainfall, and population density. We classified mean maximum temperature as "temperature" and total rainfall as "rain" for our GLMMs. We calculated λ as the dominant eigenvalue of the matrix model for each perturbation scenario. We calculated uncertainties around λ for each perturbation scenario by resampling regression coefficients 100 times using a gaussian distribution with SE given by the study; and then recalculating λ.

The Svalbard Reindeer (*Rangifer tarandus*). The study population of the wild Svalbard reindeer is located in central Spitsbergen, Svalbard, Norway *(116)*. They reach sexual maturity at the age of 1.9 years *(99)*. The climate data, population size information, and posterior samples were obtained from the authors *(116)*. The model used was an integrated population model with six female age classes. The covariates in the vital rate models were rain-on-snow (ROS), population density, and winter length. We did not include sensitivities to winter length since it was not related to temperature or rain. ROS was classified as "rain" for our GLMMs. We calculated λ as the dominant eigenvalue of the matrix model for each perturbation scenario. We calculated uncertainties around λ for each perturbation scenario by resampling regression coefficients 100 times from the MCMC posteriors, and then recalculating λ.

The African Striped Mouse (*Rhabdomys pumilio*). The short-lived African striped mouse lives in the dry regions of South Africa and reaches sexual maturity within the first year; for our study, we set this parameter to 0.7 years *(79, 117)*. The climate and population-size data, as well as the full code of the population model was provided by the corresponding author *(79)*. The model built in the study was a female-only stage-structured matrix population model *(79)*. The covariates utilized in the vital-rate models included monthly mean temperature, food availability, and population density. Monthly mean temperature was categorized as "temperature" in the analyses. We calculated λ as the dominant eigenvalue of the matrix model (which described the population dynamics over one month) for each perturbation scenario. We calculated uncertainties around λ for each perturbation scenario by resampling regression coefficients 100 times from the MCMC posteriors, and then recalculating λ. This was the only species where λ could not be calculated on an annual scale. We tested whether this affected our results by repeating the global GLMM excluding this species. Doing so did not change our results (see the R script on GitHub named MainAnalysis_without_RhabdomysPumilio.R).

The Meerkat (*Suricata suricatta*). The study population of these small social mammals is located in the Kuruman River Reserve in South Africa *(118)*. They reach sexual maturity at the age of one year *(118)*. The data and code were provided by the corresponding author of *(118)*. The model used was a mass-stage-classified integral projection model *(118)*. The covariates in the vital-rate models included population density, interannual rainfall, and temperature deviations (from seasonal means). We classified rainfall as "rain" and temperature deviations as "temperature" for our GLMMs. We calculated λ as the dominant eigenvalue of the annual integral projection model for each perturbation scenario. We obtained the uncertainties around λ for each perturbation scenario using non-parametric bootstrapping to obtain variation in vital rate parameters (following the original study, *(118)*).

The Arctic Fox (*Vulpes lagopus*). The study population of these abundant generalists and apex predators is located in Svalbard, Norway *(119)*. They reach sexual maturity at the age of 0.8 years *(119)*. The climate and population data, as well as the full code on the model was provided by the corresponding author of study *(119)*. The authors of the study built a Bayesian integrated population model *(119)*. The covariates used in the vital-rate models were sea ice extent, availability of reindeer carcasses, and goose population size. We classified sea ice extent as "temperature" and the others as biotic factors. We calculated λ as the dominant eigenvalue of the matrix model for each perturbation scenario under two hunting scenarios (low vs high pressure), and then averaged the results. We calculated uncertainties around λ for each perturbation scenario by resampling regression coefficients 100 times from the MCMC posteriors, and then recalculating λ.

The European rabbit (*Oryctolagus cuniculus*). Parameters to run an individual-based model of rabbit population dynamics in Doñana Protected Area (southwestern Spain) were obtained from Tablado and co-authors *(120)*. Rabbits are native to the Iberian Peninsula but their abundances have declined, including in Doñana, due to a combination of climate and land-use change and diseases. Rabbit are fast-lived and reach sexual maturity at around 4 months. The study by Tablado and co-authors complied demographic parameters from previous studies to develop a stochastic individual-based model (IBM). The main climatic variable in the model was mean monthly temperature, from which we obtained measures of food (or green pasture) availability and breeding season length. Population density was also considered as a covariate in vital-rate models. We ran the IBM for 16 years (1-month time steps), discarding the first 5 years to account

for transient dynamics. λ was then determined by calculating the changes in abundance per year using the formula $\lambda = \text{mean}((N_{t+1}/N_t))$, where t = abundance in June (end of the breeding season). We ran the simulations 100 times to obtain the uncertainties around λ for each perturbation scenario.

Plants

Shrubs (*Cistus libanotis, Halimium halimifolium, Lavandula stoechas*). These three common shrub species are located in Doñana National Park in Spain. *C. libanotis* reaches sexual maturity (i.e., mean age at first flowering in plants) at the age of 4.6 years, *H. halimifolium* at the age of 5.8 years, and *L. stoechas* at the age of 3 years *(121)*. The climate and population-size data, posterior samples, and code were provided by the authors, and the data and code for the population model for *Cistus libanotis* and *Halimium halimifolium*, can be found on the author's GitHub repository: https://github.com/MariaPaniw/shrub_forecast *(121)*. The demography of the latter two shrub species was described by a three-stage life cycle, from which a matrix population model was built *(121)*. The covariates used in the vital-rate models were rainfall, inter- and intraspecific densities. For *Lavandula stoechas*, we expanded the population model develop in *(121)* using individual-based data collected 2019-2023. We fit an integral projection model for this species, with vital rates were parameterized as functions of seasonal temperature and rainfall (adult plant density was used as on offset in recruitment models only). We classified seasonal temperature and rainfall as "temperature" "rain" for our GLMMs, respectively. We calculated λ as the dominant eigenvalue of the matrix model or integral projection model for each perturbation scenario. We calculated uncertainties around λ for each perturbation scenario by resampling regression coefficients 100 times from the MCMC posteriors (or multivariate Normal distribution based on the parameter covariance matrix for *L. stoechas*), and then recalculating λ.

The Pontic Dragonhead (*Dracocephalum austriacum*). The four study populations are located in the Bohemian Karst in Central Europe *(122)*. This study species reaches its sexual maturity at the age of two on average *(122)*. The data and code were provided by the corresponding author (Evers et al. in preparation). They built an integral projection model. The climatic covariates used in the vital-rate models were potential evapotranspiration (PET), precipitation, and temperature. We classified precipitation as a climatic driver "rain", and temperature as "temperature" for our GLMMs. We calculated λ as the dominant eigenvalue of the matrix model for each perturbation scenario. We obtained uncertainties around λ for each perturbation scenario by resampling

coefficients 100 times from the functional linear models, which linked climate drivers to vital rates, and then recalculating λ.

The Dewy Pine (*Drosophyllum lusitanicum*). The eight study populations of the dewy pine, a carnivorous subshrub, are located in the heathlands of Southern Spain *(123, 94)*. The dewy pine reaches sexual maturity at the age of two years *(123)*. The data and code for the analysis was provided by the corresponding author *(94)*. They built an individual-based model (IBM) and used these five covariates in the vital-rate models: temperature, rainfall, density, size, and time since last fire. The two climatic drivers temperature and rainfall were classified as such. We calculated λ by projecting the population for 50 years, discarding the first 25 years to account for transient dynamics. λ was then determined by calculating the changes in abundance per year using the formula $\lambda = (N_{t+1}/N_t)$ and averaging it over all the years. We calculated uncertainties around λ for each perturbation scenario by running the simulation 100 times, and then recalculating λ.

Spanish Trees. This study includes several tree species populations across Spain *(84)*. These include *Fagus sylvatica*, *Pinus halepensis*, *Pinus nigra*, *Pinus pinaster*, *Pinus pinea*, *Pinus sylvestris*, *Pinus uncinata*, *Quercus faginea*, *Quercus ilex*, *Quercus robur/petraea*, and *Quercus suber*. The mean age at sexual maturity of each species can be found in Table S6. The climate data and the code for the model were obtained from the corresponding author's GitHub repository: https://github.com/garciacallejas/IPM_basic *(84)*. A spatially explicit integral projection model was constructed for all tree species *(84)*. The covariates in the vital-rate models include temperature, precipitation, and their anomalies. We classified temperature and precipitation as "temperature" and "rain" for our analyses. We calculated λ by running the model for 90 years (10-year time steps), discarding the first 50 years to account for transient dynamics. λ was then determined by calculating the changes in abundance per year using the formula $\lambda = (N_{t+1}/N_t)$ and averaging it. We calculated uncertainties around λ for each perturbation scenario by running the simulation five times (due to computational demands), and then recalculating λ. In the original study, the tree species were spread across the continental territory of Spain in a 1 km x 1 km grid system *(84)*. For our study, we first calculated the scaled sensitivities and then averaged across the area.

The Tree Cholla Cactus (*Opuntia imbricata*). The study population is located at the Sevilleta National Wildlife Refuge in New Mexico, USA *(124, 125)*. This species reaches sexual maturity at the age of nine years *(126)*. The integral projection model is based on the R script from Aldo Compagnoni *(127)*. Further, two vital-rate models are from the analysis of Sanne Evers *(126)*. The data and code were provided by the corresponding author of *(126)*. The covariates in the vital-rate models were climate anomalies of the values instead of absolute values. The variables were mean average daily temperatures of two different time windows and mean minimum daily temperature *(126)*. We classified the covariates in our analyses as "temperature". We calculated λ as the dominant eigenvalue of the matrix for each perturbation scenario. We calculated uncertainties around λ for each perturbation scenario by resampling regression coefficients 100 times from the posterior distributions, and then recalculating λ.

The Common Sugarbush (*Protea repens*). This species of shrub is found throughout the Mediterranean climate of the Cape Floristic Region in South Africa *(128)*. It reaches sexual maturity at the age of four years *(129)*. All data and code were accessible online *(128)*. However, to obtain posterior samples of regression coefficients, we rebuilt and executed the regression models in JAGS *(130)*. The population model built is an integral projection model. The covariates used in the vital-rate models that we perturbed were minimum July temperature and mean annual precipitation, respectively classified as "temperature" and "rain" in the meta-regressions. We calculated λ as the dominant eigenvalue of the matrix model for each perturbation scenario. We calculated uncertainties around λ for each perturbation scenario by resampling regression coefficients 100 times from the posterior distributions, and then recalculating λ.

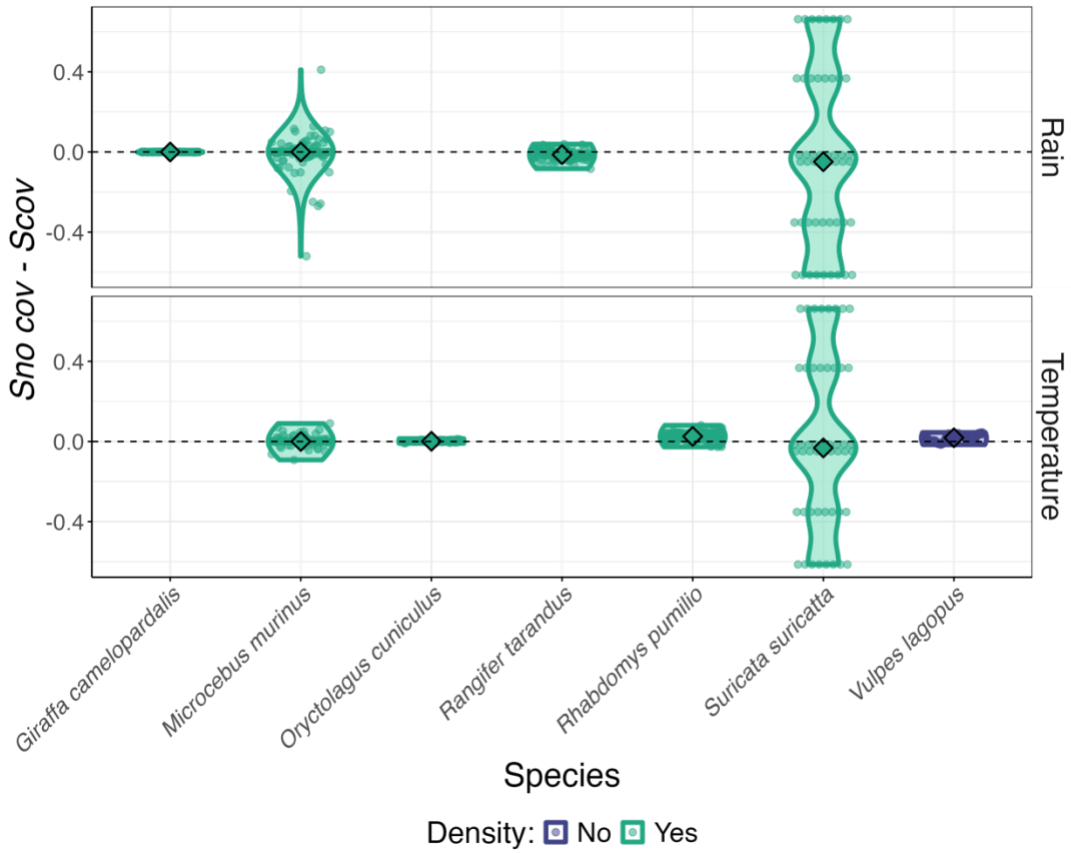

Figure S9. Differences in scaled sensitivities |S| of population growth rates of mammalian species to (A) rain and (B) temperature, without and with covarying drivers ($S_{no\ cov} - S_{cov}$). Different colors indicate models where density effects were included or not. A positive difference indicates that the sensitivities with covariation are lower than those without covariation, implying that there are dampening effects of covariation on the sensitivity of a species. The diamond symbols display the median sensitivities, while the points represent all calculated sensitivities from 100 resamplings per species ($n_{resamplings} = 100$).

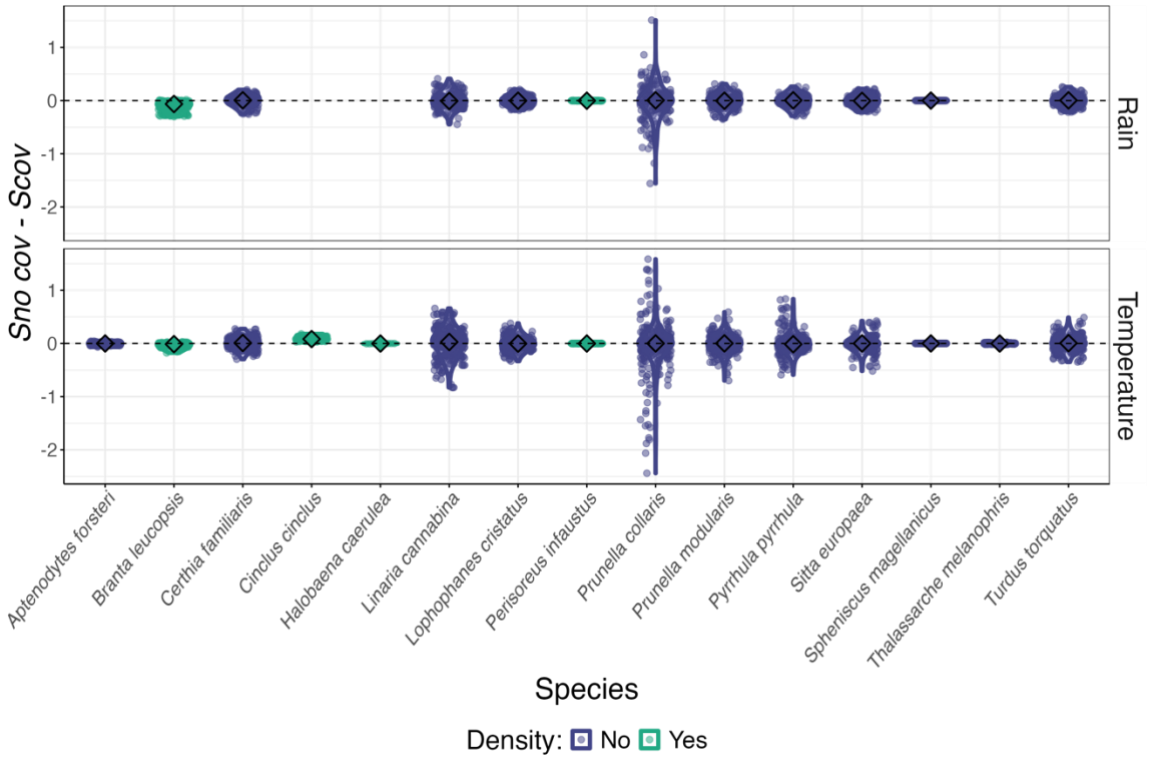

Figure S10. Differences in scaled sensitivities |S| of population growth rates of avian species to (A) rain and (B) temperature, without and with covarying drivers ($S_{no\ cov} - S_{cov}$). Different colors indicate models where density effects were included or not. A positive difference indicates that the sensitivities with covariation are lower than those without covariation, implying that there are dampening effects of covariation on the sensitivity of a species. The diamond symbols display the median sensitivities, while the points represent all calculated sensitivities from 100 resamplings per species ($n_{resamplings} = 100$, $n_{resamplings\ for\ Halobaena\ caerulea} = 50$).

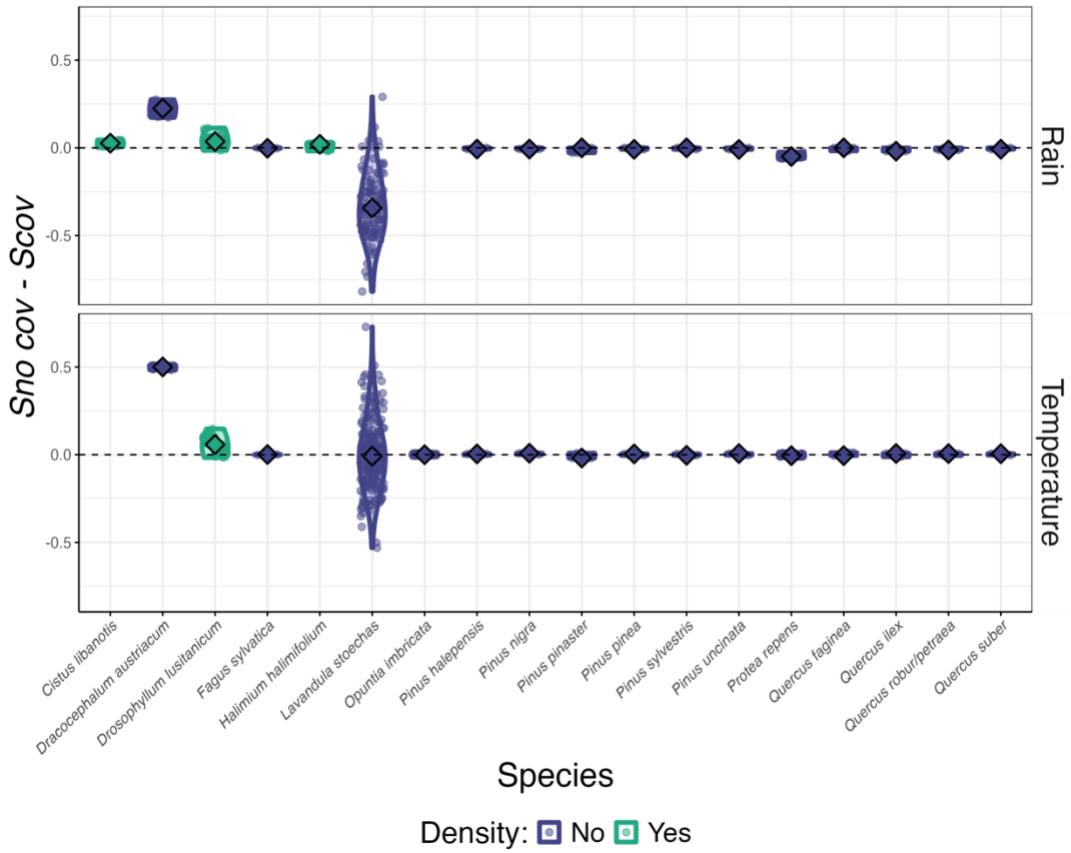

Figure S11. Differences in scaled sensitivities |S| of population growth rates of plant species to (A) rain and (B) temperature, without and with covarying drivers ($S_{no\ cov} - S_{cov}$). Different colors indicate models where density effects were included or not. A positive difference indicates that the sensitivities with covariation are lower than those without covariation, implying that there are dampening effects of covariation on the sensitivity of a species. The diamond symbols display the median sensitivities, while the points represent all calculated sensitivities from 100 resamplings per species ($n_{resamplings} = 100$, $n_{resamplings\ for\ Spanish\ Trees} = 5$).

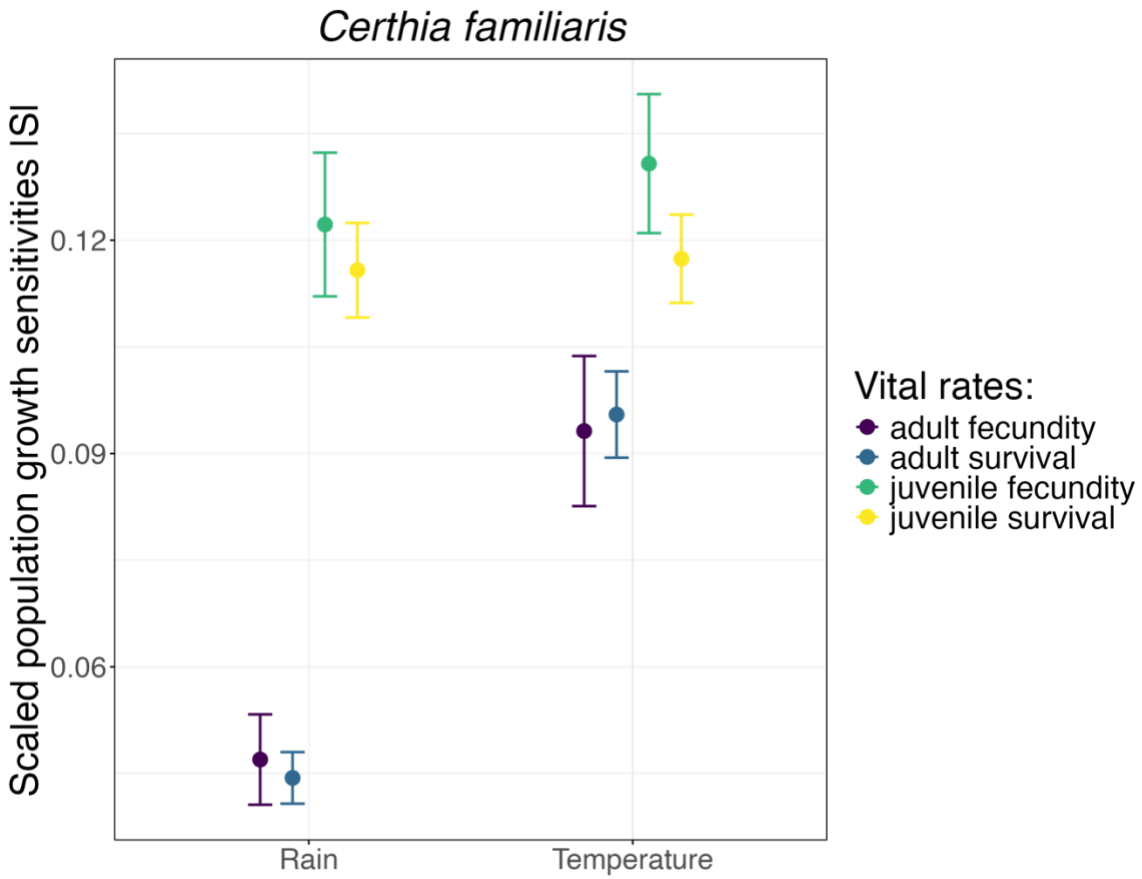

762

763 **Figure S12.** Scaled sensitivities of population growth rates per vital rate to different drivers for
764 *Certhia familiaris*. The dots represent the mean scaled sensitivities across the calculated
765 resamplings per driver and vital rate combination ($n_{resamplings}$ = 100) and the error bars display the
766 standard errors. The climatic drivers here are rain and temperature.

767

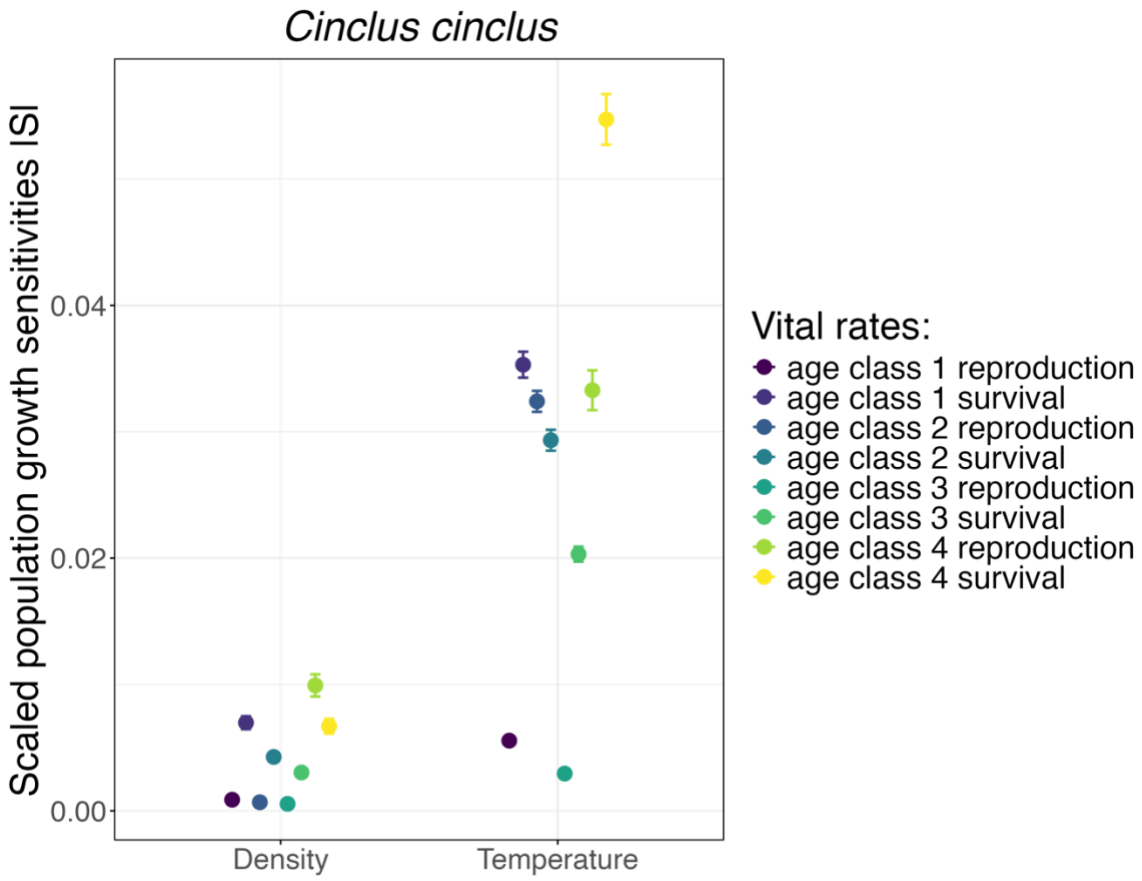

768

769 **Figure S13.** Scaled sensitivities of population growth rates per vital rate to different drivers for
770 *Cinclus* cinclus. The dots represent the mean scaled sensitivities across the calculated resamplings
771 per driver and vital rate combination ($n_{resamplings}$ = 100) and the error bars display the standard
772 errors. The climatic driver here is temperature, and the density driver refers to intraspecific
773 density.

774

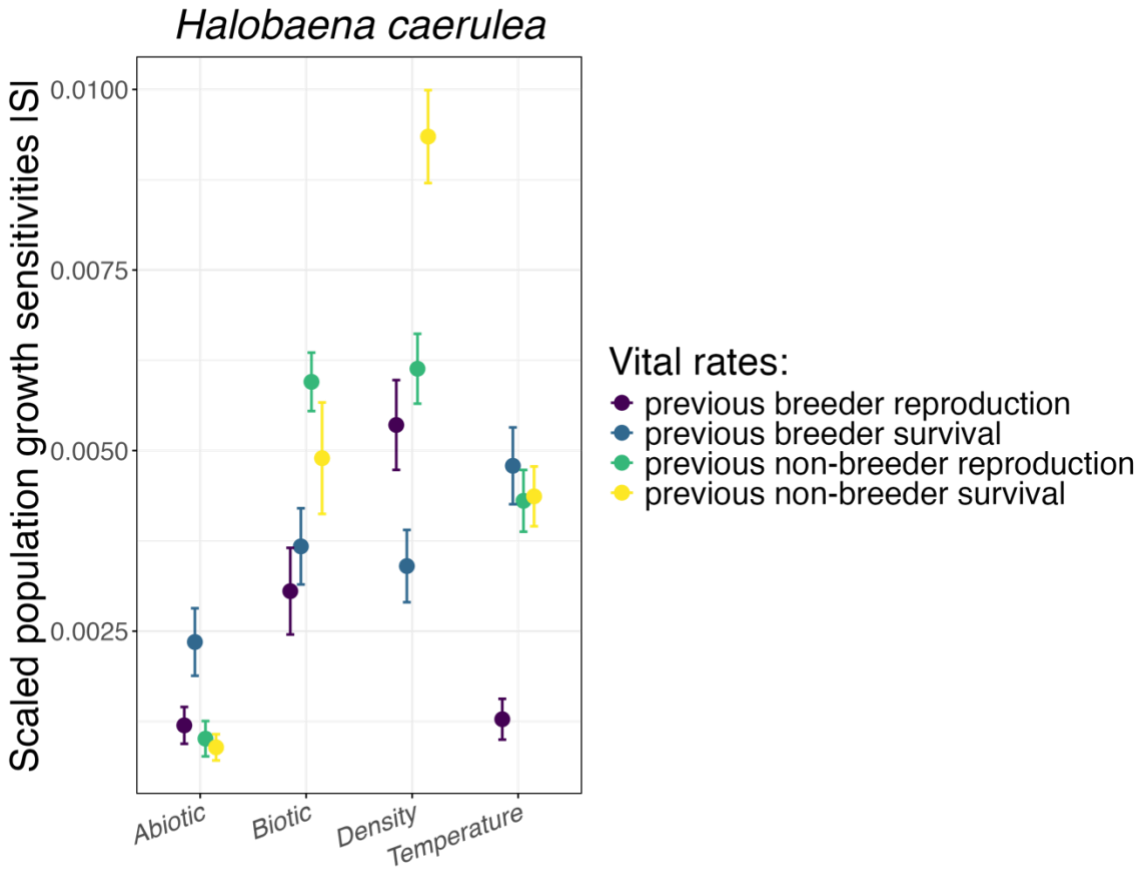

775

776 **Figure S14.** Scaled sensitivities of population growth rates per vital rate to different drivers for
777 *Halobaena caerulea*. The dots represent the mean scaled sensitivities across the calculated
778 resamplings per driver and vital rate combination ($n_{resamplings}$ = 50) and the error bars display the
779 standard errors. The abiotic driver here is the Southern Annular Mode, the biotic driver is
780 interspecific density, the density driver refers to intraspecific density, and the climatic driver is
781 sea surface temperature.

782

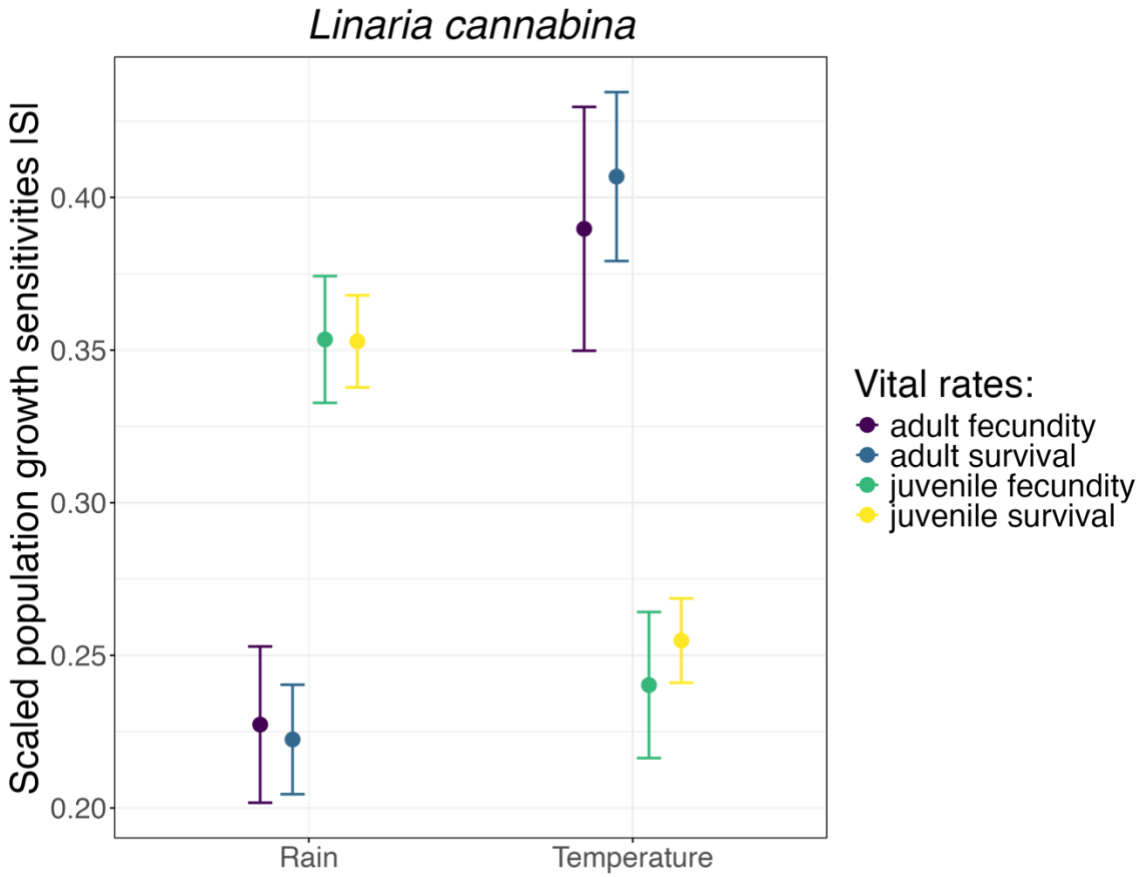

783

784 **Figure S15.** Scaled sensitivities of population growth rates per vital rate to different drivers for
785 *Linaria cannabina*. The dots represent the mean scaled sensitivities across the calculated
786 resamplings per driver and vital rate combination ($n_{resamplings}$ = 100) and the error bars display the
787 standard errors. The climatic drivers here are rain and temperature.

788

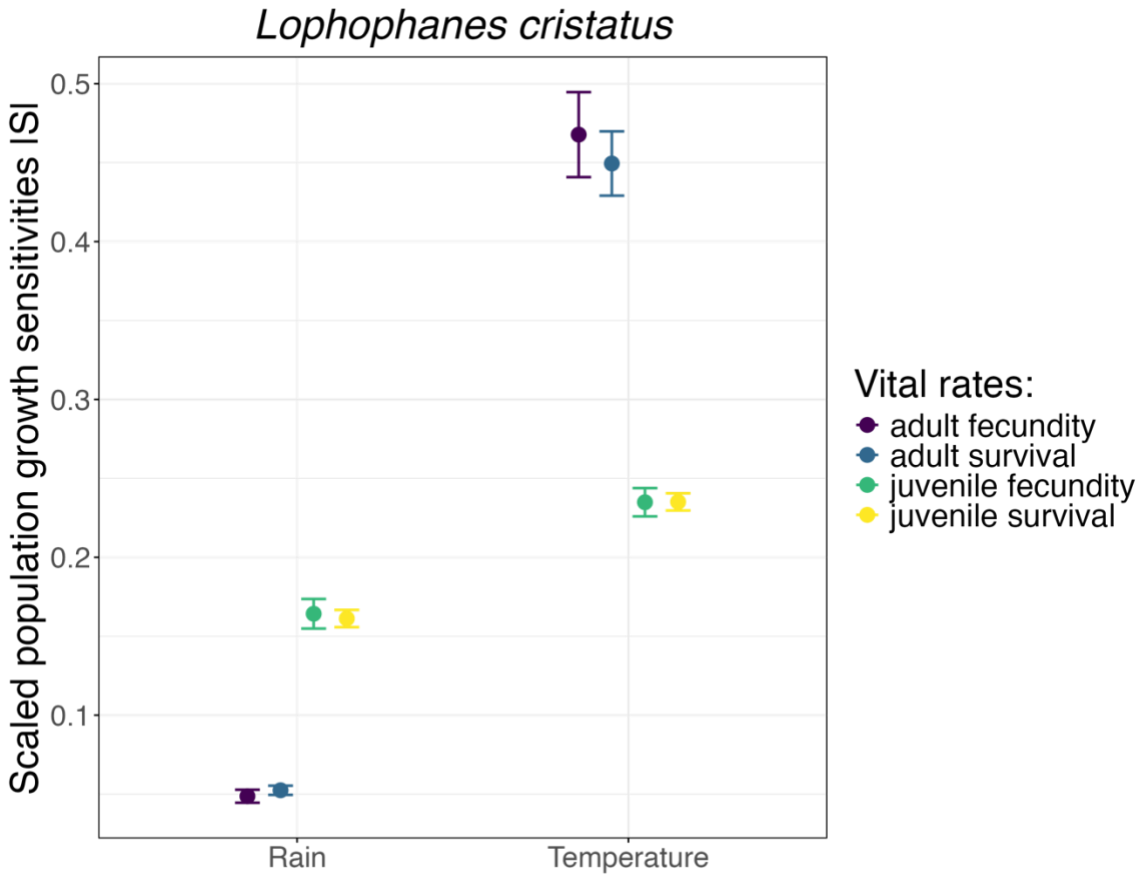

789

790 **Figure S16.** Scaled sensitivities of population growth rates per vital rate to different drivers for
791 *Lophophanes cristatus*. The dots represent the mean scaled sensitivities across the calculated
792 resamplings per driver and vital rate combination ($n_{resamplings}$ = 100) and the error bars display the
793 standard errors. The climatic drivers here are rain and temperature.

794

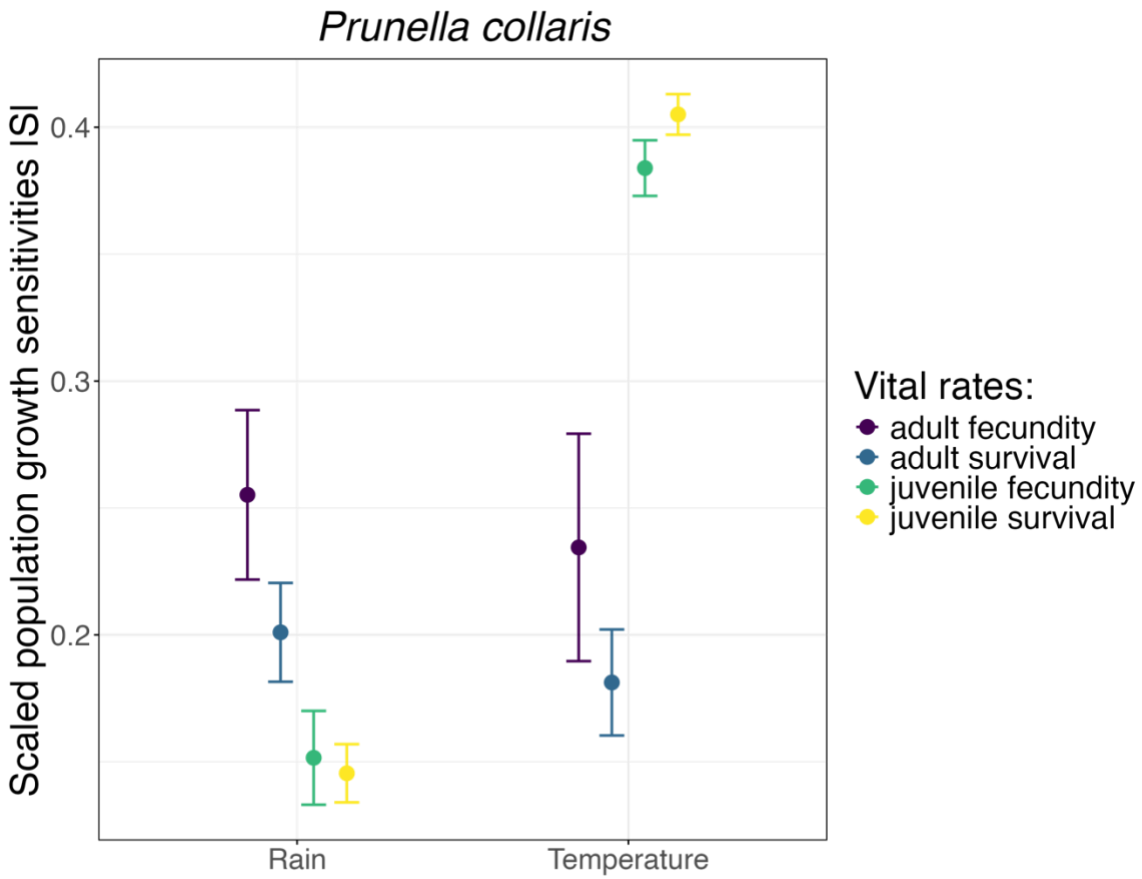

795

796 **Figure S17.** Scaled sensitivities of population growth rates per vital rate to different drivers for
797 *Prunella collaris*. The dots represent the mean scaled sensitivities across the calculated
798 resamplings per driver and vital rate combination ($n_{resamplings}$ = 100) and the error bars display the
799 standard errors. The climatic drivers here are rain and temperature.

800

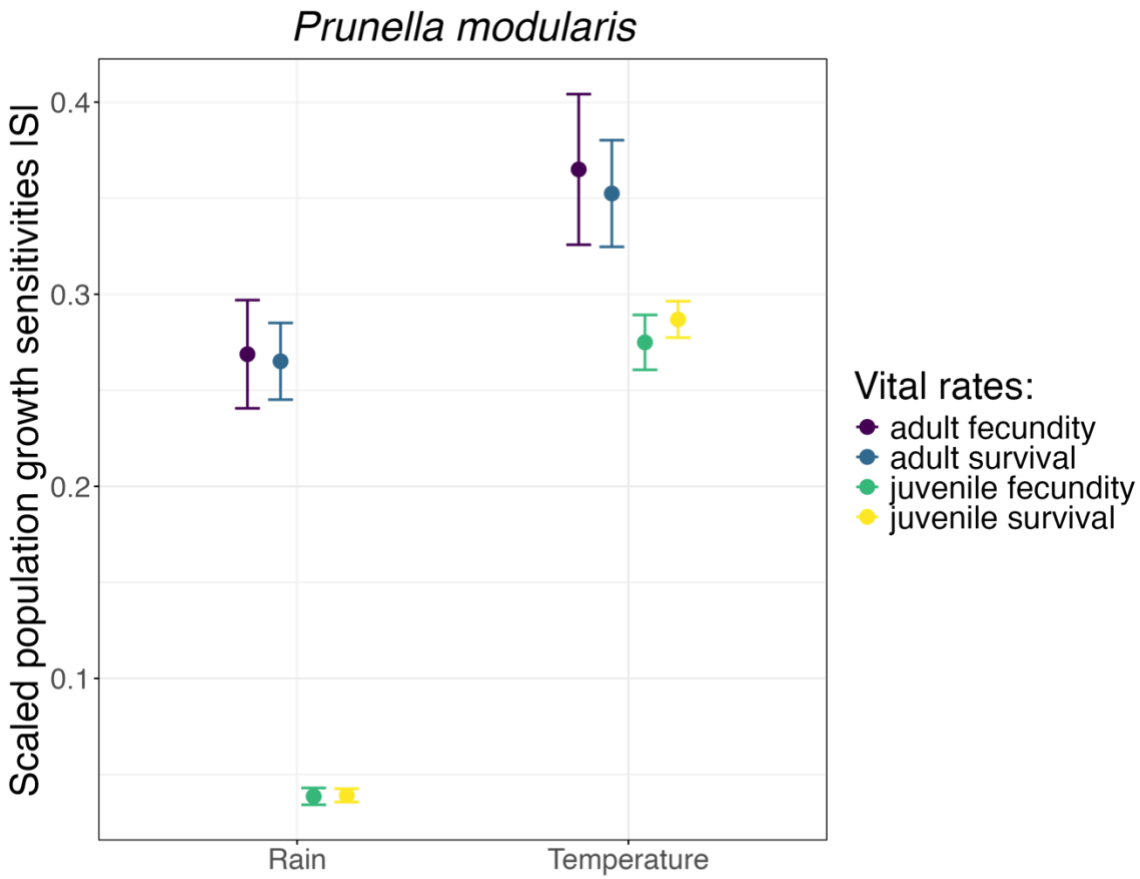

801

802 **Figure S18.** Scaled sensitivities of population growth rates per vital rate to different drivers for
803 *Prunella modularis*. The dots represent the mean scaled sensitivities across the calculated
804 resamplings per driver and vital rate combination ($n_{resamplings}$ = 100) and the error bars display the
805 standard errors. The climatic drivers here are rain and temperature.

806

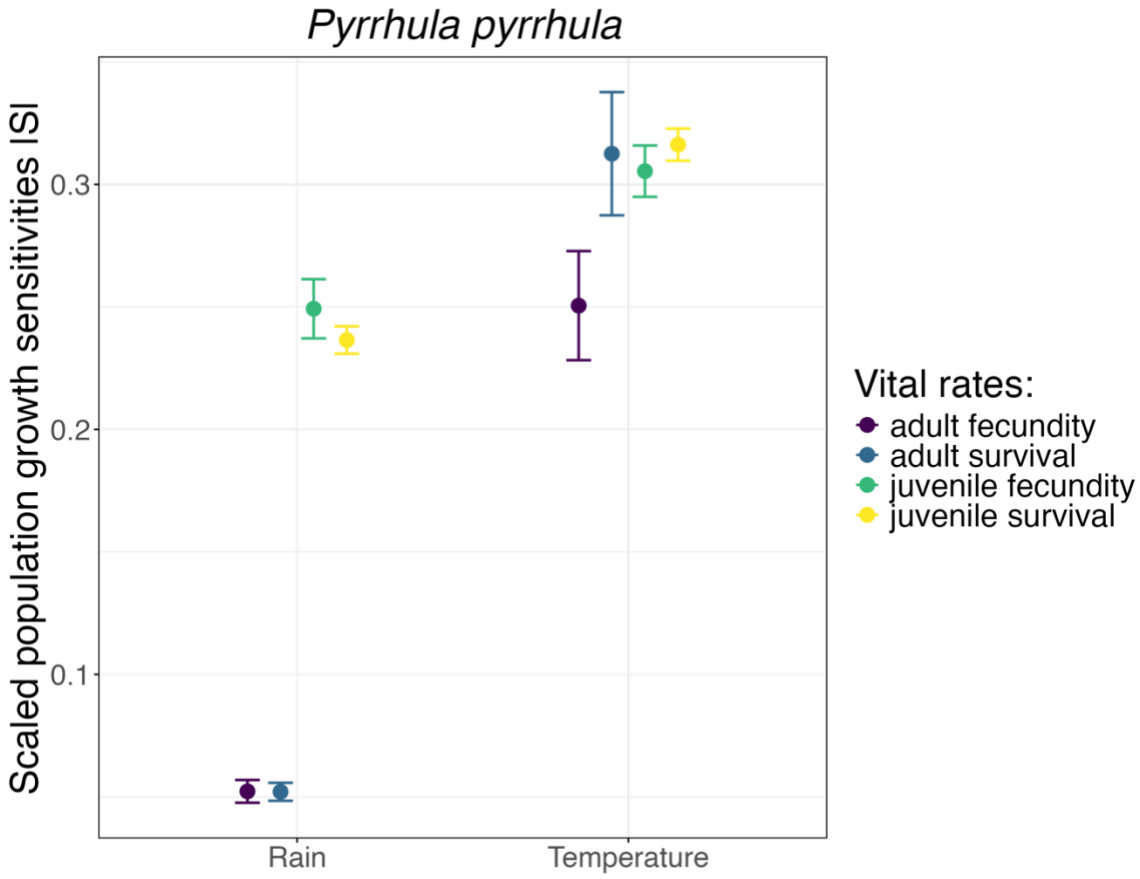

807

808 **Figure S19.** Scaled sensitivities of population growth rates per vital rate to different drivers for
809 *Pyrrhula pyrrhula*. The dots represent the mean scaled sensitivities across the calculated
810 resamplings per driver and vital rate combination ($n_{resamplings}$ = 100) and the error bars display the
811 standard errors. The climatic drivers here are rain and temperature.

812

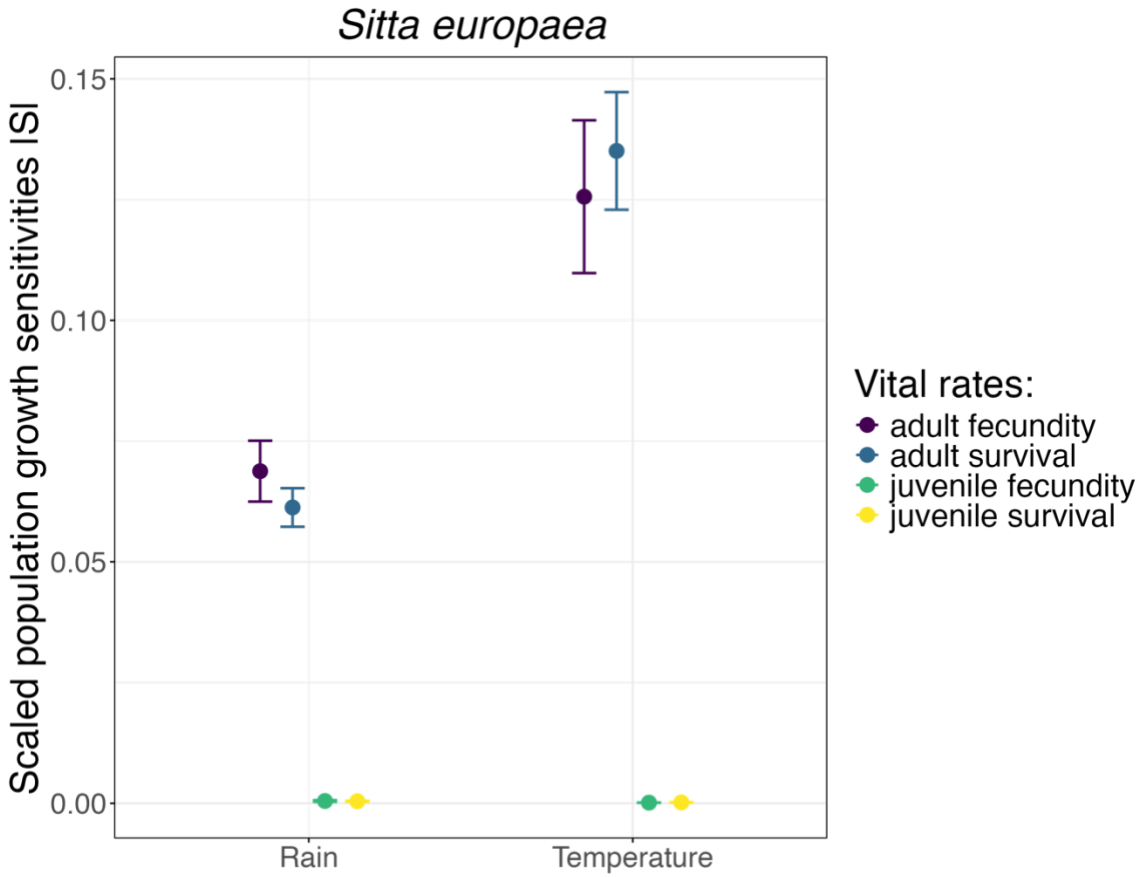

Figure S20. Scaled sensitivities of population growth rates per vital rate to different drivers for *Sitta europaea*. The dots represent the mean scaled sensitivities across the calculated resamplings per driver and vital rate combination ($n_{resamplings}$ = 100) and the error bars display the standard errors. The climatic drivers here are rain and temperature.

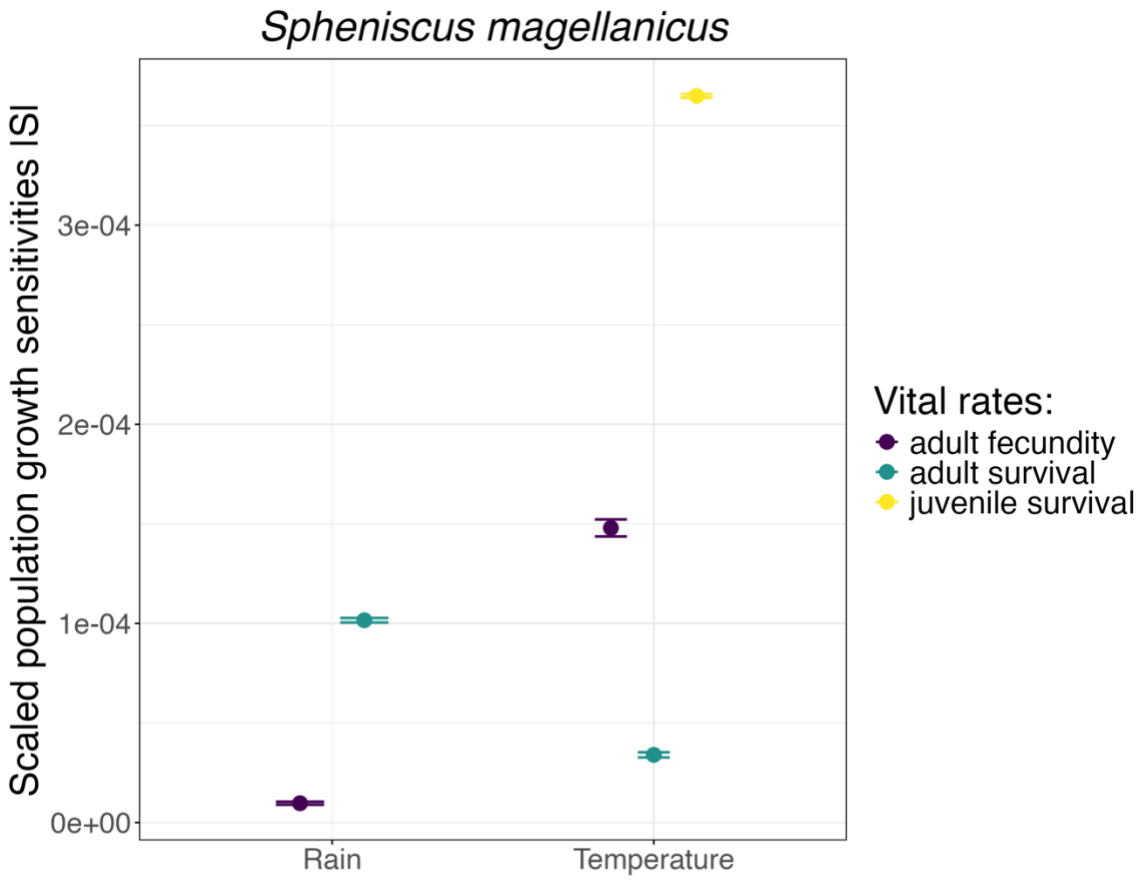

819

820 **Figure S21.** Scaled sensitivities of population growth rates per vital rate to different drivers for
821 *Spheniscus magellanicus*. The dots represent the mean scaled sensitivities across the calculated
822 resamplings per driver and vital rate combination ($n_{resamplings}$ = 100) and the error bars display the
823 standard errors. The climatic drivers here are rain, temperature, and sea surface temperature
824 anomalies (also classified as temperature).

825

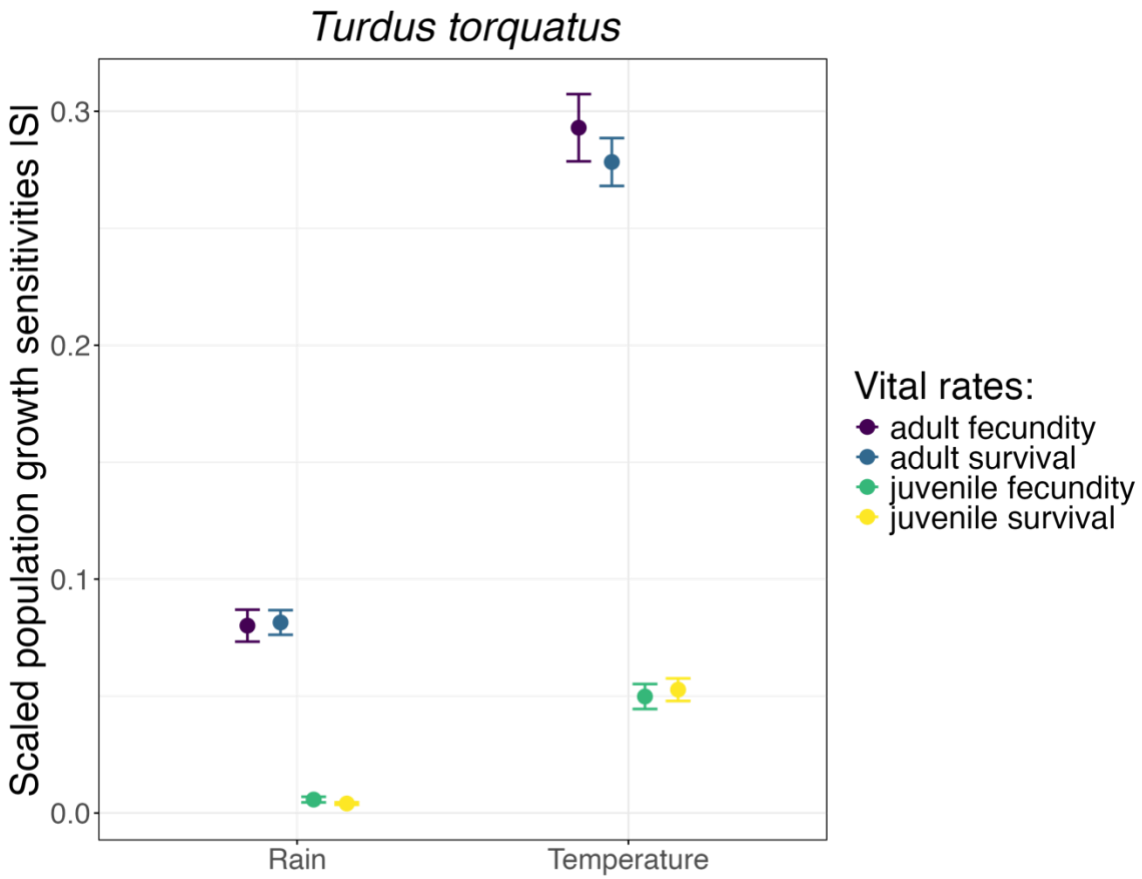

826

827 **Figure S22.** Scaled sensitivities of population growth rates per vital rate to different drivers for
828 *Turdus torquatus*. The dots represent the mean scaled sensitivities across the calculated
829 resamplings per driver and vital rate combination ($n_{resamplings}$ = 100) and the error bars display the
830 standard errors. The climatic drivers here are rain and temperature.

831

832

833

834

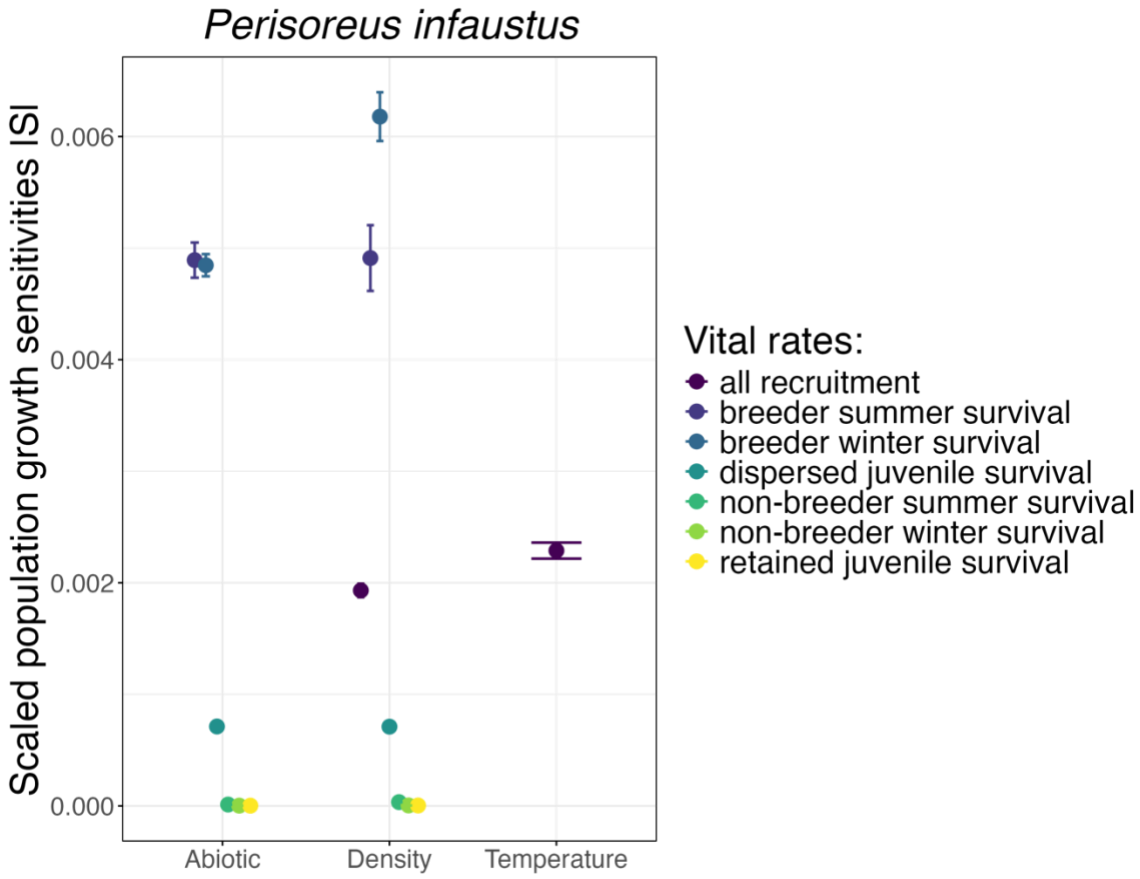

Figure S23. Scaled sensitivities of population growth rates per vital rate to different drivers for *Perisoreus infaustus*. The dots represent the mean scaled sensitivities across the calculated resamplings per driver and vital rate combination ($n_{resamplings}$ = 100) and the error bars display the standard errors. The climatic drivers here are rain and temperature.

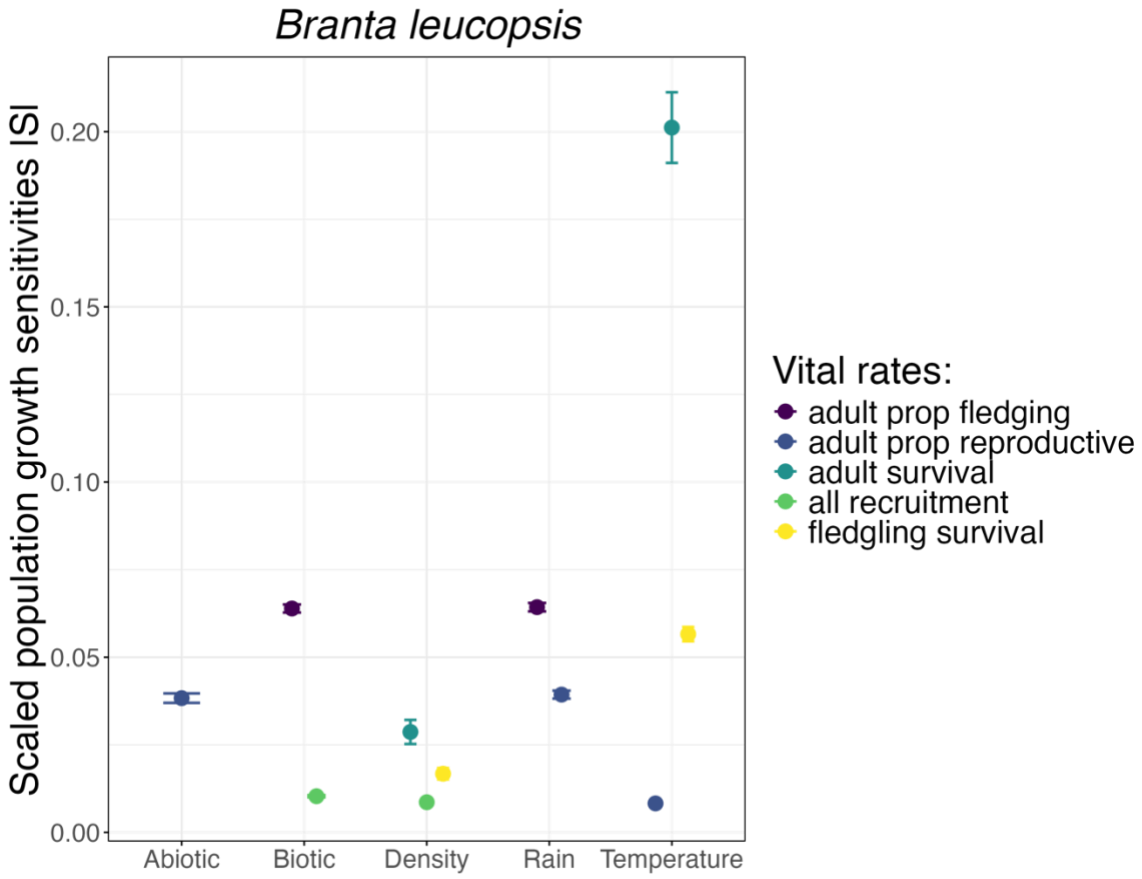

841

842 **Figure S24.** Scaled sensitivities of population growth rates per vital rate to different drivers for
843 *Branta leucopsis*. The dots represent the mean scaled sensitivities across the calculated
844 resamplings per driver and vital rate combination ($n_{resamplings}$ = 100) and the error bars display the
845 standard errors. The climatic drivers here are rain and temperature.

846

847

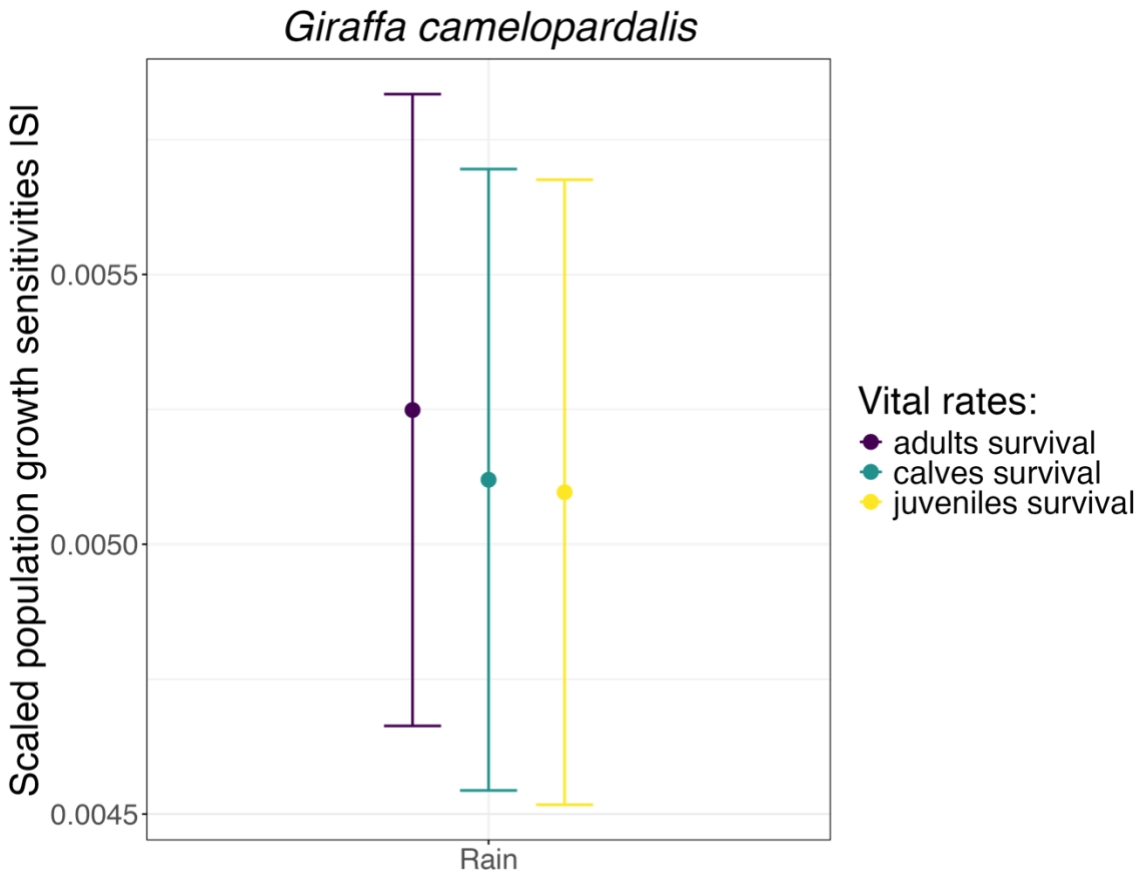

Figure S25. Scaled sensitivities of population growth rates per vital rate to different drivers for *Giraffa camelopardalis*. The dots represent the mean scaled sensitivities across the calculated resamplings per driver and vital rate combination ($n_{resamplings}$ = 100) and the error bars display the standard errors. The climatic driver here is rain.

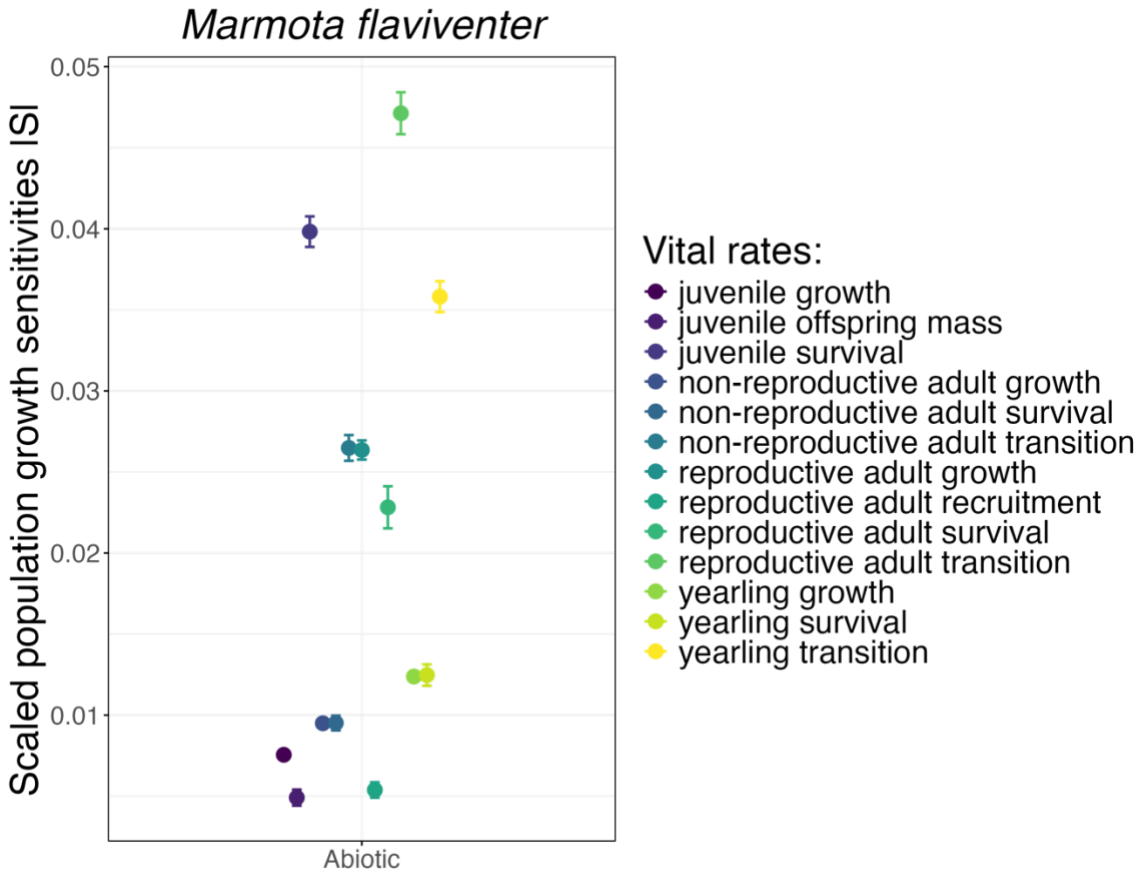

Figure S26. Scaled sensitivities of population growth rates per vital rate to different drivers for *Marmota flaviventer*. The dots represent the mean scaled sensitivities across the calculated resamplings per driver and vital rate combination ($n_{resamplings}$ = 100) and the error bars display the standard errors. The abiotic driver here is Q, which is a composite measure, including climate, representing environmental quality.

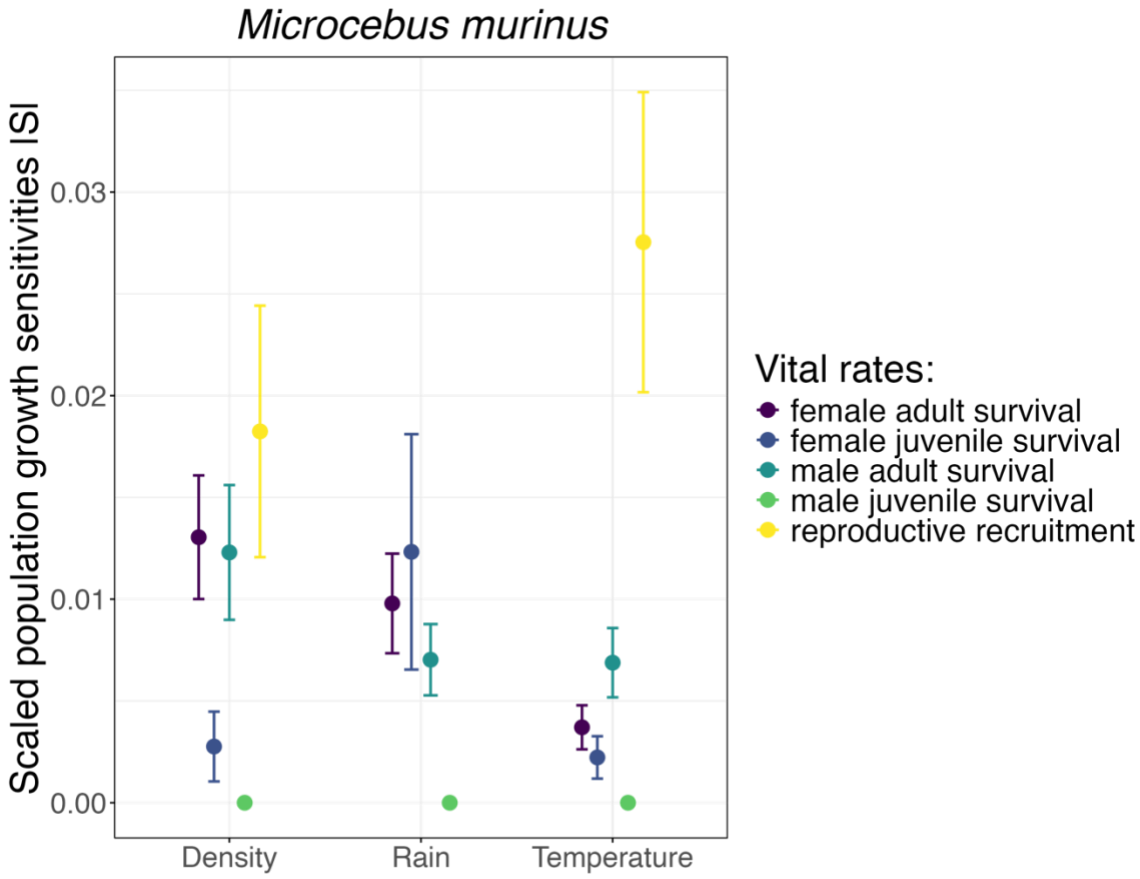

Figure S27. Scaled sensitivities of population growth rates per vital rate to different drivers for *Microcebus murinus*. The dots represent the mean scaled sensitivities across the calculated resamplings per driver and vital rate combination ($n_{resamplings}$ = 100) and the error bars display the standard errors. The density driver refers to intraspecific density, and the climatic drivers are rain and temperature.

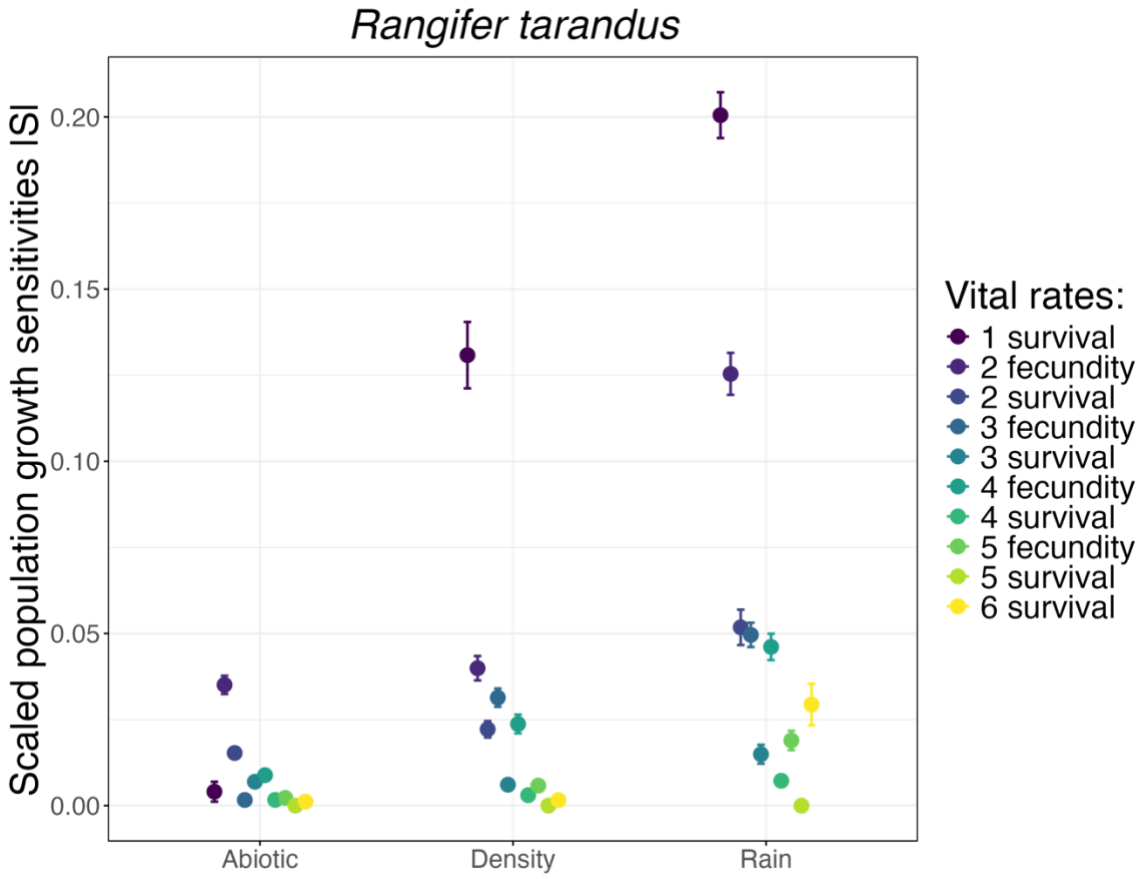

868

869 **Figure S28.** Scaled sensitivities of population growth rates per vital rate to different drivers for
870 *Rangifer tarandus*. The dots represent the mean scaled sensitivities across the calculated
871 resamplings per driver and vital rate combination ($n_{resamplings}$ = 100) and the error bars display the
872 standard errors. The abiotic driver here is winter length, the density driver refers to intraspecific
873 density, and the climatic driver is rain-on-snow, classified as rain.

874

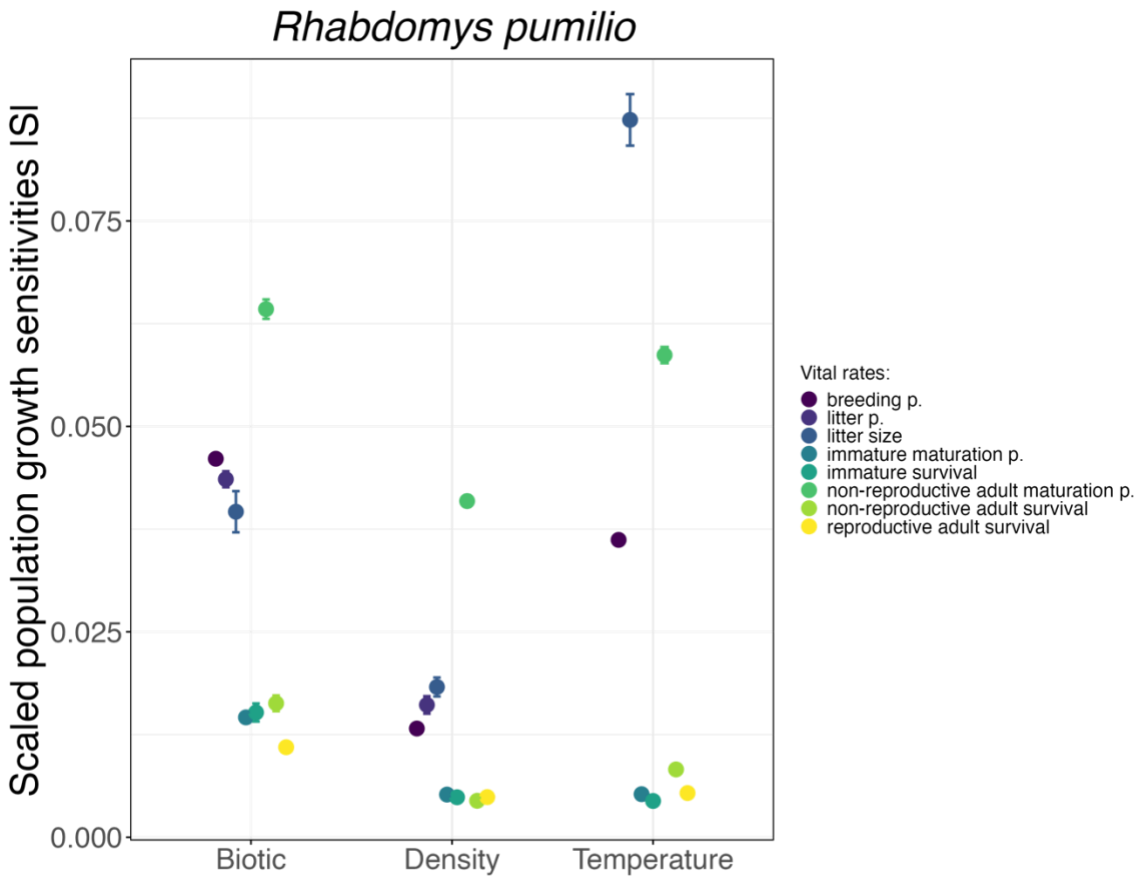

875

876 **Figure S29.** Scaled sensitivities of population growth rates per vital rate to different drivers for
877 *Rhabdomys pumilio*. The dots represent the mean scaled sensitivities across the calculated
878 resamplings per driver and vital rate combination ($n_{resamplings}$ = 100) and the error bars display the
879 standard errors. The biotic driver is food availability, the density here refers to intraspecific
880 density, and the climatic driver is temperature.

881

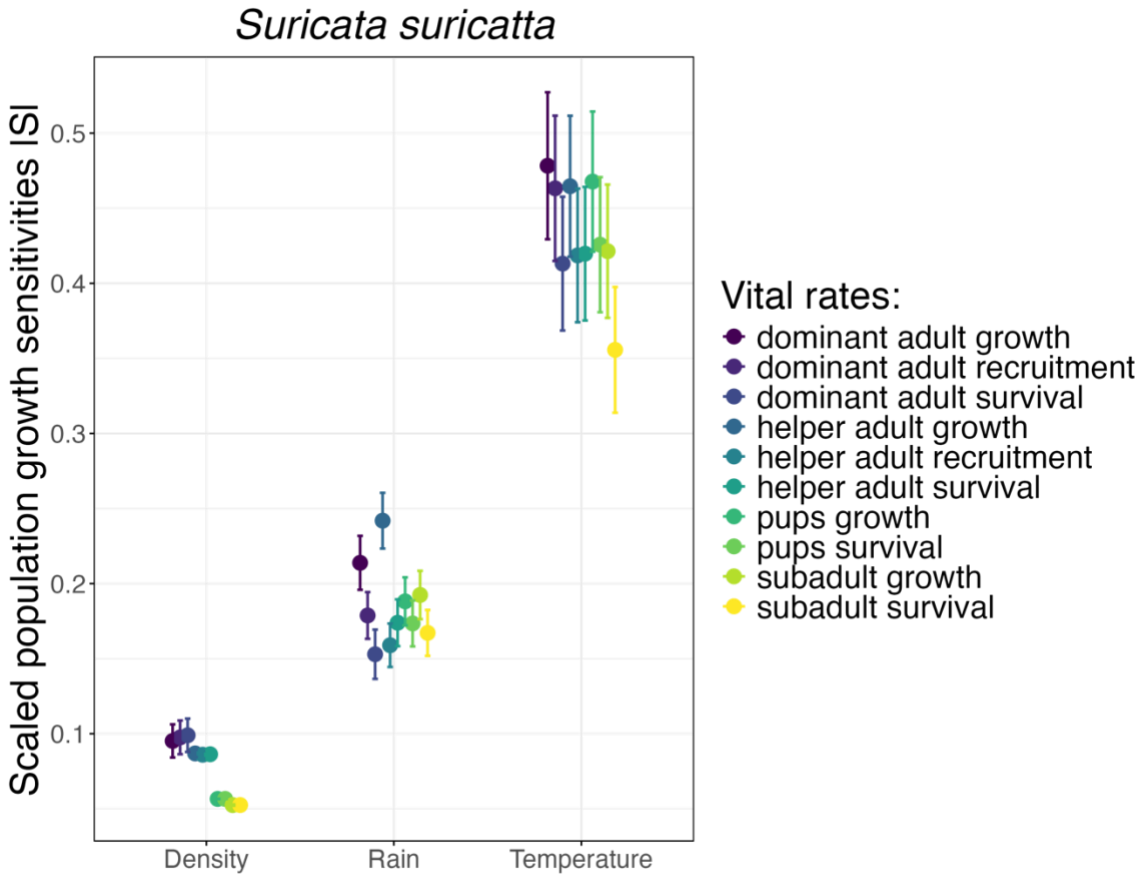

882

883 **Figure S30.** Scaled sensitivities of population growth rates per vital rate to different drivers for
884 *Suricata suricatta*. The dots represent the mean scaled sensitivities across the calculated
885 resamplings per driver and vital rate combination ($n_{resamplings}$ = 100) and the error bars display the
886 standard errors. The climatic drivers here are rain and temperature.

887

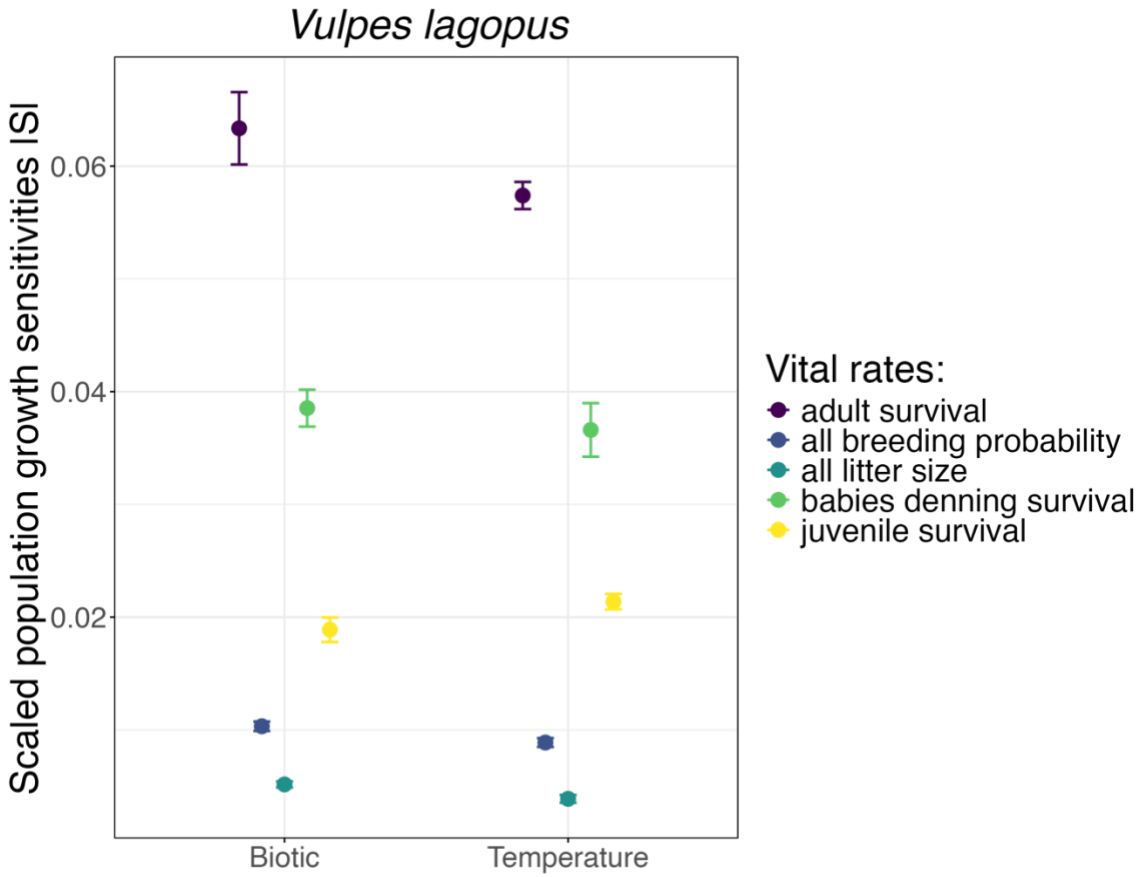

888

889 **Figure S31.** Scaled sensitivities of population growth rates per vital rate to different drivers for
890 *Vulpes lagopus*. The dots represent the mean scaled sensitivities across the calculated resamplings
891 per driver and vital rate combination ($n_{resamplings}$ = 100) and the error bars display the standard
892 errors. The biotic driver here represents reindeer carcass availability and goose abundance, and
893 the climatic driver is sea ice extent, also classified as sea ice extent.

894

895

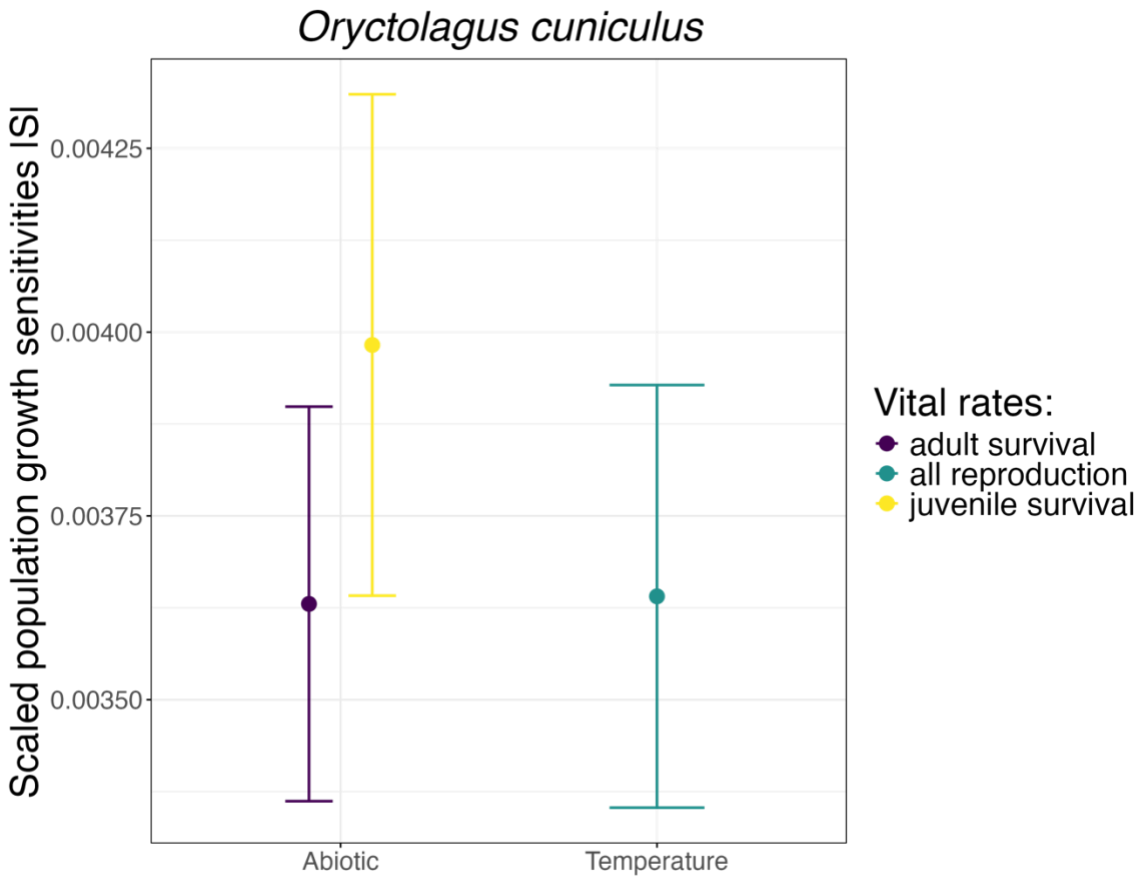

Figure S32. Scaled sensitivities of population growth rates per vital rate to different drivers for *Oryctolagus cuniculus*. The dots represent the mean scaled sensitivities across the calculated resamplings per driver and vital rate combination ($n_{resamplings}$ = 100) and the error bars display the standard errors. The biotic driver here represents reindeer carcass availability and goose abundance, and the climatic driver is sea ice extent, also classified as sea ice extent.

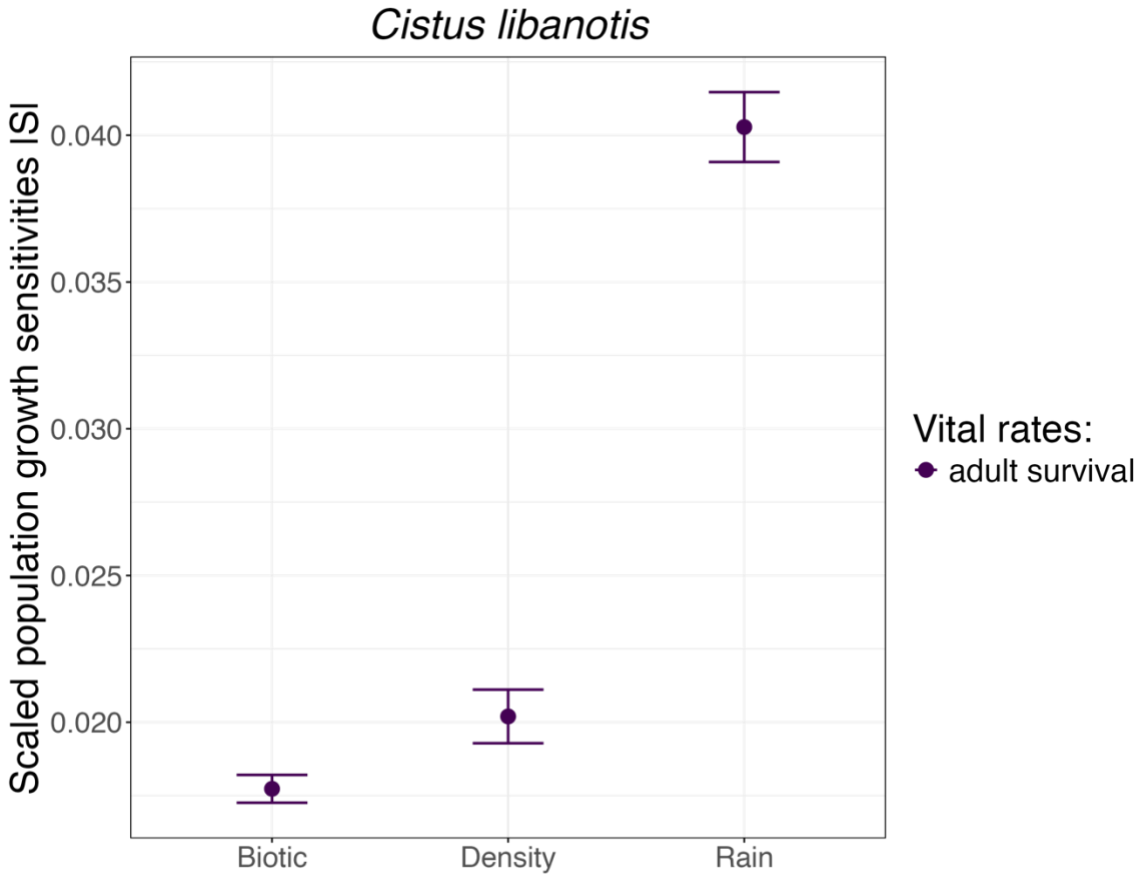

Figure S33. Scaled sensitivities of population growth rates per vital rate to different drivers for *Cistus libanotis*. The dots represent the mean scaled sensitivities across the calculated resamplings per driver and vital rate combination ($n_{resamplings}$ = 100) and the error bars display the standard errors. The biotic driver is interspecific density, the climatic driver is rain, and density represents intraspecific density.

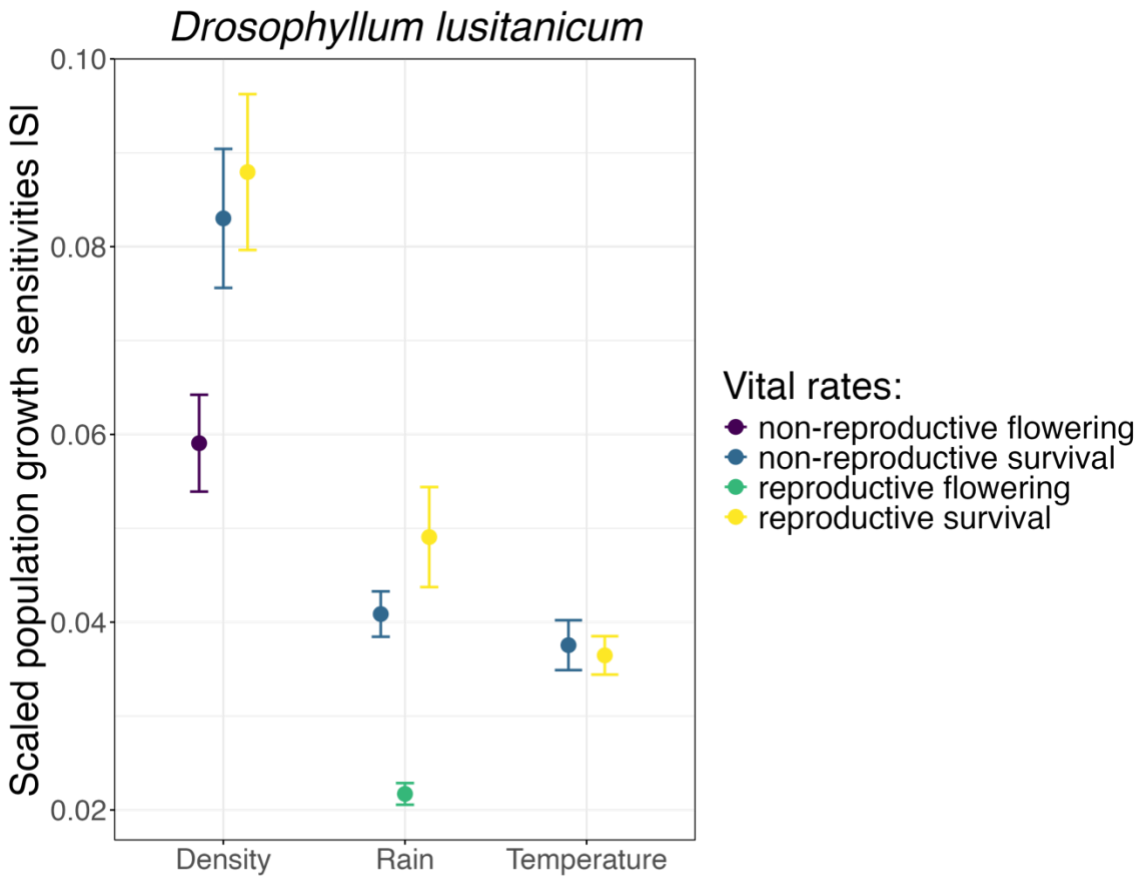

Figure S34. Scaled sensitivities of population growth rates per vital rate to different drivers for *Drosophyllum lusitanicum*. The dots represent the mean scaled sensitivities across the calculated resamplings per driver and vital rate combination ($n_{resamplings}$ = 100) and the error bars display the standard errors. The climatic drivers are rain and temperature, and density represents intraspecific density.

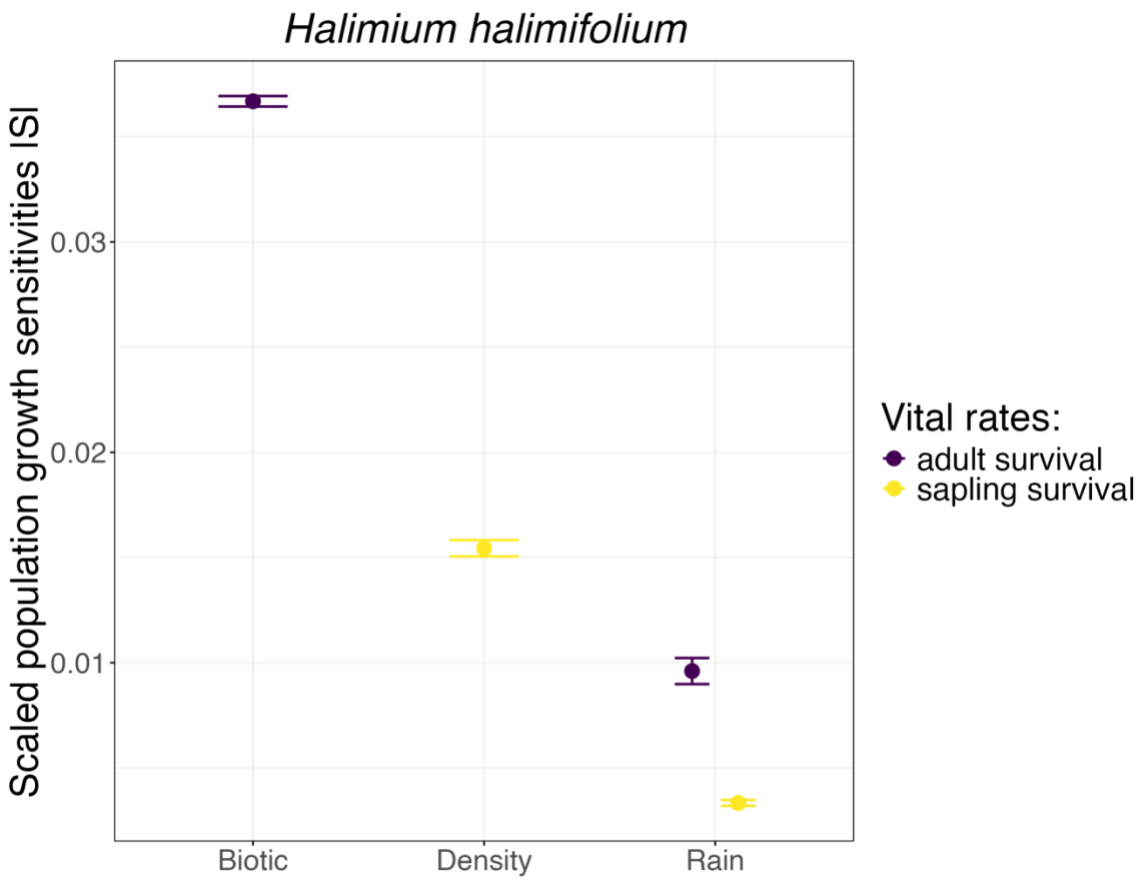

Figure S35. Scaled sensitivities of population growth rates per vital rate to different drivers for *Halimium halimifolium*. The dots represent the mean scaled sensitivities across the calculated resamplings per driver and vital rate combination ($n_{resamplings}$ = 100) and the error bars display the standard errors. The biotic driver is interspecific density, the climatic driver is rain, and density represents intraspecific density.

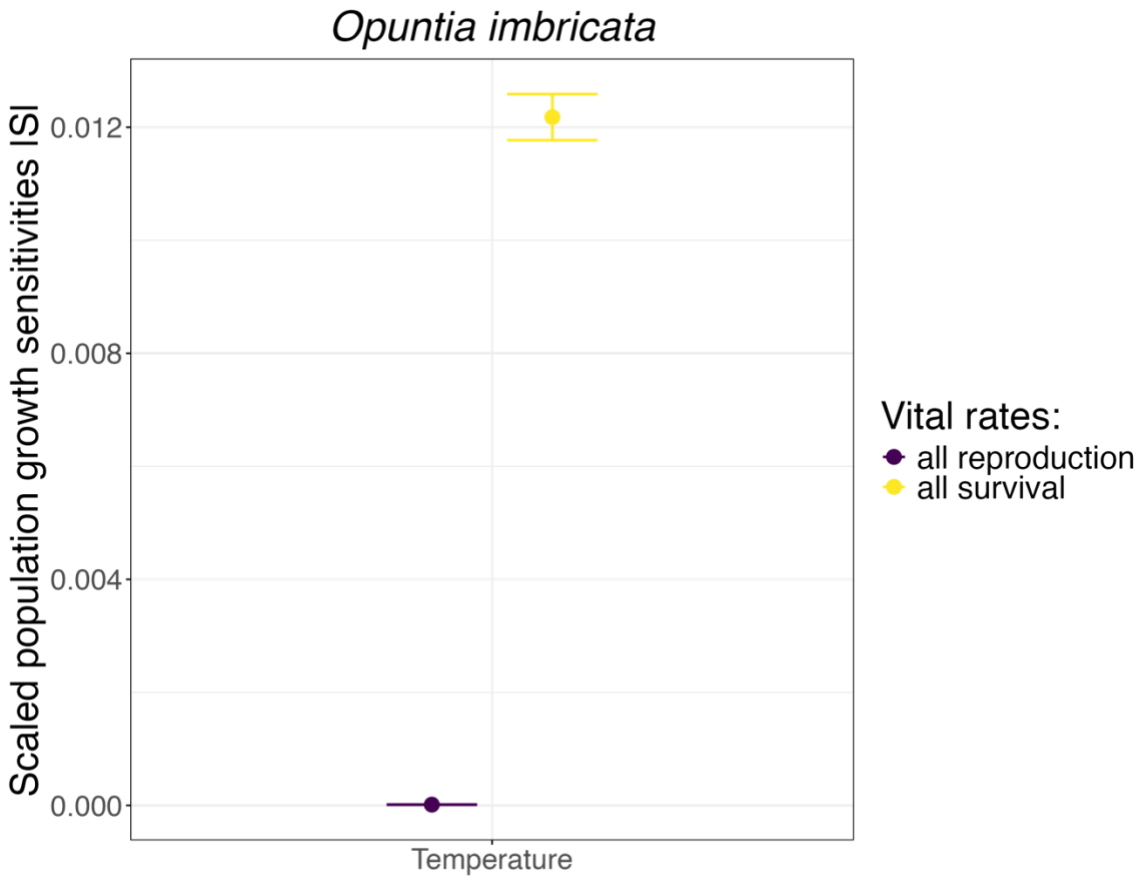

Figure S36. Scaled sensitivities of population growth rates per vital rate to different drivers for *Opuntia imbricata*. The dots represent the mean scaled sensitivities across the calculated resamplings per driver and vital rate combination ($n_{resamplings}$ = 100) and the error bars display the standard errors. The climatic driver temperature represents mean average daily temperatures of two different time windows and mean minimum daily temperature.

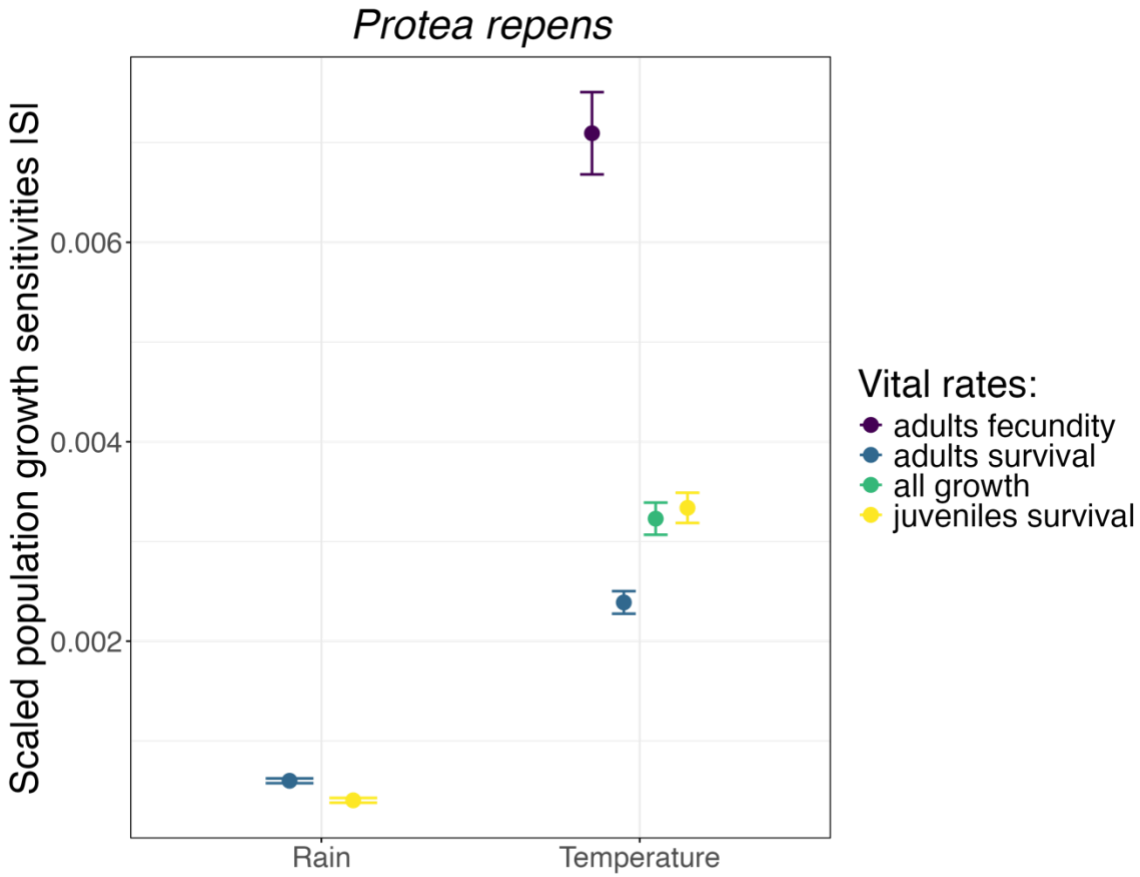

Figure S37. Scaled sensitivities of population growth rates per vital rate to different drivers for *Protea repens*. The dots represent the mean scaled sensitivities across the calculated resamplings per driver and vital rate combination ($n_{resamplings}$ = 100) and the error bars display the standard errors. The climatic drivers are rain and temperature.

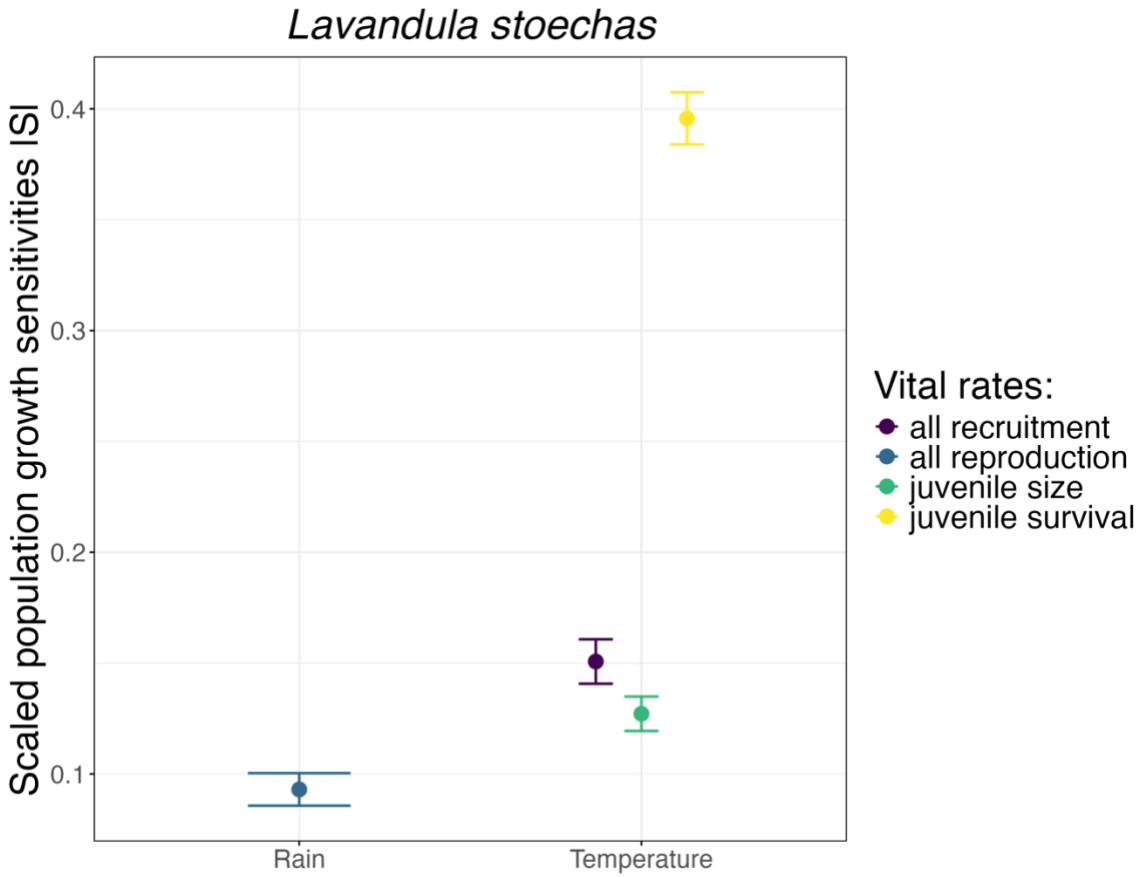

940

941 **Figure S38.** Scaled sensitivities of population growth rates per vital rate to different drivers for
942 *Lavandula stoechas*. The dots represent the mean scaled sensitivities across the calculated
943 resamplings per driver and vital rate combination ($n_{resamplings}$ = 100) and the error bars display the
944 standard errors. The climatic drivers are rain and temperature.

945

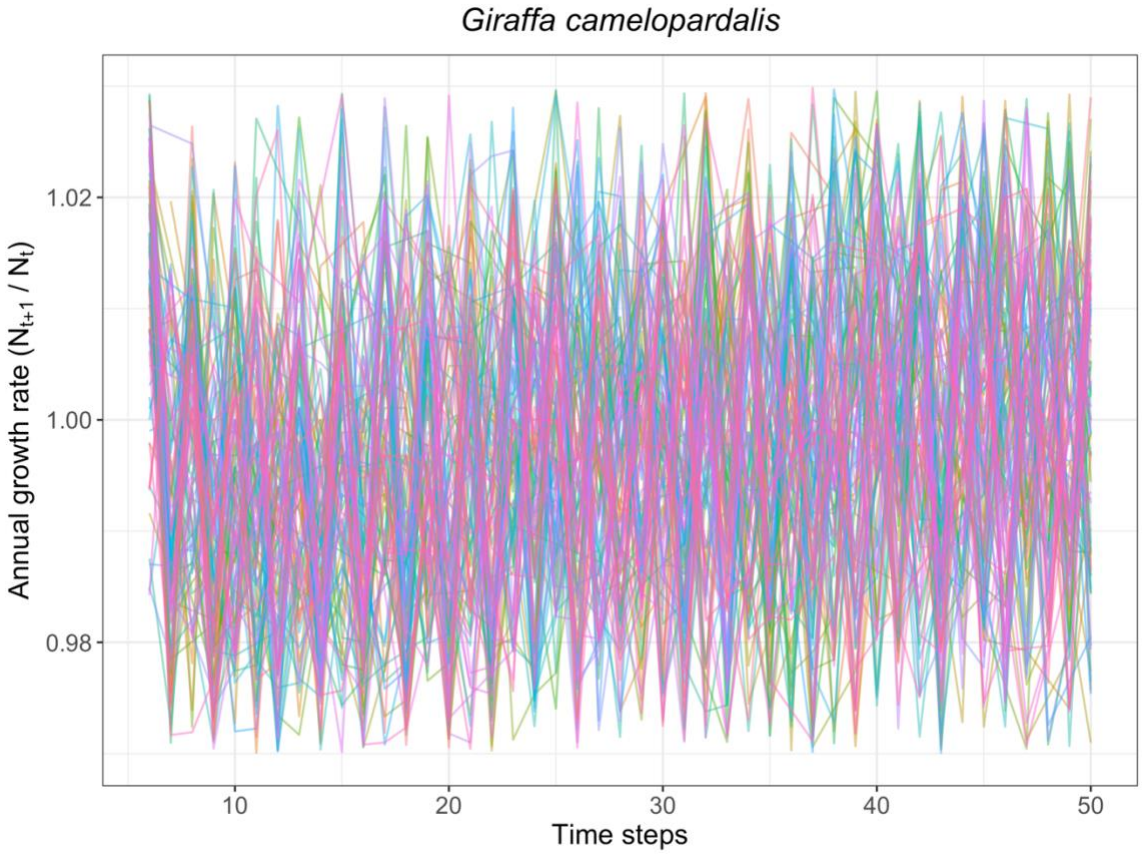

946

947 **Figure S39.** Time series of simulated annual growth rates (N_{t+1}/N_t) for *Giraffa camelopardalis*,
948 which we averaged to calculate λ (after discarding transient dynamics). The colors represent the
949 multiple simulations (n = 100).

950

951

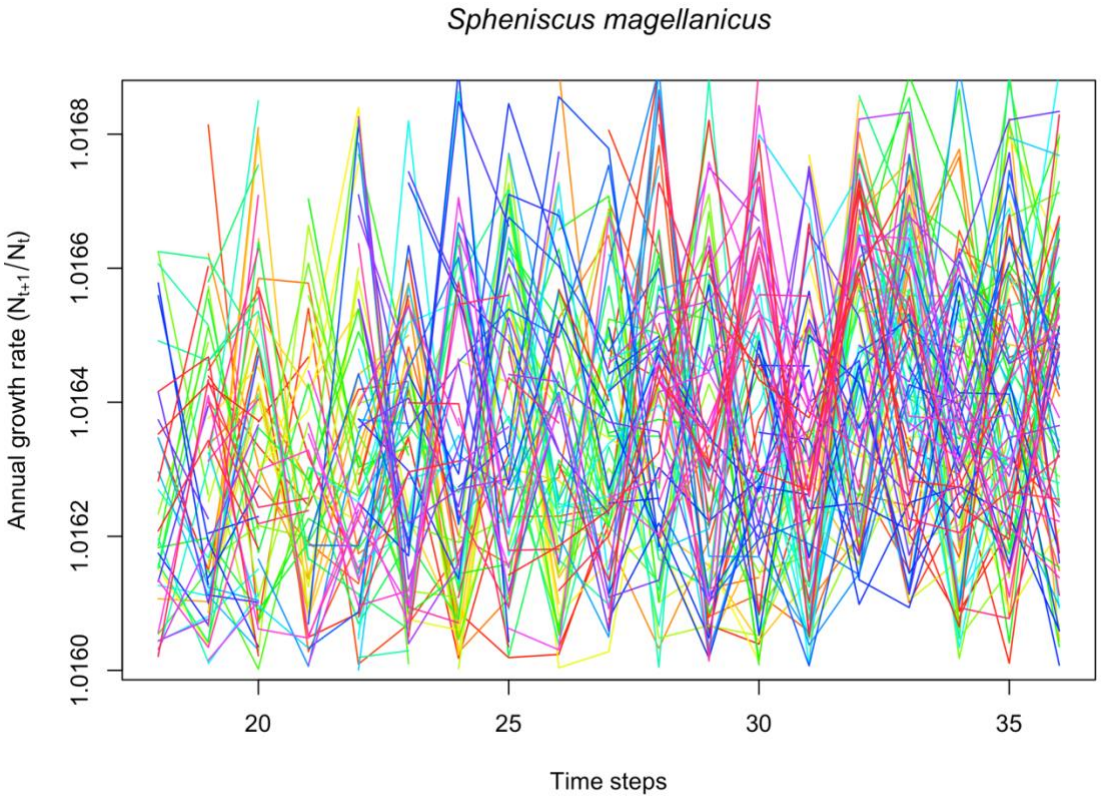

952

953 **Figure S40.** Time series of simulated annual growth rates (N_{t+1}/N_t) for *Spheniscus magellanicus*,
954 which we averaged to calculate λ (after discarding transient dynamics). The colors represent the
955 multiple simulations (n = 100).

956

957

958

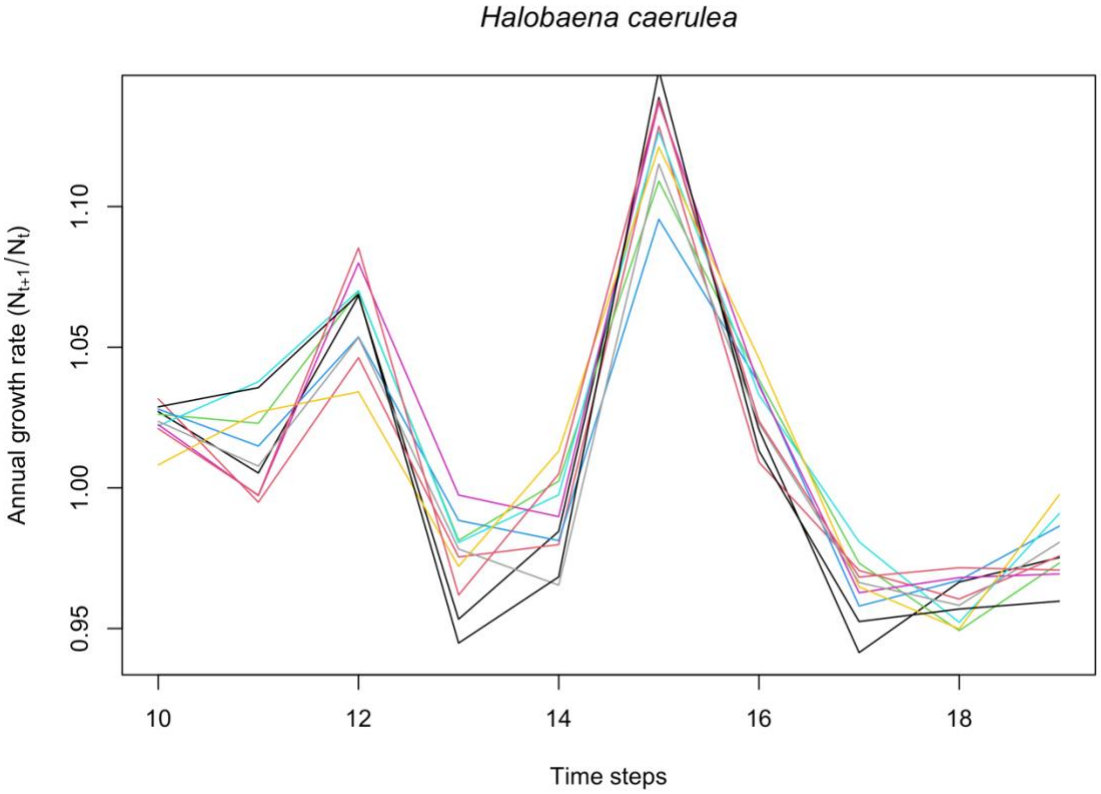

959

960 **Figure S41.** Time series of simulated annual growth rates (N_{t+1}/N_t) for *Halobaena caerulea*,
961 which we averaged to calculate λ (after discarding transient dynamics). The colors represent the
962 multiple simulations (n = 10).

963

964

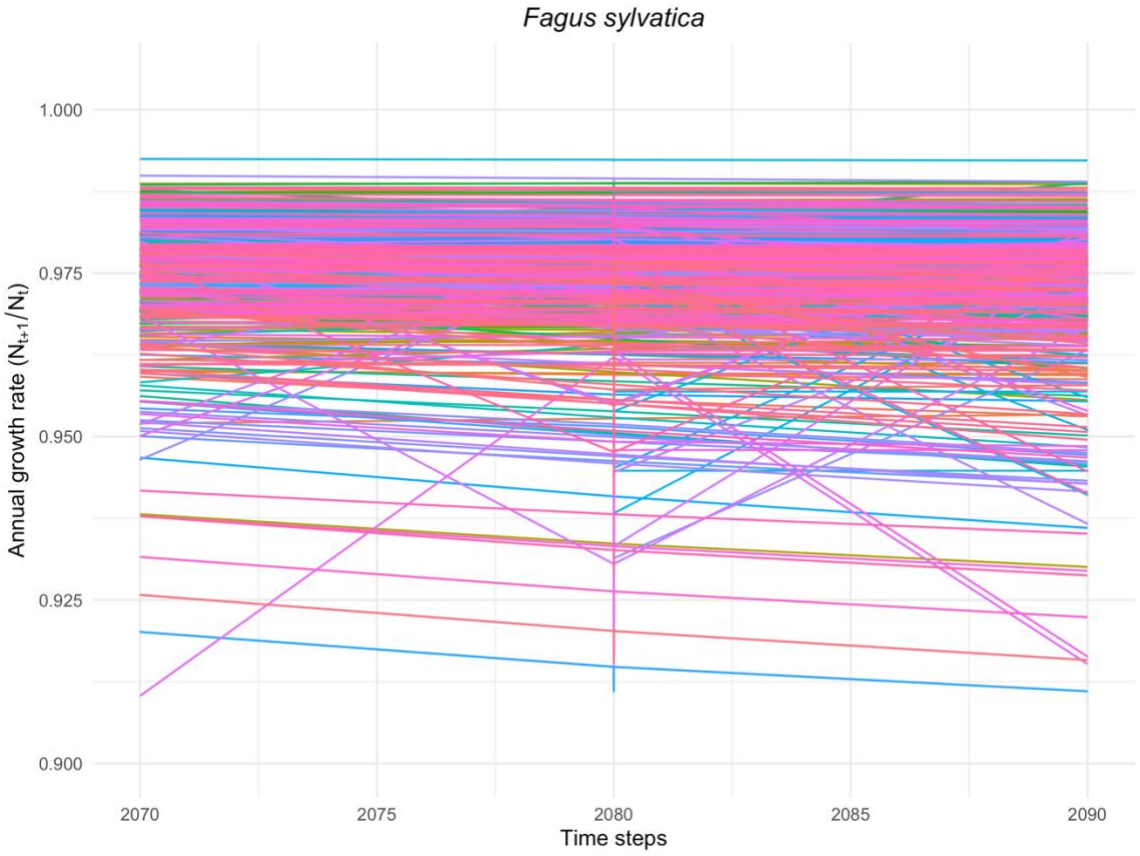

965

966 **Figure S42.** Time series of simulated annual growth rates (N_{t+1}/N_t) for *Fagus sylvatica*, which we
967 averaged to calculate λ (after discarding transient dynamics). The colors represent the multiple
968 simulations and sites (see species-specific details in SI). The variation in λ is largely attributed to
969 variation among sites as we ensured to remove sites from analyses where λ values changed
970 direction in simulations.

971

972

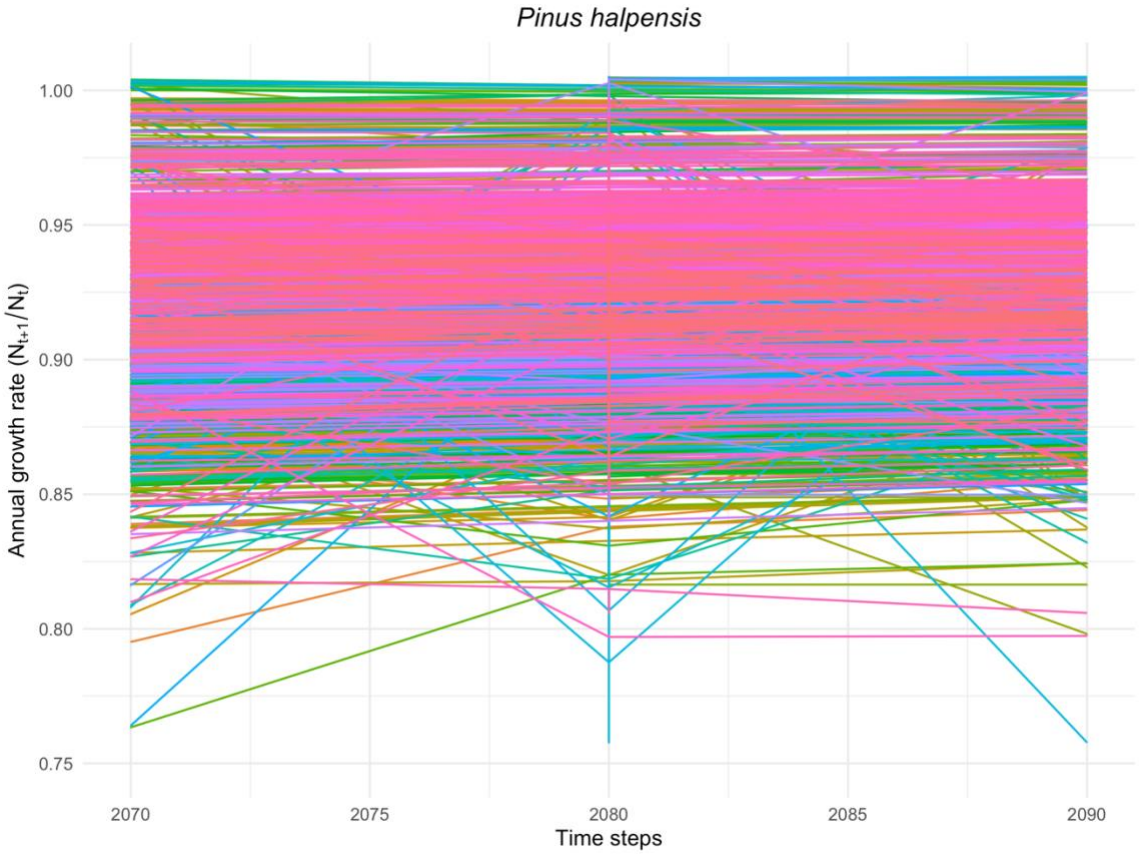

Figure S43. Time series of simulated annual growth rates (N_{t+1}/N_t) for *Pinus halepensis*, which we averaged to calculate λ (after discarding transient dynamics). The colors represent the multiple simulations and sites (see species-specific details in SI). The variation in λ is largely attributed to variation among sites as we ensured to remove sites from analyses where λ values changed direction in simulations.

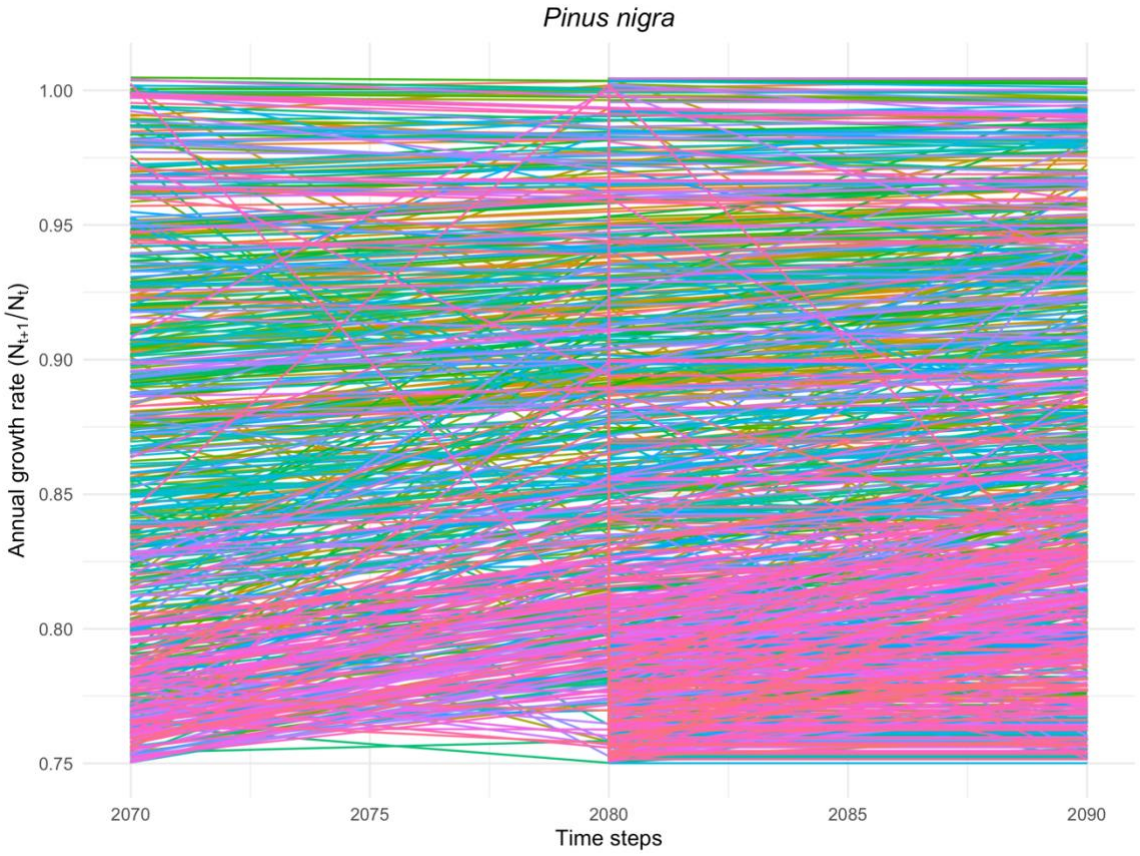

Figure S44. Time series of simulated annual growth rates (N_{t+1}/N_t) for *Pinus nigra*, which we averaged to calculate λ (after discarding transient dynamics). The colors represent the multiple simulations and sites (see species-specific details in SI). The variation in λ is largely attributed to variation among sites as we ensured to remove sites from analyses where λ values changed direction in simulations.

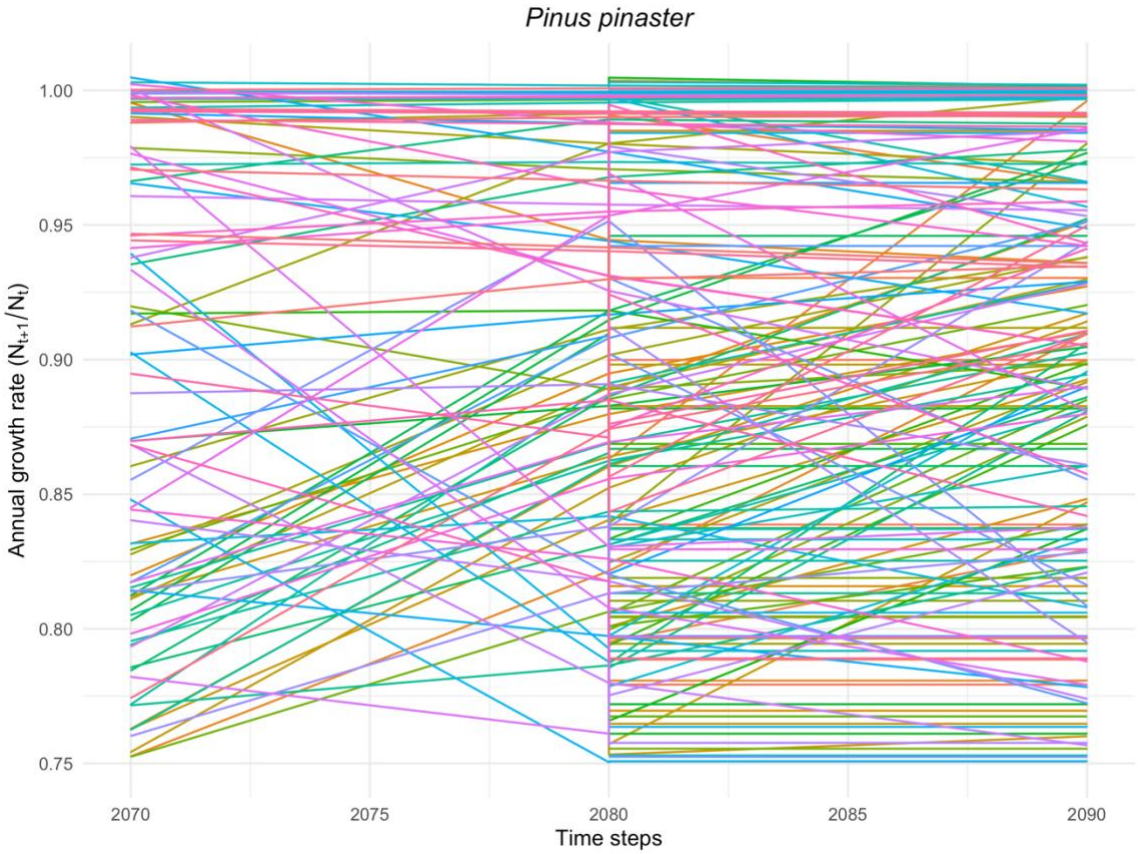

Figure S45. Time series of simulated annual growth rates (N_{t+1}/N_t) for *Pinus pinaster*, which we averaged to calculate λ (after discarding transient dynamics). The colors represent the multiple simulations and sites (see species-specific details in SI). The variation in λ is largely attributed to variation among sites as we ensured to remove sites from analyses where λ values changed direction in simulations.

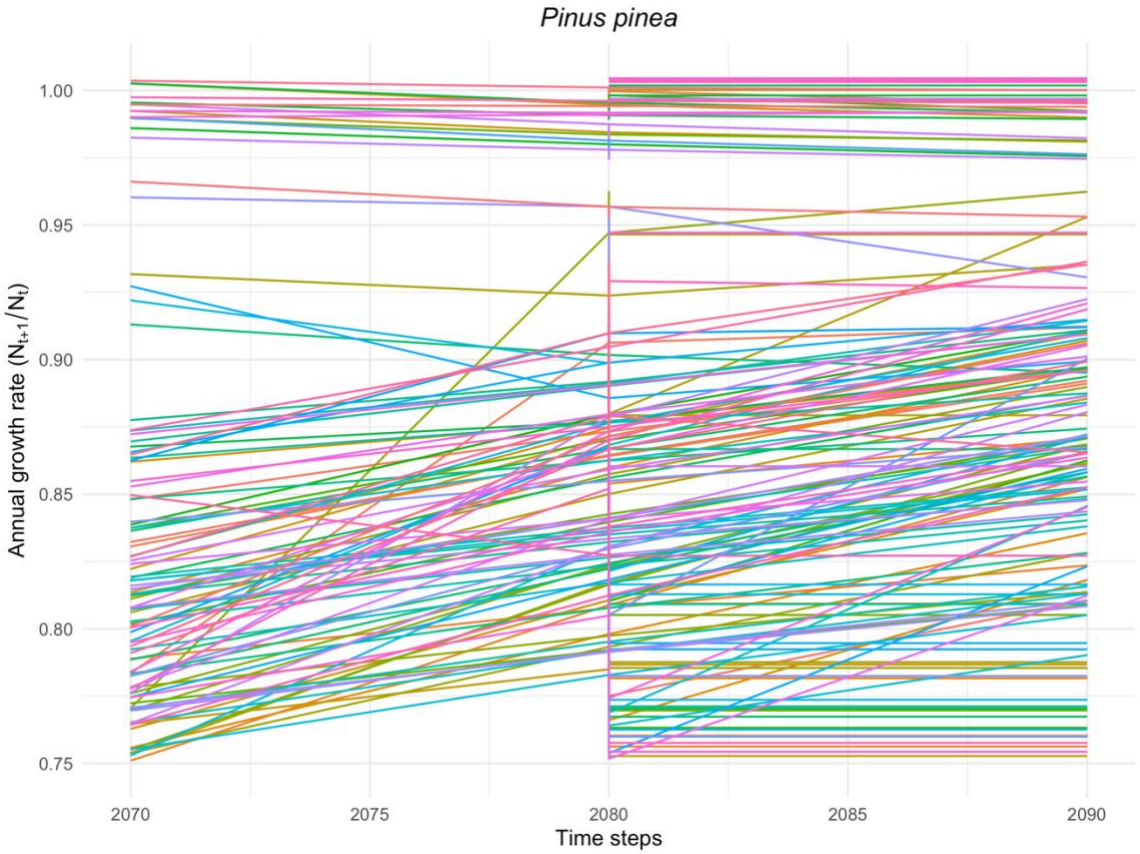

Figure S46. Time series of simulated annual growth rates (N_{t+1}/N_t) for *Pinus pinea*, which we averaged to calculate λ (after discarding transient dynamics). The colors represent the multiple simulations and sites (see species-specific details in SI). The variation in λ is largely attributed to variation among sites as we ensured to remove sites from analyses where λ values changed direction in simulations.

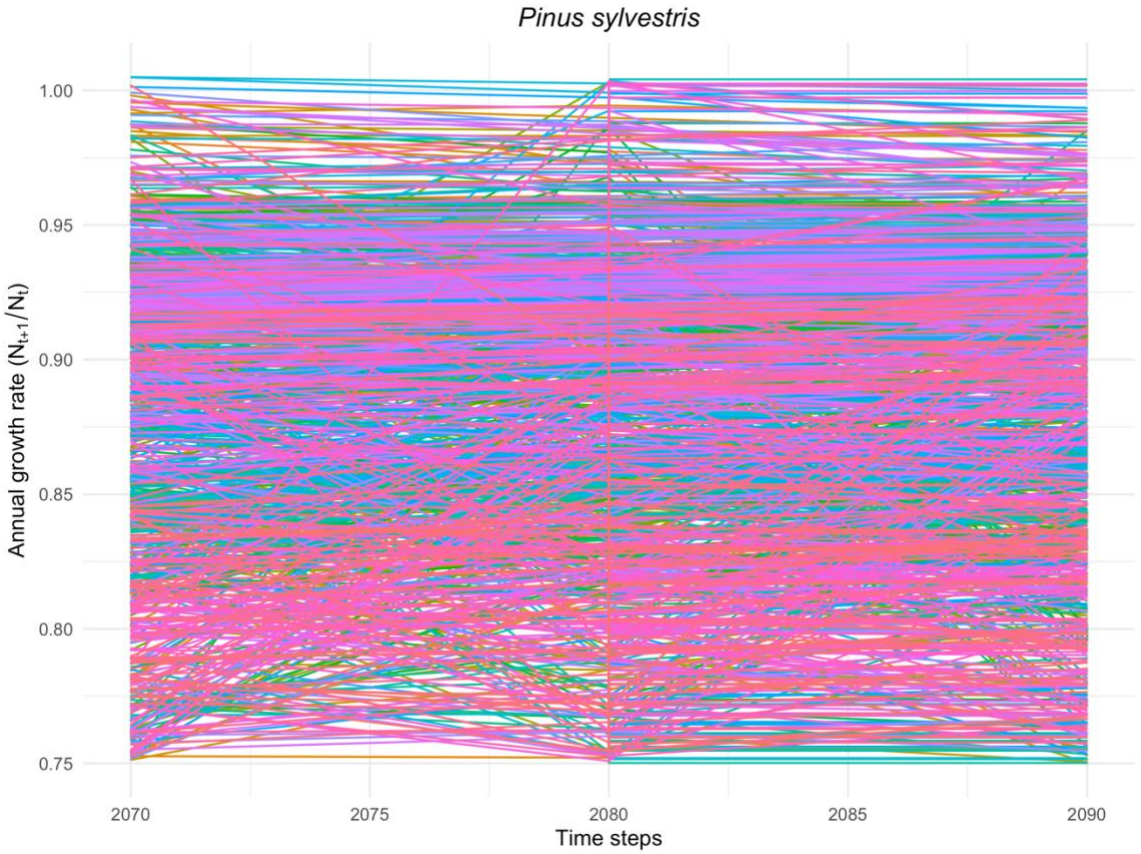

Figure S47. Time series of simulated annual growth rates (N_{t+1}/N_t) for *Pinus sylvestris*, which we averaged to calculate λ (after discarding transient dynamics). The colors represent the multiple simulations and sites (see species-specific details in SI). The variation in λ is largely attributed to variation among sites as we ensured to remove sites from analyses where λ values changed direction in simulations.

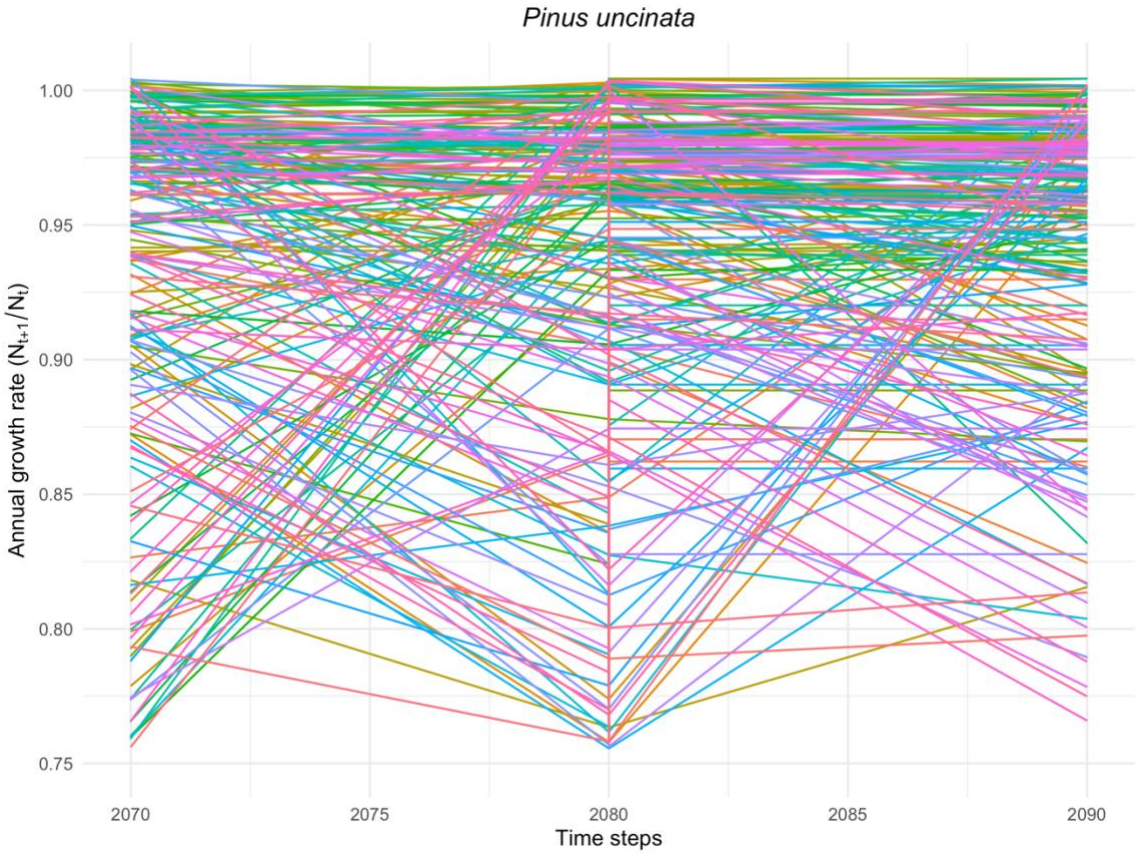

Figure S48. Time series of simulated annual growth rates (N_{t+1}/N_t) for *Pinus uncinata*, which we averaged to calculate λ (after discarding transient dynamics). The colors represent the multiple simulations and sites (see species-specific details in SI). The variation in λ is largely attributed to variation among sites as we ensured to remove sites from analyses where λ values changed direction in simulations.

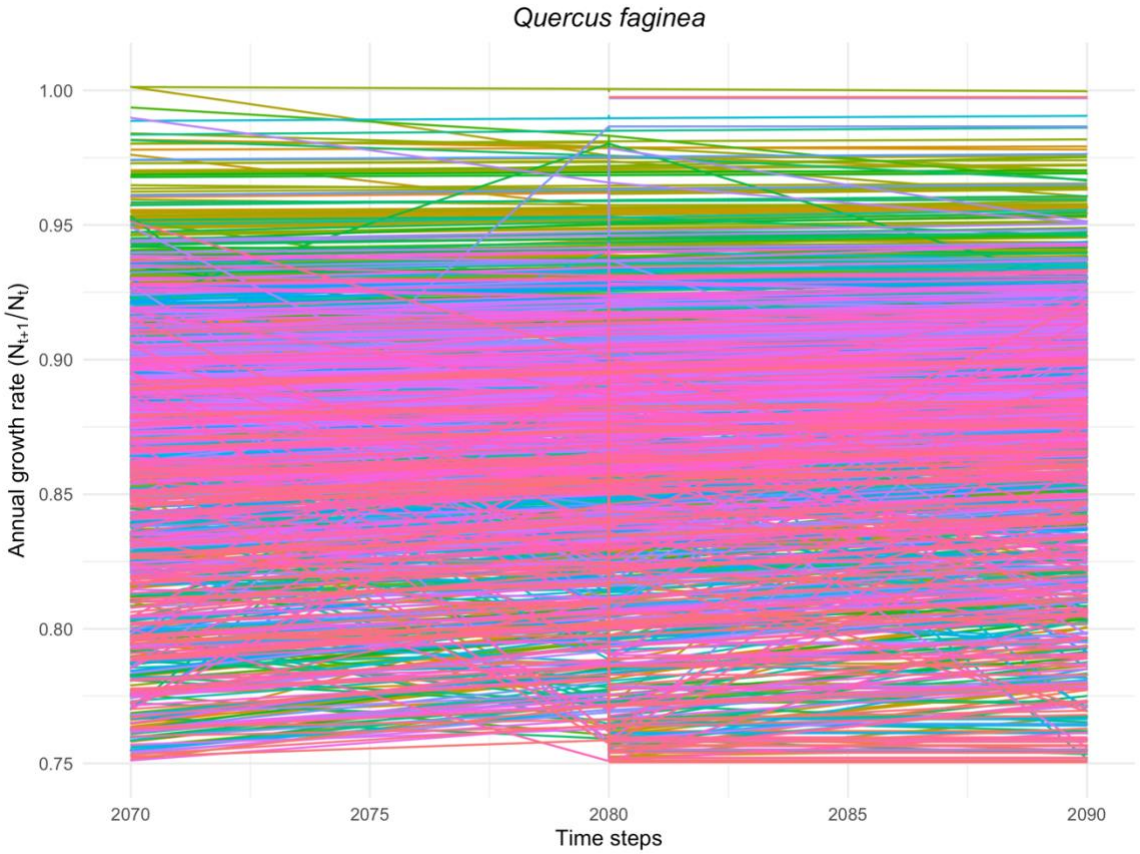

Figure S49. Time series of simulated annual growth rates (N_{t+1}/N_t) for *Quercus faginea*, which we averaged to calculate λ (after discarding transient dynamics). The colors represent the multiple simulations and sites (see species-specific details in SI). The variation in λ is largely attributed to variation among sites as we ensured to remove sites from analyses where λ values changed direction in simulations.

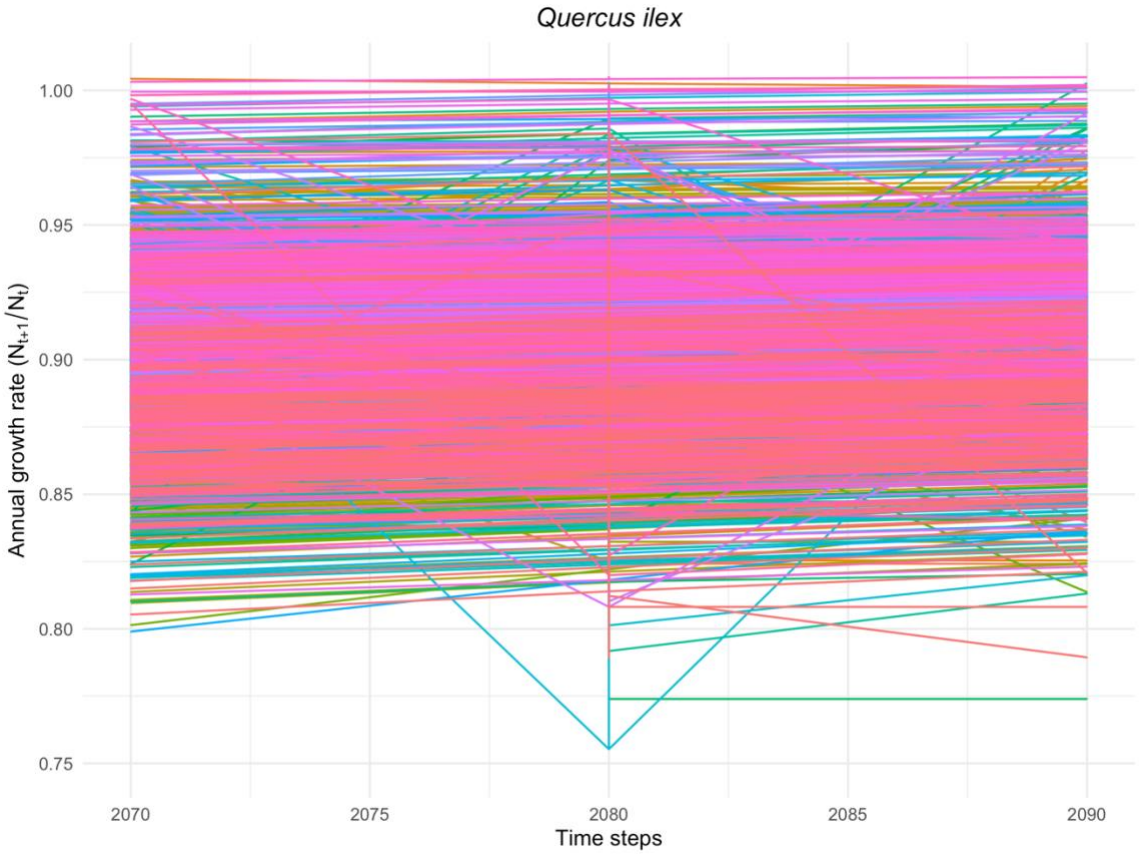

Figure S50. Time series of simulated annual growth rates (N_{t+1}/N_t) for *Quercus ilex*, which we averaged to calculate λ (after discarding transient dynamics). The colors represent the multiple simulations and sites (see species-specific details in SI). The variation in λ is largely attributed to variation among sites as we ensured to remove sites from analyses where λ values changed direction in simulations.

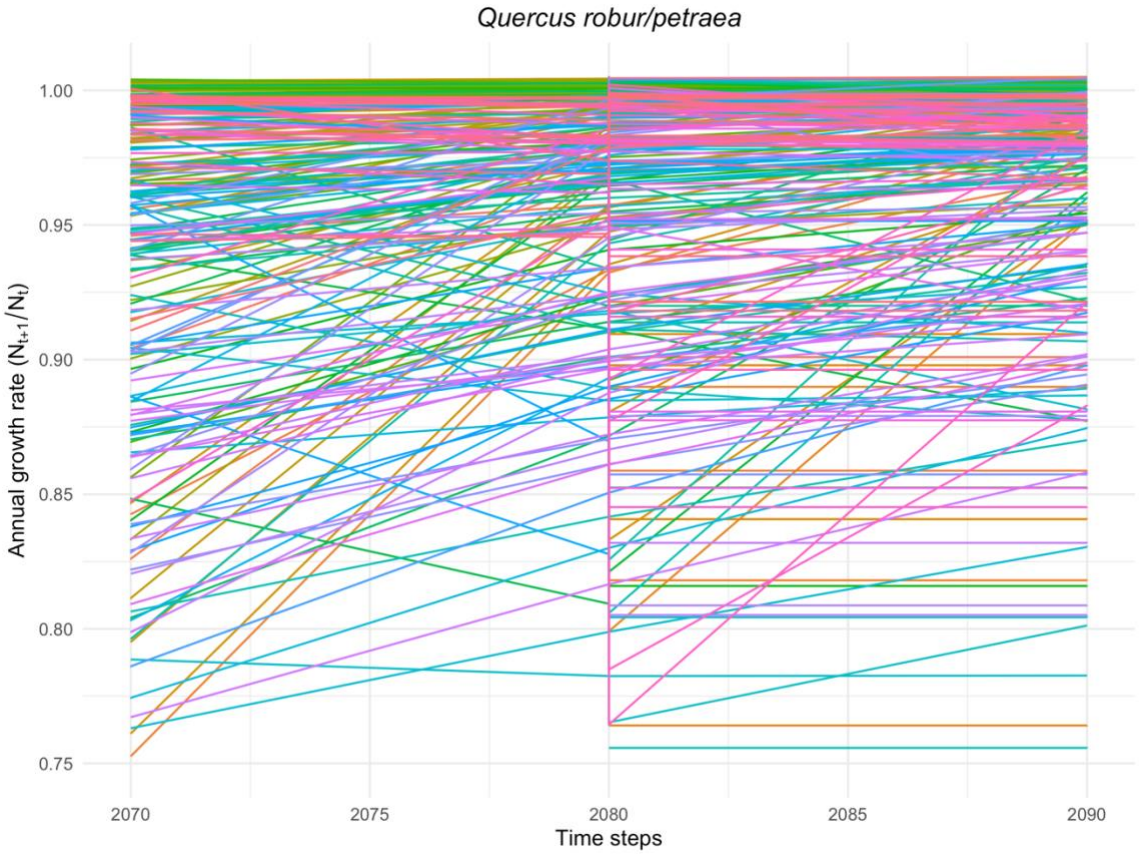

Figure S51. Time series of simulated annual growth rates (N_{t+1}/N_t) for *Quercus robur/petraea*, which we averaged to calculate λ (after discarding transient dynamics) The colors represent the multiple simulations and sites (see species-specific details in SI). The variation in λ is largely attributed to variation among sites as we ensured to remove sites from analyses where λ values changed direction in simulations.

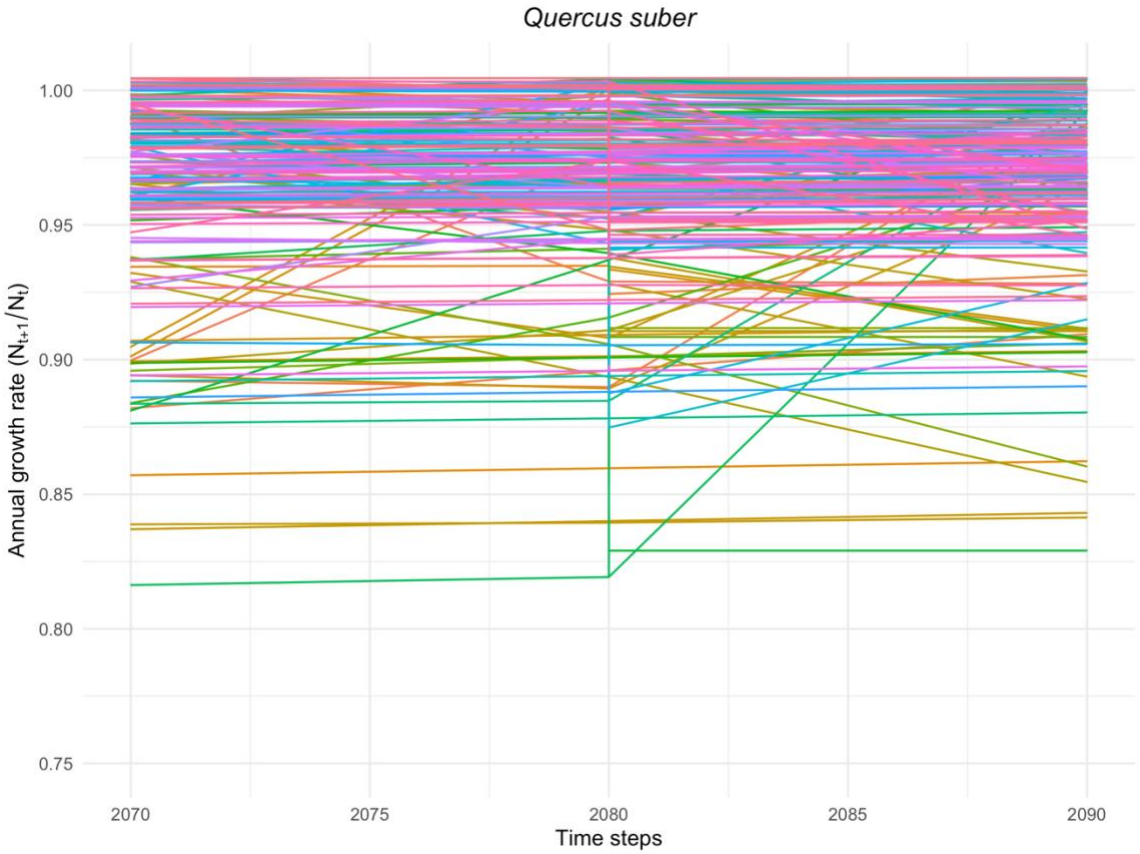

Figure S52. Time series of simulated annual growth rates (N_{t+1}/N_t) for *Quercus suber,* which we averaged to calculate λ (after discarding transient dynamics). The colors represent the multiple simulations and sites (see species-specific details in SI). The variation in λ is largely attributed to variation among sites as we ensured to remove sites from analyses where λ values changed direction in simulations.

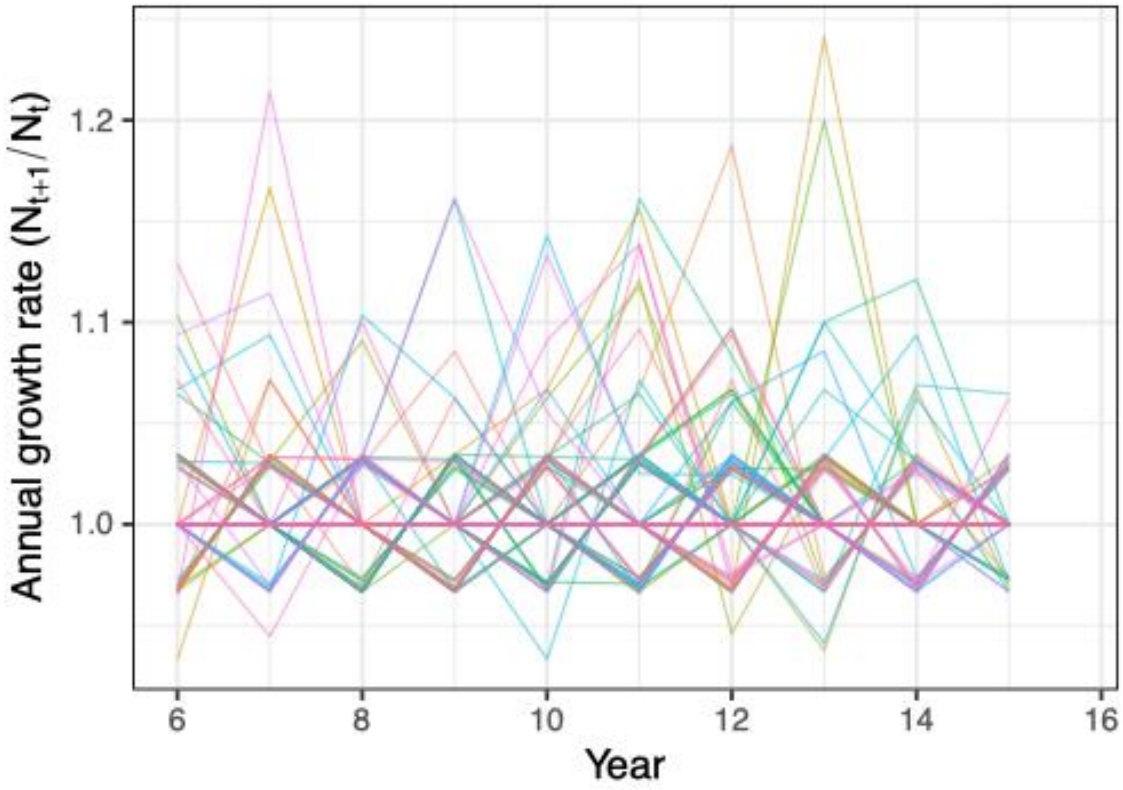

Figure S53. Time series of simulated annual growth rates (N_{t+1}/N_t) for *Oryctolagus cuniculus,* which we averaged to calculate λ (after discarding transient dynamics of year 1-5). The colors represent the multiple simulations and sites (see species-specific details in SI). The variation in λ is largely attributed to variation among sites as we ensured to remove sites from analyses where λ values changed direction in simulations. The colors represent the multiple simulations (n = 100).